Astroglial Control of Respiratory Rhythm Generating Circuits

A Thesis submitted for the Degree of
Doctor of Philosophy
to University College London

by

Shahriar Sheikhbahaei

Research Department of Neuroscience, Physiology, and Pharmacology
University College London
Gower Street
London WC1E 6BT

Declaration

I, Shahriar Sheikhbahaei, confirm that the work presented in this thesis is my own. Where information has been derived from other sources, I confirm that this has been indicated in the thesis.

Shahriar Sheikhbahaei

Abstract

Astrocytes, the most numerous glial cells of the central nervous system, are well known to provide neuronal circuits with essential structural and metabolic support. There is also evidence that astrocytes may modulate the activities of neuronal circuits controlling motor rhythms including those of the brainstem's preBötzinger complex (preBötC) that generates the rhythm of breathing in mammals. However, the extent and mechanisms of active astroglial control of the respiratory rhythm-generating circuits remain unknown. The morphological features of astrocytes in this critical brainstem region are also unknown. In this dissertation, viral gene transfer approaches designed to block or activate astroglial signaling pathways were used to determine the role of preBötC astrocytes in the control of breathing using *in vitro* and *in vivo* experimental models. Computer-aided morphometric analyses were used to investigate the structural features of brainstem astrocytes potentially contributing to their functional role.

The results from these complementary, multi-faceted experiments show that (i) morphologically, preBötC astrocytes are larger, have more branches, and longer processes when compared to astrocytes residing in other regions of the brainstem; (ii) in conscious adult rats, blockade of vesicular release mechanisms or ATP-mediated signaling in preBötC astrocytes by virally-induced bilateral expression of either the light chain of tetanus toxin (TeLC), the dominant-negative SNARE proteins (dnSNARE), or a potent ectonucleotidase – transmembrane prostatic acid phosphatase – results in a significant reduction of resting respiratory frequency and frequency of sighs, augmented breaths that engage preBötC circuits to increase inspiratory effort; (iii) hypoxic- and CO_2-induced ventilatory responses are significantly reduced when vesicular release mechanisms in preBötC astrocytes are blocked; (iv) activation of preBötC astrocytes expressing Gq-coupled Designer Receptor Exclusively Activated by Designer Drug is associated with higher frequency of both normal inspirations and sighs; (v) blockade of vesicular release mechanisms (expression of TeLC or dnSNARE) in preBötC astrocytes is associated with a dramatic reduction of exercise capacity. These data suggest that astroglial mechanisms involving exocytotic vesicular release of signaling molecules

(gliotransmitters), provides tonic excitatory drive to the inspiratory rhythm-generating circuits of the preBötC and contributes to the generation of sighs. The role of preBötC astrocytes in central nervous mechanisms controlling breathing becomes especially important in conditions of metabolic stress requiring homeostatic adjustments of breathing such as systemic hypoxia, hypercapnia, and exercise, when enhanced respiratory efforts are critical to support physiological and behavioral demands of the body.

Acknowledgements

I would like to recognize the support, enthusiasm, and passion of my exceptional supervisors, Prof. Alexander Gourine and Dr. Jeffrey Smith. Alex provided remarkable insight and working environment at UCL and patiently spent the time to teach me skills of *in vivo* experiments. Jeff provided an exceptional working environment for me at NIH to learn and apply *in vitro* experimental paradigm, guided me through scientific challenges, and mentored me in developing public engagement skills. I could not ask for better mentors, colleagues, and friends.

None of my Ph.D. work would have been possible without the help of my colleagues at UCL and NIH. I must thank Drs. Nephtali Marina and Hidehiko Koizumi for teaching me the essential surgical and electrophysiology skills required for my projects. I would like to thank my colleagues, especially Dr. Patrick Hosford, Anna Hadjihambi, Dr. Isabel Christie, and Elodie Gillard in the Gourine Lab, and Brian Morris, Sami Znati, Tibin John, Sommer Anjum, and Jared Collina in the Smith Lab who have all helped me in different ways. I am also grateful to Alla Korsak and Dr. Ruli Zhang for their technical support, and Dr. Shamshad Cockcroft for helping with PLC assay. I would like to especially thank Dr. Sergey Kasparov (University of Bristol) for providing novel molecular tools for performing experiments. I am also grateful to Dr. Doug Fields (NIH) for his great scientific input and comments, and Carly Houghton for advices on writing Python scripts.

I am also very thankful to the NIH Office of Intramural Training & Education, especially Drs. Sharon Millgram, Philip Ryan, and Gail Seabold for providing a wealth of support throughout my studies. Also, I am grateful to the NIMH Office of Fellowship Training, especially Dr. Janet Clark and Anika Reed for all their help and support through my joint PhD studies. I must also thank Prof. Bob Zucker of UC-Berkeley for his continuous support beyond my undergraduate educations.

Finally, I would like to thank my family for their support throughout my studies. My parents' love, encouragement, and support were instrumental in completing my Ph.D. I am also thankful to my cousins, Shirin, Nooshin, Shahram, Matt and their families, who made London a second home for me.

Table of Contents

List of Figures

Abbreviations

$[Ca^{2+}]_i$	intracellular calcium
$[K^+]_o$	extracellular potassium
aCSF	artificial cerebral spinal fluid
AAV	adeno-associated vector
ADP	adenosine diphosphate
ALS	amyotrophic lateral sclerosis
AMP	adenosine monophosphate
ATP	adenosine triphosphate
AVV	adenoviral vector
BötC	Bötzinger Complex
BP	blood pressure
CCHS	congenital central hypoventilation syndrome
CNS	central nervous system
DMSO	dimethyl sulfoxide
dnSNARE	dominant-negative soluble N-ethylmaleimide factor attachment protein receptor
DRG	dorsal respiratory group
EMG	electromyogram
GABA	gamma-aminobutyric acid
GFAP	glial fibrillary acidic protein (s-enhanced shortened)
GFP	green fluorescent protein (e-enhanced)
HEPES	4-(2-hydroxyethyl)-1-piperazineethanesulfonic acid
i.p.	intraperitoneal
i.v.	intravenous
IP3	inositol triphosphate
LC	Locus Coeruleus
LVV	lentiviral vector
MRS 2179	selective $P2Y_1$ receptor antagonist
NK1	N-methyl-D-aspartate
NTS	nucleus of the solitary tract (c-caudal)

P1	adenosine receptor
P2X	purinergic receptor
P2Y	purinergic receptor
*P*CO2	partial pressure arterial carbon dioxide
*P*O2	partial pressure arterial oxygen
pFRG	parafacial respiratory group
PiCo	post-inspiratory complex
PIP2	phosphatidylinositol 4,5-biphosphate
PLC	phospholipase C
PNA	phrenic nerve activity
preBötC	preBötzinger Complex
PRG	pontine respiratory group
ROS	reactive oxygen species
RTN	retrotrapeziod nucleus
SD	Sprague-Dawley
SIDS	Sudden Infant Death Syndrome
TASK	TWIK-related aid sensitive K+ channel
TeLC	tetanus light chain protein
TIRF	total internal reflection fluorescence
TMPAP	transmembrane prostatic acid phosphatase
V_E	minute ventilation
VLM	ventrolateral medulla
VRC	ventral respiratory column
VRG	ventral respiratory group (r-rostral, c-caudal)
V_T	tidal volume

Chapter 1 GENERAL INTRODUCTION

Astrocytes, the numerous glial cells of the brain, have been proposed to modulate neuronal excitability, synaptic transmission, and plasticity [1], [2]. Recent studies have suggested that astrocytes may influence neural circuits, particularly neuromodulatory circuits affecting sleep, feeding, and chemosensing [3]–[5], yet we are far from understating how astrocytes can modulate motor circuits and have an impact on complex behaviors *in vivo*. In part, the major challenge arises from the suitability of techniques to specifically target astrocytic functions and reliability of assessments of these manipulations on neuronal network output.

In this dissertation, complementary and multi-faceted experimental models were used to determine the functional consequences of genetic inhibition or activation of rodent's brainstem astrocytes on network activities controlling breathing behaviors. In this chapter, before briefly discussing the involvement of astrocytes in the central respiratory network, a general background information on the anatomy of central respiratory networks, breathing rhythm generation, and respiratory network modulators are provided.

1.1.1. Functional Anatomy of Respiratory network

Breathing activity in mammals is generated by a rhythmic neural process that ensures constant levels of oxygen and carbon dioxide in the arterial blood [6]. Disorders of the CNS affecting this process rarely occur, but if they do, the disruptions of normal breathing are life threatening [e.g., Sudden Infant Death Syndrome (SIDS) and Congenital Central Hypoventilation Syndrome (CCHS)] [7]–

[9]. Neuronal circuits controlling breathing are located in the brainstem within the pontine respiratory group (PRG), as well as bilaterally organized dorsal respiratory group (DRG) and ventral respiratory columns (VRC) of neurons in the medulla oblongata [10]–[13].

The ventral medulla is essential and sufficient to generate the respiratory rhythm. It contains several functionally distinct compartments, including (rostral to caudal) retrotrapezoid nucleus/parafacial respiratory group (RTN/pFRG), the Bötzinger complex (BötC), the preBötzinger complex (preBötC), the rostral and caudal ventral respiratory group (rVRG and cVRG). **Figure 1.1** illustrates a schematic of these functional regions. The functional role of each of these medullary regions is described briefly below. However, this thesis focuses on the preBötC which have been demonstrated to contain cellular elements essential for generating a defined motor output of basic inspiratory rhythm [10], [12], [14] even in highly reduced preparations of the mammalian CNS (such as brainstem slices in vitro) [14]–[17].

PRG, consists of Kölliker-Fuse (KF) and parabrachial (PB) nuclei, located in the dorsolateral pons. KF has a critical role in the transition from inspiration to expiratory phase of breathing cycle [18], [19]. PB complex is important for respiratory homeostasis and transmitting information from pontomedullary respiratory regions to the higher centers [19]. Since PRG also receives neuronal projections from RTN and NTS, it is also proposed that pontine group have possible roles in O_2 and/or CO_2 chemosensation [20]–[24].

DRG respiratory neurons, primarily reside within the nucleus of the solitary tract (NTS), receive information from the peripheral chemoreceptor of carotid bodies directly (see Section 1.1.3 for more details on respiratory chemosensors) [25]–[27], integrate the sensory information, and send projections to VRC [28] and PRG [29].

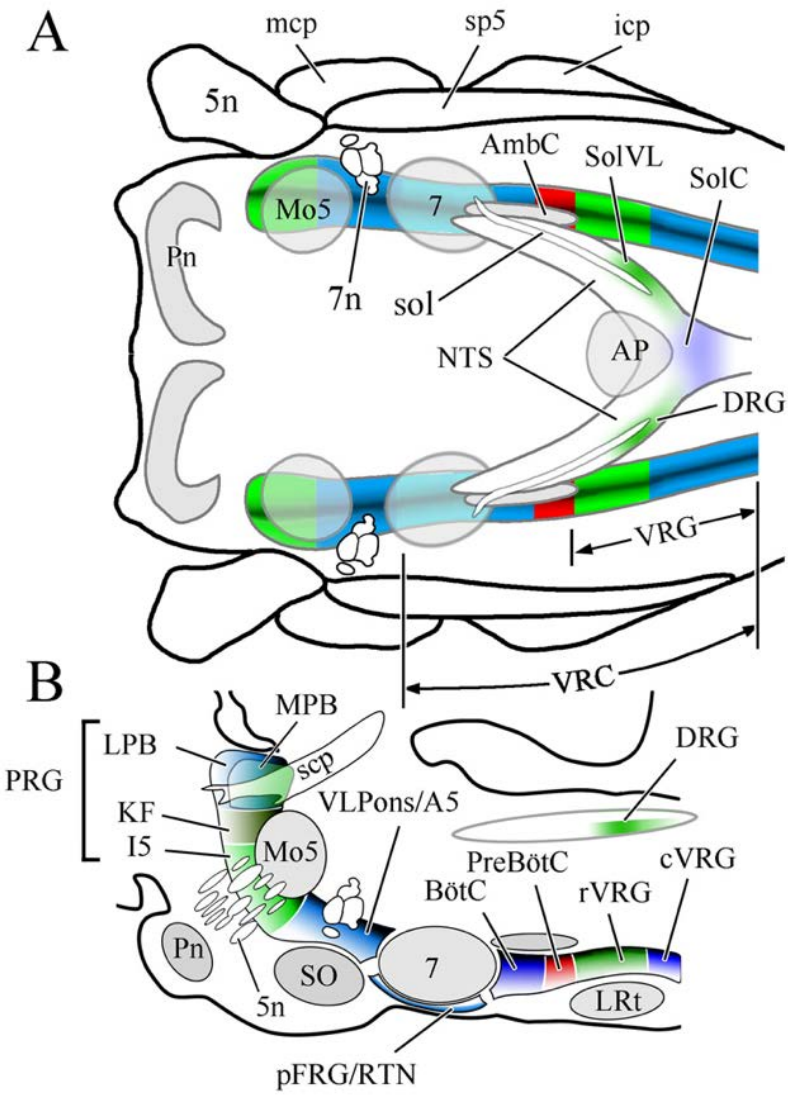

Figure 1.1| Neuroanatomy of the rat brainstem respiratory network.
The diagram illustrates a horizontal (A) and a parasagittal (B) view of the rat brainstem. The locations of the main respiratory-related regions controlling breathing in mammals have been shown. comprise a nearly continuous column in the lateral brainstem. The boundaries depicted between the various brainstem compartments reflect functional distinctions between adjacent regions relative to their impact on breathing. Abbreviations: 5n, trigeminal nerve; 7, facial nucleus; 7n, facial nerve; A5, A5 noradrenergic neuronal group; AmbC, compact part of nucleus ambiguus; AP, area postrema; BötC, Bötzinger complex; cVRG, caudal division of ventral respiratory group; DRG, dorsal respiratory group; I5, intertrigeminal area; icp, inferior cerebellar peduncle; KF, Kölliker-Fuse nucleus; LPB, lateral parabrachial region; LRt, lateral reticular nucleus; mcp, medial cerebellar peduncle; Mo5, motor nucleus of the trigeminal nerve; MPB, medial parabrachial region; NTS, nucleus of the solitary tract; pFRG, parafacial respiratory group; Pn, basilar pontine nuclei; preBötC, preBötzinger complex; PRG, pontine respiratory group; RTN, retrotrapezoid nucleus; rVRG, rostral division of ventral respiratory group; scp, superior cerebellar peduncle; SO, superior olive; sol, solitary tract; SolC, commissural subdivision of the nucleus of the solitary tract; SolVL, ventrolateral subdivision of the nucleus of the solitary tract; sp5, spinal trigeminal tract; vlPons, ventrolateral pontine region; VRC, ventral respiratory column of the medulla; VRG, ventral respiratory group. Adapted from [46]

RTN/pFRG, located ventral to the facial nucleus [30], contribute mainly to the generation of active expiration [12], [31], [32]. Putative chemosensitive neurons of the RTN are expressing the transcription factor paired-like homeobox 2b (Phox2b) and proposed to have a central role in CO_2 chemosensitivity [33] (I have discussed the role of RTN neurons in control of breathing in more details in Sections 1.1.2 and 1.1.3.2, and Chapter 5).

BötC, a defined group of mainly expiratory neurons [10], [34], [35], is located caudal to the RTN and provide inhibitory (GABAergic and glycinergic) projections through the VRC [10], [36]. BötC neurons are shown to be important in the transition of breathing phase from inspiration to expiration [10], [37]. However, BötC receives tonic excitatory inputs from the pons and removing of the pons (in *in situ* preparation) changes the pattern of normal breathing from a three-phase to a two-phase breathing pattern [10]. The role of BötC neurons in respiratory rhythm generation has been discussed in more details in section 1.1.2 .

PreBötC, a group of heterogeneous interneurons with intrinsic inspiratory rhythm-generating properties [14], is located ventral to the semi-compact division of the nucleus ambiguus (NAsc) and caudal to the BötC region [12]. Pacemaker-like cells of the preBötC can support the rhythm even when they are isolated in medullary slices *in vitro* [14]. It is believed that the preBötC is essential for normal inspiratory activity *in vivo* [12], receives afferent inputs from the respiratory chemosensors, and sends extensive projections [38] to other respiratory nuclei in VRC, DRG, and PRG to provide inspiratory drive and/or modulate breathing pattern [37]. The preBötC has been described several species including rodents [14], cats [39] and humans [40], [41], and it is shown that rhythmogenic neurons of the preBötC are derived from progenitor cells that express the developing brain homeobox 1 (*Dbx1*) gene [42]–[44]. In an innovative and well-designed experiment to explore the minimum number of neurons necessary for generating rhythm in the preBötC, it was shown that in mouse rhythmically-active brainstem slice *in vitro*, generated rhythm was stopped after laser ablations of ~ 15% of preBötC Dbx1 neurons [45].

rVRG neurons, which contains a cluster of inspiratory bulbospinal premotor neurons [46], are modulated by excitatory neuronal projections from preBötC and RTN, as well as inhibitory neurons of BötC. rVRG neurons transmit the inspiratory drive to the diaphragm via phrenic motoneurons [46], [47]. *cVRG* contains expiratory bulbospinal excitatory neurons, receive similar convergent inputs from the preBötC, BötC and RTN/pFRG, and mainly project to abdominal motoneurons [48], [49].

1.1.2. Inspiratory Rhythmogenesis.

The eupneic respiratory cycle consists of three distinct phases: inspiration (phase 1), post-inspiration (phase 2), and late-expiration (phase 3), which translate into coordinated activities of inspiratory and expiratory muscles [13], [18]. Traditionally, three-phased respiratory rhythm was thought to emerge from neuronal cross-talk between preBötC and BötC, where preBötC generates rhythmic inspiratory phase and BötC orchestrates post-inspiration and late-expiration phases [36], [50]–[52]. However, the role of BötC inhibitory neurons in expiration and regulation of phase change from inspiratory to expiratory activities has been recently challenged [53], [54]; injections of a bicuculline ($GABA_A$ receptors antagonist) and strychnine (glycine receptors antagonist) mix into the BötC did not interrupt normal breathing rhythm [54]. Instead, it has been proposed that a subpopulation of the pFRG neurons (located outside of the BötC) function as a separate/distinct expiratory oscillator which interacts with the preBötC to control active expiration and coordinate transitional patterns of inspiratory to expiratory activities [12], [55]. Recently , post-inspiratory complex (PiCo), located dorsomedial to the NA and dorsal to BötC, has been suggested as the putative region for the coordination of the post-inspiratory activity in a triple oscillatory hypothesis [56], though prior data suggested KF might play such a role [57], [58]. The details of these proposed models of respiratory rhythmogenesis are beyond the scope of this thesis. Nevertheless, in all the proposed models, it is now accepted that the preBötC is the main source of rhythmic excitatory drive in the brainstem network, which is transmitted via polysynaptic pathways to

the respiratory motoneurons such as phrenic motoneurons [10], [14], [15].

Although the intrinsic cellular properties and the circuit features that underlie the generation of the respiratory rhythm are not fully understood, it is accepted that rhythmogenic mechanisms of the brainstem may change based on metabolic demand, environmental circumstances, and behavioral conditions [18], [37], [59], [60]. Brainstem respiratory control system receives feedback from lung mechanosensors (to adapt the breathing pattern to the position of respiratory muscles) and chemosensors (to match the respiratory activity with metabolic demand). Changes in the arterial PO_2 and PCO_2/pH are sensed by specialized chemosensors of the central and peripheral nervous systems. The activity of the respiratory network is under constant modulation by inputs from the central and peripheral chemoreceptors as the respiratory activity requires a certain level of CO_2.

1.1.3. Chemoreception

1.1.3.1. Peripheral chemoreceptors

Oxygenation of the arterial blood is continuously monitored by peripheral chemoreceptors located in the carotid and (in some species) aortic bodies [61]–[63]. These chemoreceptors detect changes in blood PO_2 in a manner also dependent on blood PCO_2/pH, and convey chemosensory information to the brainstem respiratory control networks [25], [26], which adjust the respiratory activity in accordance with prevailing physiological and behavioral needs.

Located bilaterally at the bifurcation of the common carotid arteries, carotid body chemoreceptors are believed to be the major site for respiratory oxygen sensing [64], [65]. When arterial PO_2 decreases (e.g., during systemic hypoxia), the carotid bodies signal to the brainstem circuits, which increase the rate and depth of breathing [61]and also trigger adaptive increases in sympathetic activity [66], [67].

In addition to hypoxia, other stimuli, including hypercapnia [as it is believed that peripheral chemoreceptors in the carotid bodies contribute to about one-third of

the hypercapnic ventilatory response [65], [68]], and acidosis [69] have been shown to activate carotid body chemoreceptors.

However, conscious rats (and some other mammals, but not humans) with denervated peripheral chemoreceptors display robust ventilatory responses to hypoxia [70]–[75] and even display partial or almost complete recovery of the ventilatory response to hypoxia [76], which suggest that the central nervous system may contain a functional respiratory oxygen sensor.

1.1.3.1.1. Hypoxic Ventilatory Response

Acute hypoxia causes a biphasic ventilatory response including an initial rapid increase followed by a secondary depression in ventilation [76], [77]. It is believed that the peripheral chemoreceptors (of the carotid body) are responsible for the initial response, though hypoxia sensitive regions in the CNS (such as the caudal hypothalamus, NTS, and preBötC) could potentially contribute to this initial increase in ventilation [78], [79].

Recent studies in rodents also reported (but did not comment on this particular aspect) robust respiratory responses to hypoxia in awake mice and rats with chronically denervated carotid bodies [80], [81]. The latest studies of the mechanisms underlying peripheral oxygen sensitivity using transgenic animal models reported that during the early postnatal period in mice, chemosensitive carotid body glomus cells do not express critical components (olfactory receptor Olfr78) of the O_2 signaling pathway [82]. Yet, neonatal mice displayed robust and sustained hypoxic ventilatory responses [83], [84]. These data provided further evidence for the existence of a central respiratory oxygen sensor ([76]; see also Section 5.1) located (most likely) in the brainstem which contributes to the development of the ventilatory response to hypoxia [76]. It has been shown that purinergic signaling plays a significant role in mediating both phases of the hypoxic ventilatory response, at both central and peripheral sites [77]. However, the source these signaling molecules is not identified.

1.1.3.2. Central chemoreceptors

Significant evidence suggests that changes in the arterial levels of PCO_2/pH are detected by specialized chemoreceptors located in the brainstem [61]–[63], [85], [86]. It is believed that brainstem central chemosensors mediate about two-thirds of the hypercapnic ventilatory response [87]–[91]. Intrinsically chemosensitive neurons reside in several areas within the brainstem [92]–[95] including the RTN [33], respiratory rhythm-generating region of the preBötC [96]–[98], and in the raphe nuclei [99]. However, the current prevailing model is that central respiratory CO_2 chemosensitivity is brought about by functions of a defined group of pH-sensitive glutamatergic neurons residing in the RTN located in the ventral regions of the medulla oblongata, in near proximity to the populations of respiratory and autonomic neurons that generate coordinated respiratory and sympathetic activities [85], [100], [101]. This view is supported by experimental evidence which demonstrated that the permanent loss or acute inhibition of RTN neurons abolishes or significantly reduces the amplitude of ventilatory responses induced by increases in the arterial PCO_2 [32], [33], [102]–[105].

1.1.3.2.1. Hypercapnic Ventilatory Response

Breathing activity is tightly modulated by the level of partial pressure of carbon dioxide (PCO_2) as the respiratory network is not active in the absence of CO_2 and requires a threshold level of CO_2 to operate [88], [106]. Carbon dioxide (produced in the mitochondria in proportion to the metabolic rate) is mainly excreted through the process of alveolar ventilation [6], [107]. In situations where ventilation is impaired, CO_2 elimination becomes inadequate leading to accumulation of H^+ ions and a reduction in extracellular pH, a condition that is rapidly corrected by adjustments in ventilatory and cardiovascular activities that ensure the removal of excess CO_2 from the circulation.

The mechanisms by which central chemoreceptors sense CO_2/H^+ have been recently reported to depend on the activity of the proton-sensitive receptor GPR4 in

putative pH-sensitive chemosensory neurons of RTN [108]. However, there is also evidence suggesting that the chemosensitivity of RTN neurons is (to a large extent) indirect and mediated by the responses triggered by changes of $PCO_2/[H^+]$ in neighboring glial cells [5]. While extracellular adenosine triphosphate (ATP) acting via purinergic receptors plays a significant role in central CO_2 chemoreception and involves in mediating CO_2-induced respiratory responses at the RTN [5], [101], [109], [110] and maybe at the preBötC [95], [96], recent work has demonstrated a significant contribution of purinergic signaling by astroglial cells [5], [109], [111]–[114].

1.1.4. Astrocytes.

Astrocytes, the numerous glial cells of the brain, have recently been implicated in the modulation of neuronal activity [115]–[118]. These electrically silent cells provide metabolic support for neurons [119]–[121] and alter the extracellular space [122], [123] that can affect neuron and circuit activity. Astrocytes enwrap all intracerebral and penetrating arterioles and capillaries controlling local blood flow [124]. Astrocytes also enwrap neuronal somata, supplying neurons with lactate and controlling the ionic and metabolic neuropil environment [125]–[127], which includes recycling and providing pre-synaptic terminals with a renewable source of transmitters, as well as mediating neurovascular coupling [128]–[131]. Moreover, astrocytes display Ca^{2+} excitability and release of gliotransmitters, such as ATP/adenosine, glutamate, D-serine, lactate and possibly many others [132]–[134]. There is evidence that astrocytes play an active role in some CNS homeostatic mechanisms, including central mechanisms of controlling breathing [5], [71], [135]–[141].

1.1.5. Astroglial Control of Respiratory Rhythm Generating Circuits

In vivo experiments in anesthetized and mechanically ventilated rats revealed

that astrocytes residing within the RTN region have an intrinsic capacity to detect physiological changes in extracellular pH (generated by excess CO_2), responding with robust elevations in intracellular Ca^{2+} which triggers the exocytosis of ATP-containing vesicles [5], [142]. Thus, astrocytes are likely to be at the center of the brainstem chemosensory mechanisms that adjust patterns of the respiratory activity in response to changes in PCO_2/pH [5], [113], [114], [143], [144]. Chemosensory stimuli are known to stimulate breathing centrally via decreases in brain extracellular pH associated with increases in blood/brain PCO_2 that independently triggers astrocytic release of ATP, which has been identified as the key gliotransmitter responsible for astrocytic control of the respiratory network [4], [5], [11], [137], [145]–[147]. This astrocytic release of ATP occurs via several mechanisms, such as vesicular exocytosis in response to acidification [5] and hypoxia [71], or opening of connexin hemichannels following an increase in PCO_2 [144]. Activation of individual respiratory neurons including preBötC rhythm-generating respiratory circuits in response to ATP-mediated signaling mechanisms have been demonstrated before [5], [12], [148]–[150]. Therefore, preBötC astroglial signaling molecules, such as ATP/adenosine, can initiate an adaptive respiratory response that may alter the function of surrounding neurons.

Astrocytes modulate neural activity in many other brain regions. For instance, ATP/Adenosine released by astrocytes has been shown to participate in the accumulation of sleep pressure [4], [133]; vesicular release of transmitters from cortical astrocytes has been shown to contribute to long-term [151] and acute [152] changes in cortical state and memory retention; D-serine and ATP/adenosine released from cortical astrocytes have been also shown to contribute to slow oscillations *in vivo* [153].

Purinergic signaling is not unique to the respiratory system; for instance, in the hippocampus, it has been shown that astrocytes continuously [154], [155], and phasically released ATP in a SNARE-dependent manner [155], [156]. Released ATP in this region is rapidly degraded to adenosine, which modulates the activity of neurons [155]. In motor networks of the spinal cord, another rhythmic motor circuit, tonic purinergic signaling from astrocytes is also reported to regulate motor circuit activities [157]. Also, it has been shown that ATP excites the locomotor centers

[158], [159], whereas its metabolite, adenosine, inhibits the network activity [160]–[162]. In mice, application of the glial toxins (methionine sulfoximine or fluoroacetate) blocked most of the adenosine induced modulation of circuit activities in spinal motor networks, suggesting that astroglia cells are the major source of this purinergic signals [160]. Similarly, in respiratory rhythm-generation of the preBötC, ATP-mediated excitation, and adenosine-induced inhibition of the inspiratory neurons are reported [149], [150], [163]. Therefore, it is also plausible that astrocytes are likely to be at the center of this purinergic regulation of the preBötC respiratory rhythm-generating circuits.

1.1.6. Conclusion

This chapter has provided a scientific background and an overview of the organization of central respiratory control networks; inspiratory rhythm generation in the preBötC; peripheral and central chemosensors; hypoxic and hypercapnic ventilatory response; and astrocytes as new players in the respiratory control system. There is overwhelming evidence that that gliotransmitters may influence neural circuits, particularly neuromodulatory circuits affecting sleep, feeding, and chemosensing [3]–[5]. However, the physiological significance and mechanisms of astroglial control of the respiratory rhythm-generating circuits of the preBötC remain unresolved.

1.1.7. Summary of Aims

Experimental studies described in this thesis tested the hypothesis that *exocytotic release of gliotransmitters by preBötC astrocytes controls the activity of the respiratory rhythm-generating circuits and modulates breathing behaviors at rest and during metabolic challenges.* Methods of genetic cell targeting using viral gene transfer combined with *in vivo* approaches (anesthetized and conscious adult rats) were used to address the following specific aims that will be addressed in the subsequent results chapters:

1. To study the anatomical features of brainstem astrocytes and to determine

whether preBötC astrocytes are morphologically different from astrocytes residing in other regions of the brainstem.

2. To determine the effect of activation and blockade of signaling pathways in preBötC astrocytes on breathing behavior (conscious behaving rats).
3. To determine the effect of activation and blockade of signaling pathways in preBötC astrocytes on breathing behavior during hypoxia, hypercapnia, and exercise (conscious behaving rats).

Chapter 2 METHODS

2.1.1. Animal experimentations

All animal experiments were performed in accordance with the European Commission Directive 2010/63/EU (European Convention for the Protection of Vertebrate Animals used for Experimental and Other Scientific Purposes), the UK Home Office (Scientific Procedures) Act (1986), and the National Institutes of Health Guide for the Care and Use of Laboratory Animals, with project approval from the respective Institutional Animal Care and Use Committees. Animals were housed in temperature-controlled facilities with a normal light-dark cycle (12h:12h, lights on at 7:00 A.M.). Tap water and laboratory rodent chow were provided *ad libitum*.

Juvenile (60 – 90 g) and adult Sprague-Dawley rats (250 – 300 g) were used for *in vivo* studies. Novel molecular approaches designed to activate or inhibit signaling pathways in preBötC astrocytes (see **Table 2.1**) were applied.

2.1.2. Molecular approaches to block astroglial signaling

Vesicular exocytosis is one of the main mechanisms that astrocytes use to release signaling molecules (i.e., gliotransmitters). To interfere with astroglial vesicular release pathways, adenoviral vectors (AVV) were used to express specific proteins under the control of the enhanced shortened astrocytic specific GFAP promoter (GfaABC1D). The AVVs were produced by homologous recombination as

described in detail previously [164], [165] in collaboration with Prof. Sergey Kasparov (University of Bristol).

2.1.2.1. Adenoviral vector (AVV) for the expression of dominant-negative SNARE (dnSNARE) protein in astrocytes

To block vesicular release mechanisms in preBötC astrocytes, novel AVV was used to drive the expression of a dominant-negative SNARE (dnSNARE) protein [155] under the control of the astrocytic specific GFAP promoter (AVV-sGFAP-dnSNARE-EGFP; **Table 2.1**). The layout of the vector is shown in **Figure 4.1**. In this vector, a bicistronic construct was produced in which the enhanced shortened GFAP promoter (GfaABC1D) was used to drive the expression of dnSNARE linked to EGFP (**Figure 4.1**). Validation of the transgene efficacy in blocking vesicular release mechanisms in cultured astrocytes is provided in Chapter 4 .

2.1.2.2. AVV for the expression of light chain of tetanus toxin (TeLC) in astrocytes

PreBötC astrocytes were also targeted to express the light chain of tetanus toxin (TeLC), which blocks vesicular exocytosis by proteolytic degradation of SNARE proteins responsible for vesicular docking and fusion (AVV-sGFAP-EGFP-skip-TeLC; **Table 2.1**). This vector is similar to the AVV vector used to express dnSNARE in astrocytes, except that the enhanced shortened GFAP promoter (GfaABC1D) drives the expression of EGFP linked to TeLC via a "SKIP" sequence [71]. With this construct placing TeLC second in the cassette after the SKIP sequence, TeLC expression is attenuated to minimize toxicity to transduced cells. The validation of the TeLC efficacy in blocking vesicular release and signaling between astrocytes have been described in detail in Angelova et al. [71].

Since dnSNARE or TeLC expression in astrocytes is likely to block exocytosis of several putative gliotransmitters, the specific contribution of ATP was determined by blocking ATP-mediated signaling within the preBötC by virally-driven

expression of a potent ectonucleotidase (TMPAP, see below).

2.1.2.3. Lentiviral vector for the expression of transmembrane prostatic acid phosphatase (TMPAP)

To block ATP-mediated signaling, a lentiviral vector (LVV) was used to overexpress a potent ectonucleotidase - transmembrane prostatic acid phosphatase (TMPAP) [166]. Expression of TMPAP was driven under the control of an elongation factor 1α (Ef1α) promoter (LVV-Ef1α-TMPAP-EGFP; **Table 2.1**). Efficacy of TMPAP in preventing vesicular ATP accumulation in astrocytes and blocking ATP-mediated signaling between astrocytes was described in detail previously[167], [168]. Despite the use of the generic promoter Ef1α, EGFP expression driven by LVVs is almost exclusively confined to astroglia [167] (**Figure 4.11**).

2.1.3. Molecular approach to activate astrocytes

2.1.3.1. AVV for the expression of Gq-coupled Designer Receptor Exclusively Activated by Designer Drug (DREADD$_{Gq}$) in astrocytes

To stimulate Gq-coupled signaling pathways in astrocytes, a novel AVV was used to express Gq-coupled Designer Receptor Exclusively Activated by Designer Drug (DREADD$_{Gq}$) fused with EGFP (AVV-sGFAP-DREADD$_{Gq}$-EGFP; **Table 2.1**). DREADD$_{Gq}$ at the level of the expression provided by our vector appeared to be constitutively active as evident from higher resting PLC activity, enhanced fusions of putative ATP containing vesicles and facilitated ATP release in astrocytes expressing DREADD$_{Gq}$ (see Chapter 4 for details).

2.1.4. Molecular approach to inhibit neurons

Current models of central respiratory CO_2 chemosensitivity are centered on a defined group of pH-sensitive neurons residing in the medullary retrotrapezoid nucleus (RTN). To determine the role of preBötC astrocytes in central respiratory chemosensitivity, viral vectors were used to drive the expression of an inhibitory receptor in the RTN neurons (see below).

2.1.4.1. Adenoassociated vector (AAV) for the expression of Gi-coupled DREADD ($DREADD_{Gi}$) in neurons

In order to stimulate Gi-coupled signaling pathways in the RTN neurons to inhibit these cells, I used an adeno-associated viral vector (AAV) to express $DREADD_{Gi}$ under the control of the synapsin (hSyn) promoter (AAV-2/5 hSyn-$DREADD_{Gi}$-mCitrine; University of North Carolina Vector Core, Chapel Hill, NC; **Table 2.1**). Efficacy of $DREADD_{Gi}$ in inhibiting RTN neurons was described previously [169].

2.1.1. Control transgenes

2.1.1.1. CatCh

Since $DREADD_{Gq}$ is a membrane protein, a control transgene with a membrane-bound protein was needed. Thus, an AVV to express calcium translocating channelrhodopsin variant (CatCh) fused with EGFP (CatCh-EGFP) under the

Table 2.1. Viral vectors used in the experimental studies

Abbreviated name	Full virus name	Group size	Type	Titer	Target cells
TeLC	AVV-sGFAP-EGFP-skip-TeLC	n = 12	adenovirus	$2.1x10^{8}$	astrocytes
dnSNARE	AVV-sGFAP-dnSNARE-EGFP	n = 5	adenovirus	$7.7x10^{9}$	astrocytes
$DREADD_{Gq}$	AVV-sGFAP-$DREADD_{Gq}$-EGFP	n = 8	adenovirus	$8.6x10^{9}$	astrocytes
CatCh (control)	AVV-sGFAP-CatCh-EGFP	n = 5-12	adenovirus	$2.1x10^{9}$	astrocytes
TMPAP	LVV-Ef1α-TMPAP-EGFP	n = 7	lentivirus	$1x10^{10}$	all brain cells
EGFP (control)	LVV-Ef1α-EGFP	n = 7	lentivirus	$1x10^{10}$	all brain cells

control of the same GFAP promoter (AVV-sGFAP-CatCh-EGFP; **Table 2.1**) was used as a control. CatCh-EGFP is more appropriate control since it incorporates into the membrane similar to DREADDs. In addition, parts of both CatCh and DREADDs are facing the extracellular space and (as foreign proteins) may potentially trigger a local immune response. Thus, expression of CatCh-EGFP is a much harsher control than a cytoplasmic expression of EGFP which has hardly ever been reported to cause any detectable adverse cellular effects. AVV-sGFAP-CatCh-EGFP was used as a control in the experiments when AVVs were used to drive the expression of TeLC, dnSNARE, or $DREADD_{Gq}$

2.1.1.2. EGFP

A lentiviral vector (LVV) to express EGFP under the control of EF1α promoter was used as a control for LVVs that drive the expression TMPAP (**Table 2.1**).

2.1.1.3. ChR2

An AAV to express ChR2 fused with EGFP (ChR2-EGFP) under the control of hSyn promoter (AAV-hSyn-ChR2-EGFP; University of North Carolina Vector Core, Chapel Hill, NC despite) was used as a control for $GREADD_{Gi}$ (**Table 2.1**).

Each experimental animal groups (expressing dnSNARE, TeLC, $DREADD_{Gq}$, TMPAP, $DREADD_{Gi}$) and control groups (expressing CatCh-EGFP, EGFP, or ChR2) were injected with the appropriate viral vector at the same time, and the experimental groups were compared to their control groups. Although some variations in the baseline respiratory frequency were observed (**Figure 4.13**), these differences in resting respiratory activity between animals from different control groups expressing CatCh-EGFP, ChR2-EGFP, or EGFP in the preBötC and naïve (non-transduced) rats were not statistically significant (**Figure 4.13**).

2.1.2. *In vitro* methods to validate transgene functionality

2.1.2.1. Cell culture

Primary astroglial cell cultures were prepared from the brainstem tissue of rat pups (P2 – P3 of either sex) as described in detail previously [71], [142]. The animals were killed by isoflurane overdose, the brains were removed, and the ventral regions of the medulla oblongata were dissected out. Brainstem tissue cuts from 2-3 animals were used for each cell culture preparation. After isolation, the cells were plated on poly-d-lysine-coated glass coverslips and maintained at 37°C in a humidified atmosphere of 5% CO_2 and 95% air. Viral vectors to drive the expression of a transgene of interest (dnSNARE, DREADDGq, CatCh or EGFP, **Table 2.1**) were added to the incubation medium at the time of cell culture preparation at $5x10^8$ – $5x10^{10}$ transducing units ml^{-1}. Experiments were performed after 7 – 10 days of incubation.

2.1.2.2. Total internal reflection fluorescence (TIRF) microscopy

In cultured brainstem astrocytes, vesicular compartments were visualized by quinacrine staining (5 μM, 15 min incubation at 37°C). The acridine derivative quinacrine is a weak base which binds ATP with high affinity and can be used to identify putative ATP-containing vesicles in living cells, including astrocytes [170]. An Olympus TIRF microscope was used to monitor fusion events of ATP-containing vesicles as described in detail previously [142]. Briefly, quinacrine-loaded (i.e., ATP-containing) vesicles were excited at 488 nm, and the fluorescent was collected at 500-530 nm, and the motility of vesicles was analyzed using time-lapse imaging. The imaging setup included a high-numerical-aperture oil-immersion objective (60x, 1.65 NA), an inverted microscope (IX71; Olympus) and a cooled charge-coupled-device camera (Hamamatsu). Rapid destaining of quinacrine-loaded vesicles in different experimental conditions was quantified and interpreted as release of quinacrine (and ATP) from the astrocyte into extracellular space [171]. Images were analyzed using Olympus Cell^tool software (Olympus). The experiments were performed at 37°C. These experiments were performed in

collaboration with Dr. Egor Turovsky.

2.1.2.3. Ca^{2+} imaging

Optical $[Ca^{2+}]_i$ recordings in cultured astrocytes were performed as described in detail previously [71], [113]. $[Ca^{2+}]_i$ responses in individual astrocytes were visualized by recording changes in fluorescence of conventional Ca^{2+} indicators Fura-2 (Molecular Probes) or Rhod-2 (Thermo Fisher). Cells were loaded with Fura-2 (5 μM; 40 min incubation; 37°C) or Rhod-2 (10 μM; 40 min incubation; 37°C) with the addition of pluronic F-127 (0.005%). After incubation with the dye, cultures were washed three times prior to the experiment. Changes in $[Ca^{2+}]_i$ were monitored by an inverted Olympus microscope with 20x oil immersion objective. Excitation light provided by a Xenon arc lamp was passed sequentially through a monochromator at 340, 380 and 490 nm (Cairn Research); emitted fluorescence was measured at 515 nm (Fura-2) or 565 nm (Rhod-2). The experiments were performed at 37°C. These experiments were performed in collaboration with Dr. Egor Turovsky.

2.1.2.4. PLC activity assay

Cultured naïve astrocytes and astrocytes transduced to express $DREADD_{Gq}$ or CatCh were incubated for 18 h in M199 medium containing 10% dialyzed fetal calf serum (FCS) and 1 μCi/ml of [^{3}H]-inositol (specific activity 18.5 Ci/mmole) (37°C; 5% CO_2, 95% O_2). Immediately before the assay, the incubation medium was replaced with HBSS buffer. Lithium chloride was then added to reach a final concentration of 10 mM, and cultures were incubated at 37°C for an additional 30 min. To activate $DREADD_{Gq}$, clozapine-N-oxide (CNO, 5 μM) was added for 20 min. Reactions were terminated by removal of the medium and the addition of 500 μl of ice-cold methanol. [^{3}H]-inositol phosphate ([^{3}H]-InsP) production was determined by adding the samples to 2 ml Dowex columns pre-washed with a mixture of ammonium formate (2M) and 0.1M formic acid. Double-distilled water

and a mixture of sodium tetraborate (5mM) and sodium formate (60mM) were used to elute unbound [^{3}H]-inositol and glycosylphosphatidylinositol, respectively. Then, a mixture of ammonium formate (1M) and formic acid (0.1M) was added to the column to elute total [3H]-InsP into scintillation vials. 500 µl aliquots of the eluted samples were then transferred in duplicates to liquid scintillation vials. Concentrations of [^{3}H] in [^{3}H]-InsP and total [^{3}H]-inositol lipids were detected using a Beckman LS 5801 scintillation counter (4 min, [^{3}H] DPM program). The results are presented as percentages of radioactive InsP ([^{3}H]-InsP) in the total inositol lipid pool.

2.1.2.5. Measurements of ATP release in acute brainstem slices using microelectrode biosensors

Adult rats were transduced to express $DREADD_{Gq}$ and CatCh by astrocytes of the left and right preBötC regions. After 7 days following microinjections of viral vectors, the animals were humanely killed by isoflurane inhalation overdose, and the brainstem was quickly removed and placed in chilled (4-6°C) artificial cerebrospinal fluid (aCSF; 124 mM NaCl, 3 mM KCl, 2 mM $CaCl_2$, 26 mM $NaHCO_3$, 1.25 mM NaH_2PO_4, 1 mM $MgSO_4$, 10 mM D-glucose saturated with 95% O_2/ 5% CO_2, pH 7.4) with an additional 9 mM Mg^{2+}. The medulla was isolated, and a horizontal 400 µm thick slice was cut parallel to the ventral medullary surface using a vibrating microtome as described in detail previously [101], [144]. Once cut, the slice was stored before use in aCSF saturated with 95% O_2 and 5% CO_2 (pH 7.4) at room temperature. Recordings were made in a flow chamber (3 ml min^{-1}) at ~35°C from the slices placed on an elevated grid to permit access of aCSF from both sides of the slice.

The design and operation of the ATP biosensors (Sarissa Biomedical) are described in detail elsewhere [101], [172]. To control for the release of non-specific electroactive interferents, a dual recording configuration of the ATP biosensor and control (null) biosensor was used, as described [101]. A "null" biosensor (lacking enzymes but otherwise identical) current was subtracted from the current recorded

by the ATP biosensor to give "net-ATP" readings, reporting release of ATP. Sensors were calibrated before and after every recording by application of ATP (10 μM) (**Figure 4.6**) To convert changes in the biosensor current to changes in ATP concentration, an average of sensor calibrations before and after the recording was used. These experiments were performed in collaboration with Dr. Patrick Hosford and Ms. Anna Hadjihambi.

2.1.3. Physiological Experiments

The physiological experiments described in the thesis were conducted using *in vitro* and *in vivo* experimental models from rats as described in this section.

2.1.3.1. In vivo experiments in conscious rats

2.1.3.1.1. In vivo viral gene transfer

Adult male Sprague-Dawley rats (240 – 280 g) were anesthetized with a mixture of ketamine (60 mg kg^{-1}, i.m.) and medetomidine (250 μg kg^{-1}, i.m.) and placed in a stereotaxic frame. The tooth bar was adjusted so that Bregma was positioned 5 mm below Lambda. PreBötC areas were targeted bilaterally by advancing a pipette from the dorsal surface of the medulla oblongata. Viral vectors (see **Table 2.1** for viral titers) were delivered via a single microinjection (0.2 – 0.25 μl) per side using the following coordinates: 0.9 mm rostral, 2 mm lateral, and 2.7 mm ventral from the *calamus scriptorium*. After the microinjections, the wound was sutured and anesthesia was reversed with atipamezole (1 mg kg^{-1}, i.m.). For post-operative analgesia, rats received buprenorphine (0.05 mg^{-1} kg^{-1} d^{-1}, s.c.) for two days. No complications were observed after the surgery, and the animals gained weight normally.

2.1.3.1.2. Ablation of the carotid body chemoreceptors

Rats were anesthetized with a mixture of ketamine (60 mg kg^{-1}, i.m.) and medetomidine (250 µg kg^{-1}, i.m.). Using aseptic technique, an anterior midline neck incision was performed, and the sternohyoid and sternocleidomastoid muscles were retracted. The carotid bifurcation was exposed, the occipital artery was retracted, the carotid sinus nerve and its branches were cut, and the carotid bodies were removed. Sham-operated rats underwent the same surgical procedures to expose the carotid bifurcation, but the carotid sinus nerves and the carotid bodies were left intact. After the surgery, the wound was sutured, and anesthesia was reversed with atipemazole (1 mg kg^{-1}). No mortalities occurred, and animals gained weight normally. Carotid body ablations were performed 10 weeks before the main experiments.

2.1.3.1.3. Assessment of sleep efficiency

Established behavioral criteria [173] were used to calculate sleep efficiency (SE) score before, during, and after the hypoxic challenge with an epoch length of 2 s. Briefly, rats were considered to be awake (W: grooming, eyes open, gross body movement, such as crawling and changing position), in quiet sleep (QS: eyes closed, absence of movement except for periodic sighs and intermittent brief startles or a gross body movement lasting < 2 s during a relatively long period of QS), or in active sleep [AS: eyes closed, frequent twitches of the whiskers, ears, and extremities or very brief (< 2 s) and small movements of the head or limbs]. The state was recorded as indeterminate (IN) when it was difficult to establish the state. After rats had habituated to the plethysmography environment (below) and were asleep for ~30 min, room air supplying the chamber was exchanged with the 10% O_2/90% N_2 gas mixture for 10 min. SE score was then assessed for 10 min after the termination of the hypoxic stimulus. The SE score was calculated according to the following formula: SE = 100 x (QS+AS) / (QS+ AS+W+IN) [71], [174], [175].

2.1.3.1.4. Measurements of respiratory activity by plethysmography

Whole-body plethysmography was used to record respiratory activity in conscious

adult rats [176]–[178]. The rats were placed in a Plexiglas recording chamber (~1 L) that was flushed continuously with humidified air (21% O_2, 79% N_2; temperature 22-24°C), at a rate of 1.2 L min^{-1}. In order to take into the account circadian variations of the physiological parameters, respiratory activity in all the animals was assessed at the same time of the day, between 11.00 – 15.00. The animals were allowed to acclimatize to the chamber environment for ~60 min before baseline respiratory activity was recorded. For the experiments involving hypoxic challenges, the O_2 concentration in the inspired air was reduced to 10% (balanced with N_2) for 10 min. In a separate series of experiments, hypercapnia was induced by stepwise increases in CO_2 concentration in the respiratory gas mixture to 3% and 6% in the hyperoxic environment (~60% O_2, balanced with N_2) to minimize the drive from the peripheral chemoreceptors. Each CO_2 concentration was maintained for 5 min. Concentrations of O_2 and CO_2 in the plethysmography chamber were monitored online using a fast-response O_2/CO_2 analyzer (ML206, AD Instruments,). Data were acquired using Power1401 interface and analyzed off-line using *Spike2* software (Cambridge Electronic Design, CED).

2.1.3.2. Biotelemetry transmitter implantation

Biotelemetry was used to record the systemic arterial blood pressure and heart rate in exercising animals. The rats were anesthetized with ketamine (60 mg kg^{-1} i.m.), and medetomidine (250 μg kg^{-1}, i.m.) and a laparotomy was performed to expose the abdominal aorta. The catheter connected to a telemetry pressure transducer (model TA11PA-C40, Data Science International) was advanced rostrally into the aorta and secured with Vetbond (3M). The transmitter was secured to the abdominal wall, and the incision was closed by successive suturing of the abdominal muscle and skin layers. Anesthesia was reversed with atipamezole (1 mg kg^{-1}; i.m.). Carprofen (5 mg kg^{-1}; s.c.) was given, and the animals were returned to their home cages where they were allowed to recover for at least 7 days. Blood pressure and heart rate were sampled every second and averaged every 30-seconds. The analysis was performed using a custom-made *Spike2* script in accord with previously reported protocols [179], [180].

2.1.3.2.1. Measurements of exercise capacity

Exercise capacity of experimental rats was determined in a forced exercise experimental paradigm using a single lane rodent treadmill (Harvard Apparatus) with an electrical shock grid set to the minimum perceived threshold (0.1 mA). The animals were selected on the basis of their exercise compliance and subjected to daily recruitment/training sessions involving running speeds of 20 – 30 cm s^{-1} over a 5-minute period after 15 min of acclimatization to the treadmill environment. To determine the exercise capacity, treadmill speed was raised from 25 cm s^{-1} in increments of 5 cm s^{-1} every 5 min until the animal's hind limbs made contact with the grid four times within a two-minute period, which is the humanely defined point of exhaustion. The distance covered by the animal was recorded, and exercise capacity was expressed as work done in Joules (kg m^{-2} s^{-2}).

2.1.3.2.2. Data Analysis of the respiratory activity and statistics

The respiratory cycle duration (T_{TOT}) was measured for each respiratory cycle after the animals had habituated to the plethysmography chamber environment for at least 1 hr. The average T_{TOT} was calculated for respiratory cycles recorded continuously over a ~1 hr period, and used to determine the resting respiratory frequency (number of breaths per minute, f_R). Variability of T_{TOT} was determined by calculating the irregularity score (IS) for each respiratory cycle defined as the absolute value of ($T_{TOT}n$ – $T_{TOT}n$-1)/$T_{TOT}n$-1 for the nth respiratory cycle and expressed as a percentage. Tidal volume (V_T, normalized to the body weight) was determined by measuring the pressure changes in the chamber. Poincaré plots of T_{TOT} for the nth cycle versus T_{TOT} for the nth+1 cycle were used to evaluate the temporal dispersion of T_{TOT}. Calculated values of minute ventilation ($V_E = f_R \times V_T$) were averaged and reported in arbitrary units. In addition to quantifying f_R, we also determined the frequency of sighs – augmented breaths that occur on top of normal inspirations *in vivo* [181]. A sigh was defined as a high-amplitude, biphasic augmented inspiratory

breath that started near the peak of a normal inspiration and lasted for a period that exceeded the duration of the previous inspiration [182]. Sigh rate was calculated (and verified manually) offline using *Spike2* software (CED) as the frequency of augmented breaths with V_T that was at least two times larger than the mean V_T and the T_{TOT} that was >50% longer than the average T_{TOT} of the previous 5 respiratory cycles.

Data are reported as box-and-whisker or mean ± SEM and analyzed and plotted with Prism 7.0 software (GraphPad Software Inc). In box and whisker plots, central black dot (or cross) sign illustrates the mean, central line shows the median, the edges of the box define the upper and lower quartile values, and whiskers show the minimum-maximum range of the data. Data were tested for normality using Shapiro-Wilk normality test and compared by Kruskal-Wallis ANOVA by ranks followed by Dunn's post hoc or Student's unpaired *t* test for normally distributed data sets passing the normality test. Mann-Whitney U or Wilcoxon matched-pairs signed-rank test were used as appropriate for comparing data sets that were not normally distributed. Values of $p < 0.05$ were considered to be statistically significant.

Justification of the sample size. One experimental and one control group were compared using the abovementioned statistical tests, whereas the significance was set at 0.05. We expect to detect a significant difference with 5-6 animals per group. If the treatments cause differences between means that are as large as 2.25 SD, it is likely that the difference is due to a physiologically significant difference. If the difference was as small as 1.75 SD, we increased sample sizes per group to 9 or 12. Although, increasing the sample sizes per group to 15 may enable us to detect a difference between means of 1.25 SD, it is doubtful these differences will have a biological significance.

2.1.3.3. In vivo experiments in anesthetized artificially-ventilated rats

2.1.3.3.1. In vivo gene transfer

Male Sprague-Dawley rats (60 – 80 g) were anesthetized with intramuscular injection of a mixture of ketamine (60 mg kg^{-1}) and medetomidine (250 μg kg^{-1}). Animals were placed in a stereotaxic frame (tooth bar −18 mm below the interaural line), and the RTN area received two 24° and 16° angled microinjections per side (~100 nl of each, ~ 50 nl min^{-1}) of the AAV-2/5 hSyn-$DREADD_{Gi}$-mCitrine or control (ChR2-EGFP) viral vectors (**Table 2.1**). The injections were made ±1.7 mm lateral from the midline and −3.7 mm ventral from calamus scriptorius. Anesthesia was reversed with atipamezole (1 mg kg^{-1}). No complications were observed after the surgery, and the animals gained weight normally. 2-3 weeks after the first injection, rats received a second bilateral injection of AVV-sGFAP-EGFP-TeLC or control vectors (AVV-sGFAP-CatCh-EGFP) targeting preBötC at the coordinance provided in the previous section. The animals were allowed to recover for at least 7 days before the experiments. After each surgery, Carprofen (5 mg kg^{-1}; s.c.) was given for post-operative analgesia, and the weight gain by the animal was monitored for 5 days.

2.1.3.3.2. Measurements of central respiratory drive

The rat was anesthetized with urethane (1.3 g kg^{-1}; i.v.) following femoral vein cannulation under isoflurane (3%) induction. The trachea was cannulated, and the animal was ventilated artificially with artificial oxygen−enriched air (~30% O_2, 70% N_2, < 0.04% CO_2). Core temperature was maintained at ~37°C using a heating blanket. The end-tidal level of CO_2 was monitored continuously using fast-response O_2/CO_2 analyzer (AD Instruments, ML206) and blood gasses were measured regularly. The right phrenic nerve (PN) was dissected, and its activity (PNA), as well as abdominal electromyogram (EMGABD), were recorded as indicators of central inspiratory and expiratory drives, respectively. The ventral brainstem surface was exposed as described previously [32], [101], [146]. 20 minutes after recording an initial response to the hypercapnic challenge (5 min, 10-12% CO_2), carotid body nerves were sectioned bilaterally to eliminate inputs from the peripheral chemoreceptors. 20 minutes after the carotid body denervation (CBD), the rat was exposed to another hypercapnic challenge to measure the contribution of carotid

bodies to the hypercapnic ventilatory response. Shortly after blood gasses returned to their normal physiological ranges (PO_2 ~120 mmHg, PCO_2 30 – 40 mmHg, pH at 7.3 – 7.4), clozapine-N-oxide (CNO, $DREADD_{Gi}$ ligand) was applied to inhibit RTN neurons (2 mg kg−1, i.v.), which followed by the 3rd hypercapnic challenge that enables us to investigate the contribution of RTN neurons to the overall hypercapnic ventilatory response (**Figure 5.7**). The hypercapnic augmentation of PNA before (initial) and after each treatment (CBD and application of CNO) was determined as the percent change of the peak of every CO_2-evoked response with respect to the baseline (normocapnic) recording and expressed as percent change in PNA (CO_2-evoked ΔPNA; **Figure 5.7**). PO_2, PCO_2, and pH of the arterial blood were measured before each hypercapnic challenge. The PNA signal was amplified (20,000x), filtered (500-1500 Hz), rectified and smoothed (τ = 50 ms). At the end of the experiments, the animals were humanely killed by an overdose of pentobarbitone sodium (200 mg kg^{-1}, i.v.).

2.1.3.3.3. Quantification of the respiratory parameters and statistics

Respiratory parameters were analyzed off-line. Inspiratory peak times were defined using derivatives of smoothed rectified PNA, from which instantaneous inspiratory frequency was calculated. For the statistical analyses, PNA was determined during normocapnia and at the peak of the CO_2-evoked response before and after carotid body denervation as well as after administration of CNO. The data were digitized (3 kHz sampling rate) and analyzed offline (*Spike2*, CED, Cambridge, UK). Data are reported as mean ± SEM and analyzed and plotted with Prism 7.0 software (GraphPad Software Inc). Data were tested for normality using Shapiro-Wilk normality test and compared by Kruskal-Wallis ANOVA by ranks followed by Dunn's post hoc or Student's unpaired *t* test for normally distributed data sets passing the normality test. Mann-Whitney U or Wilcoxon matched-pairs signed-rank test were used as appropriate for comparing data sets that were not normally distributed. Values of $p < 0.05$ were considered to be statistically significant.

2.1.4. Histology and immunohistochemistry

2.1.4.1. Immunostaining

At the end of the experiments, the rats were given an anesthetic overdose (pentobarbitone sodium, 200 mg kg-1, i.p.), perfused transcardially with 4% paraformaldehyde (PFA) in 0.1 M phosphate buffer (pH 7.4), the brain was removed and post-fixed in the same solution for 4-5 days at 4°C. After cryoprotection in 30% sucrose, serial transverse sections (30-40 μm) of the medulla oblongata were cut using a freezing microtome. Free-floating tissue sections were incubated with chicken anti-GFP (1:250; Aves Labs, Cat. GFP- 1020), rabbit anti-GFAP (1:1000; DAKO, Cat. z-0334), mouse anti-NeuN (1:1000; EMD Millipore, Cat. MAB377), and/or goat anti-ChAT antibody (1:200, EMD Millipore, Cat. AB144P) overnight at 4°C. The sections were subsequently incubated with specific secondary antibodies conjugated to the fluorescent probes (each 1:250; Life Science Technologies) for 1 h at room temperature. Images were obtained using a confocal laser scanning microscope (Zeiss LSM 510). For cell counting, two randomly selected, non-consecutive transverse sections of the medulla oblongata at the level of the preBötC were used for tallying the number of cells expressing the transgene. As a negative control for immunoreactivity, I obtained fluorescent images from slices treated with secondary but not primary antibodies. All images were color/contrast enhanced and adjusted with a thresholding filter in Photoshop (Adobe Photoshop CC 2015.5).

2.1.4.2. Morphometric analysis of brainstem astrocytes

2.1.4.2.1. Tissue processing and immunohistochemistry

Five adult rats (~350 g) were deeply anesthetized with overdose of urethane (3 g/kg^{-1}) and perfused transcardially with ~250 ml phosphate-buffer (PB, 0.1 M) solution and then with 4% paraformaldehyde (PFA) in PB solution. The brains were removed

and post-fixed in 4% PFA for 3-5 days. Brains were then cryoprotected at 4°C in 30% sucrose (in 0.1 M PB solution) over 2-3 days and coronally sectioned at 30-50 µm on a freezing microtome (Leica). Free-floating sections (1 in 4 series) were then incubated in phosphate buffer saline (PBS) containing 10% methanol and 3% H_2O_2 to suppress background fluorescence. Antigen retrieval was performed in 1% citrate buffer warmed to 80°C to unmask the proteins. Tissue sections were then incubated for 1-3 days at 4°C with primary antibodies against GFAP (rabbit anti-GFAP, 1:1000, DAKO, catalog# z-0334; or cy3-conjugated mouse anti-GFAP, 1:1000. MiliporeSigma, catalog# MAB3402C3), choline acetyltransferase (ChAT; to label motoneurons; goat anti-ChAT, 1:200; EMD MilliporeSigma, catalog #AB144P) and/or endothelial cells (mouse anti-RECA1, 1:1000, Abcam, catalog# ab9774). Negative controls, in which the primary antibody was excluded, were performed for all antibodies to determine the level of nonspecific binding. The sections were subsequently incubated with specific secondary antibodies (except for mouse anti-GFAP) conjugated to the fluorescent probes (each 1:250; Lifescience Technologies) for 1.5 h at room temperature. Individual sections were mounted on slides and covered with an anti-fading medium (Fluoro-Gel; Electron Microscopy Sciences). The tiled image of each location was obtained automatically under low magnification (10x). For reconstruction of astrocytes, image stacks of GFAP-positive astrocytes within the preBötC, RTN, nucleus tractus solitarius (NTS), and an intermediate reticular formation (IRf) were obtained using an inverted confocal laser scanning microscope (Zeiss LSM 510) at high magnification (40x objective). In order to minimize differences in the background fluorescence and in the immunostaining of astrocytes in different animals, all the brains were fixed simultaneously using the identical protocol and solutions. Brainstems were sectioned, processed, and developed in the identical immunostaining solution for the same time period.

2.1.4.2.2. Three-dimensional (3D) reconstruction Astrocytes and blood vessels

The image stacks of astrocytes were imported into Neurolucida 360 (MBF

Bioscience), where reconstructions were completed with the software's tracing tools by an investigator blinded to the region of the brain that the images were taken. GFAP-positive astrocytes that exhibited intact morphological processes were randomly chosen for reconstruction (2 – 5 astroglia per animal per region), and astrocytic processes were traced throughout the thickness of the section

Similar to astrocyte reconstruction, the image stacks of blood vessels were imported into Neurolucida 360 (MBF Bioscience) and reconstructed with the software's tracing tools. Blood vessels labeled with RECA1 were traced throughout the thickness of the section by an investigator and verified by a second investigator. Morphometric data was normalized with respect to the total volume containing the reconstructed vasculature. These experiments were done in collaboration with the NIH summer intern students Brian Morris, Sami Znati, Sommer Anjum, and Jared Collina.

2.1.4.2.3. Morphometric Analysis of Reconstructed Astrocytes and Vasculature

Astrocytes. A file containing the 3D tracing information was then imported into the NeuroExplorer software (MBF Bioscience), where the tracing was rendered as a maximum projection (flat) image (**Figure 3.3**). This image was used to collect metrics including total process length, the total number of nodes (branch points), number of primary branches (processes originating from soma), and the total number of terminal points. Sholl analysis was also used since the complexity of astrocytes increases with radial distance from the soma. This analysis utilized regions of interest between concentric circles, centered at the soma, with radii increasing by 5 μm (Sholl 1965) and quantified the number of Nodes (branch points), number of processes, and process length out to a given radius not including the area of any smaller radii (see **Figure 3.3B**). 3D Convex Hull analysis, which calculated the volume enclosed by and surface area of a polygon that joins terminal points of the processes, was used to estimate the volume occupied by the astrocytic process field and surface area of the encased region occupied by an astrocyte (see **Figure 3.3C**). Complexity Index [183] was defined automatically by the

NeuroExplorer software (MBF Bioscience) according to the following equation: (Σ terminal orders + number of terminals) × (total process length/total number of primary branches).

Blood vessels. Similar to astrocyte reconstruction, a file containing the tracing information was then imported into the NeuroExplorer software (**Figure 3.9**). Total volume and surface area of the reconstructed blood vessels was calculated.

2.1.4.2.4. Statistical Analysis for morphometric dataset

The data is reported as mean ± SEM. The data were compared using nonparametric Mann-Whitney U test ranks, one-way ANOVA followed by Tukey's *post hoc* test, or Kruskal-Wallis ANOVA by ranks followed by Dunn's *post hoc* test, as appropriate. Differences with $p < 0.05$ were considered to be significant.

2.1.5. Drugs

Clozapine N-oxide (CNO) was obtained from Tocris Bioscience. Vasopressin was purchased from APP Pharmaceuticals. All other chemicals were obtained from Sigma.

Chapter 3 MORPHOMETRIC ANALYSIS OF ASTROCYTES IN BRAINSTEM RESPIRATORY REGIONS

In the experiments described in this chapter, I have used computer-aided reconstruction to systemically compare the morphology of astrocytes residing within brainstem respiratory regions. These experiments tested *the hypothesis that the morphology of preBötC astrocytes is different from that of astrocytes residing within other brainstem respiratory regions*.

3.1.1. Background

In the rodent hippocampus and cortex, astrocytes residing in the gray matter exhibit high anatomical complexities [184], [185]. A single astrocyte may enwrap thousands of synapses [186]–[188] and a multitude of parenchymal blood vessels [130], putting this cell in a key position to simultaneously modulate synaptic activity as well as regulate local blood flow to match cerebral circulation and levels of neuronal activity. Although the functional significance of these complex astrocytic arrangements has not been definitively established [124], it has been suggested that astrocytic morphology is closely related to their crucial function in regulating brain physiology [184], [189], [190].

Although it has been proposed that astroglia can modulate the activity of CNS neural circuits and affect behavior [153], [191]–[194], evidence for such modulation has only recently emerged [5], [195]. In the rodent brainstem, astrocytes have been shown to play a certain role in the modulation of the respiratory control circuit activity [5], [134], [138], [139], [143], [144], [196]–[198], including the rhythm-generating circuits of the preBötC [12], [14] located within the Ventral Respiratory

Column (VRC) [12]. However, morphological arrangements of astrocytes that may be associated with glial-neuronal interactions in these regions have not been investigated. Considering the critical function of the preBötC for life, we hypothesized that preBötC astrocytes and neurons might have special structural arrangements. Astrocytes provide structural and nutritional support, but also, they are critically important for glutamate re-cycling [glutamate is critical for the generation of the inspiratory rhythm [12]], and release of ATP/adenosine which have powerful effects on the preBötC inspiratory circuit activity [137], [149], [150], [196], [199].

Here, in adult Sprague-Dawley rats, immuno-labeled glial fibrillary acidic protein (GFAP)-positive astrocytes residing within the preBötC region. For comparison, we analyzed morphology of two other areas associated with respiratory function, namely nucleus tractus solitarius (NTS), and an intermediate reticular formation (IRf) region dorso-medial to preBötC in which some of the neurons have been shown to have respiratory activity and a premotor function [15], [200], were morphometrically analyzed.

3.1.2. Material and Methods

Confocal image stacks of the GFAP-positive astrocytes or RECA1 labeled blood vessels within the preBötC, IRf, RTN, and NTS were obtained from 5 different adult rats. The image stacks were imported to Neurolucida 360 (MBF Bioscience), where reconstructions were completed using the software's tracing tools.

Tracing information was then imported into the NeuroExplorer software (MBF Bioscience), and subsequently, the metrics were exported and compared.

3.1.3. Results

GFAP-labeled astrocytes were initially surveyed in several regions of the medulla associated with respiratory function including preBötC, IRf, NTS, and RTN. The anatomical locations of astrocytes were determined using anti-choline

acetyltransferase (ChAT) immunoreactivity to label motor neurons of the nucleus ambiguus (NA), hypoglossal nucleus (XII), and facial nucleus (VII), as illustrated in **Figure 3.1**. PreBötC is located ventral to the semi-compact division of the nucleus ambiguus (NAsc; **Figure 3.1A**). The IRf region [200] was imaged dorso-medial to the NAsc (**Figure 3.1A**), and NTS was imaged dorsolateral to XII, at the same medullary level containing the preBötC (**Figure 3.1**). The location of the RTN region was defined previously [30], [33], and the images were taken ventral to the facial nucleus and rostral to the preBötzinger Complex (BötC; **Figure 3.1**).

3.1.3.1. Morphological arrangements of astrocytes in respiratory-related regions

In ventral regions of the medulla at the level of the preBötC, processes of the parenchymal astrocytes projected deep into the brainstem tissue (**Figure 3.2**). This organization became less apparent moving rostrally, as an extra layer of thin astrocytic processes appeared at the RTN level between the ventral surface pial membrane and the parenchymal tissues. These laminar astrocytes abundantly populate the ventral surface to create a dense network of astrocytic fibers (**Figure 3.2F&G**). Cell bodies of these laminar astrocytes are located close to the pial surface and have numerous long processes parallel to the ventral surface in the medio-lateral

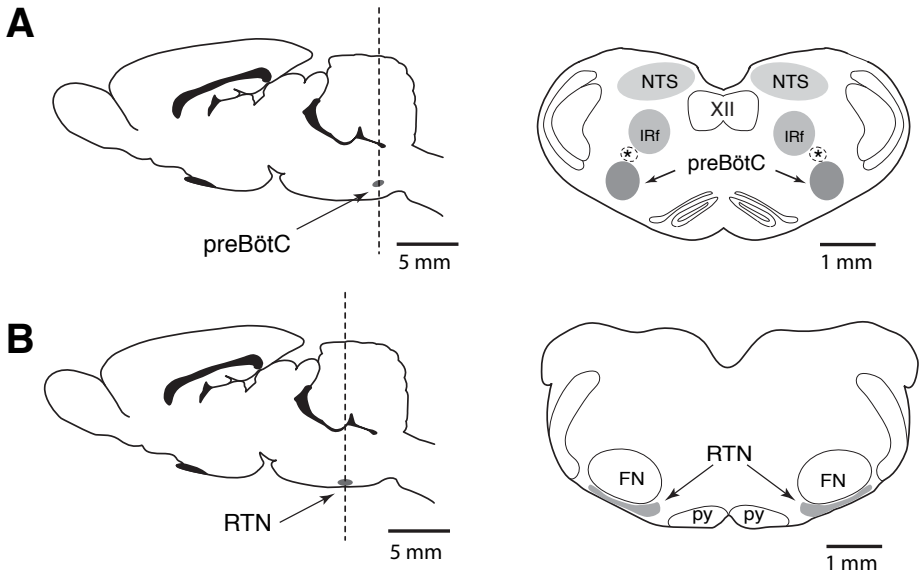

Figure 3.1| Schematic drawings of adult rat brain in sagittal (*left*) and coronal (*right*) projections illustrating the anatomical locations of the preBötC (preBötzinger complex, **A**), an intermediate reticular formation region (IRf), **A**), nucleus tractus solitarius (NTS, A), and retrotrapezoid nucleus (RTN, gray color; **B**). Other abbreviations: *, semi-compact division of nucleus ambiguous (NAsc); XII, hypoglossal nucleus; py, pyramids. FN, facial motor nucleus.

plane. (**Figure 3.2G**). This nexus of dense GFAP-positive fibers was not observed in the other regions surveyed and represents a feature unique to the ventral surface of the medulla at the level of RTN. In the preBötC, IRf, and NTS regions, the astrocytes were less densely arrayed and individual astrocytes, and their proximal processes could be readily distinguished from GFAP immunostaining. We, therefore, selected these regions for more detailed reconstruction of astrocyte morphology. The GFAP staining of the densely intermingled, nexus-like processes of RTN astrocytes did not permit accurate tracing of processes, and these astrocytes were not considered for detailed morphometric analyses.

3.1.3.2. Morphometric features of reconstructed astrocytes

To analyze the morphology of astrocytes, Sholl analysis [201] was applied to the reconstructed astrocytes from preBötC, NTS and IRf regions, by overlaying a

series of concentric circles (in 5 μm steps) outwardly from the center

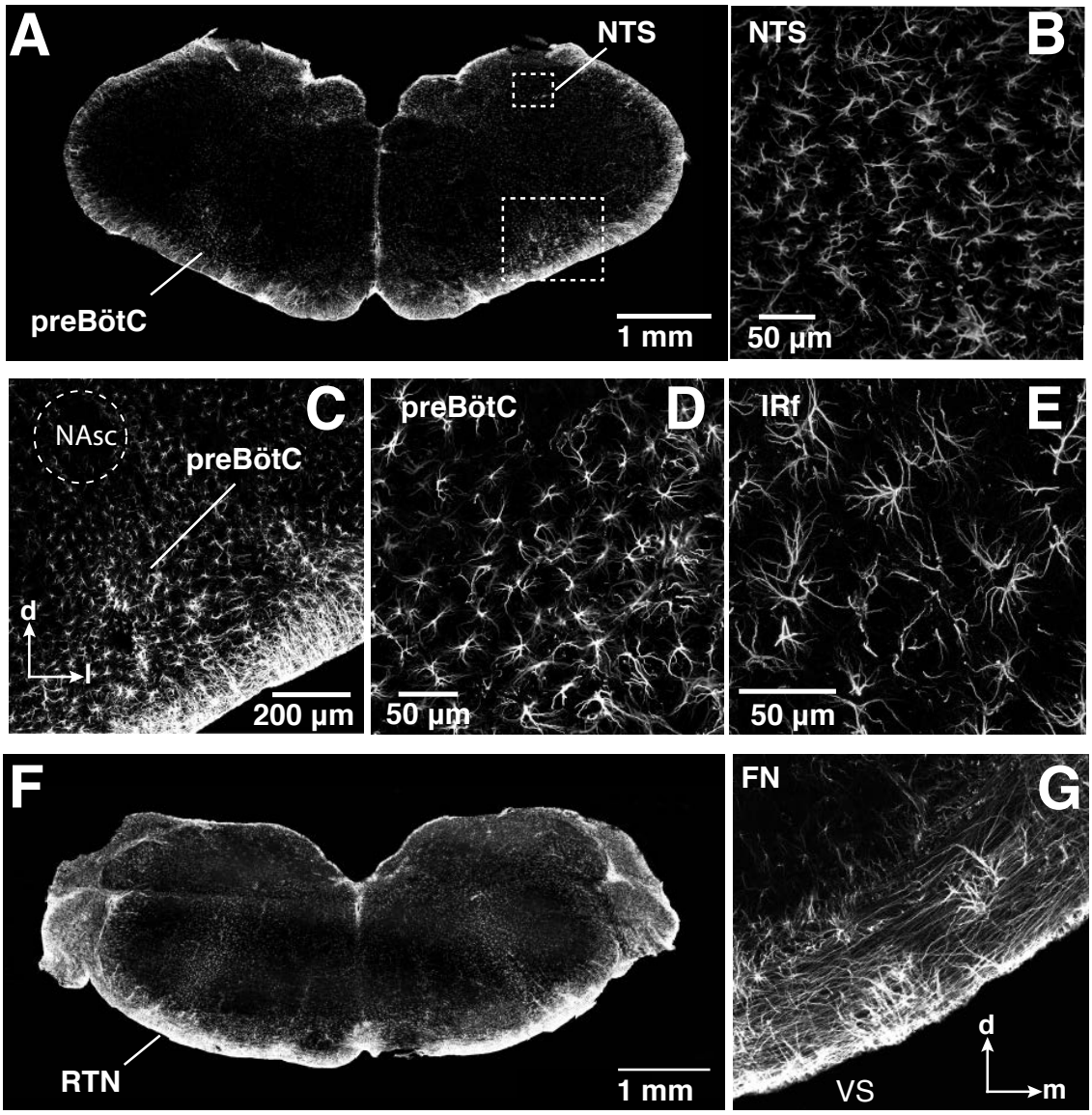

Figure 3.2| Immunostaining of GFAP-positive astrocytes in rat brainstem. A) Tiled low magnification confocal image of GFAP-positive brainstem astrocytes at the level of the preBötC. **B**) High magnification immunostained NTS astrocytes. **C&D**) Low and high magnification confocal images of preBötC astrocytes. **E**) GFAP-positive astrocytes reside within intermediate reticular formation region (IRf). **F**) Tiled low magnification confocal image of GFAP-positive astrocytes at the level of the RTN. **G**) High magnification image of laminar astrocytes making a network of processes at the level of RTN near the ventral brainstem surface. See **Figure 3.1** for details. NAsc, semi-compact division of the nucleus ambiguus; VS, ventral surface of the brainstem; d, dorsal; m, medial; l, lateral; FN, facial nucleus.

of astroglial soma (**Figure 3.3A,B)**. In the preBötC, NTS, and IRf regions, the average number of terminals (**Figure 3.3B**), nodes (branch points), and primary branches, as well as the total length of processes, volume, and surface area of the reconstructed astrocytes were comparatively analyzed. This analysis (**Figure 3.4-Figure 3.7**) revealed that preBötC astrocytes have a higher average number of

terminals (62 ± 5, n = 19) than IRf (41 ± 2, n = 10; p = 0.026) and NTS astrocytes (37 ± 5, n = 10; p = 0.007). Similarly, the average number of nodes was higher in preBötC astrocytes (52 ± 4, n = 19) than in IRf (30 ± 2, n = 10; p = 0.014) or NTS (28 ± 6, n = 10; p = 0.011) astrocytes (**Figure 3.7**). On the other hand, the number of primary branches (**Figure 3.7**) was only different between IRf and NTS astrocytes (8 ± 0.7, n = 10 *vs* 11 ± 1, n = 10; p = 0.014). The total length of all the GFAP-stained processes of preBötC astrocytes (1039 ± 64 µm, n = 19 astrocytes) was significantly larger than that of IRf (691 ± 56 µm, n = 10 astrocytes; p = 0.028) and NTS (454 ± 80 µm, n = 10; p < 0.001) astrocytes (**Figure 3.7**).

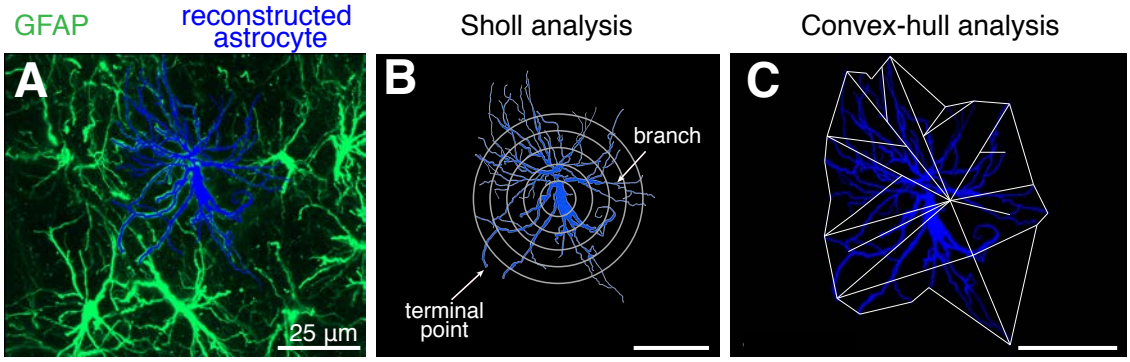

Figure 3.3| Morphometric analysis of brainstem astrocytes. A) Reconstructed astrocyte (blue) identified by GFAP immunoreactivity (green) in the preBötC region. Reconstruction of astrocyte morphology using Neurolucida 360 (MBF) to produce a 2D maximum projection image delineating the appearance of each cell. **B**) Sholl analysis was performed by applying concentric circles with 5 µm increments from the center of the astroglial soma (see Materials and Methods for detail). **C**) The convex-hull analysis was performed to determine the volume and surface area of astrocytes (see Materials and Methods for detail).

The convex hull surface area of the preBötC astrocytes (7727 ± 345 μm^2, n = 19) was significantly larger than that of astrocytes residing in the IRf (5461 ± 609 μm^2, n = 10; p < 0.001) and NTS (2676 ± 340 μm^2, n = 10; p < 0.001) (**Figure 3.7F**). The mean convex hull surface area of the IRf astrocytes was also larger than that of the NTS astrocytes (p < 0.001; **Figure 3.7F**). Convex hull volume (**Figure 3.3**) of preBötC astrocytes (42310 ± 2600 μm^3, n = 19) was found to be significantly larger than that of the IRf (23351 ± 3741 μm^3, n = 10; p < 0.001) and NTS (7220 ± 2056 μm^3, n = 10; p < 0.001) astrocytes (**Figure 3.7E**).

To compare the complexity of astrocytes from these different areas, Complexity Index was determined using the NeuroExplorer software (see Material and Methods). The Complexity Index of preBötC astrocytes (44368 ± 5359, n = 19) was found to be significantly higher than that of IRf (16854 ± 1545, n=10; $p < 0.001$) and NTS astrocytes (4768 ± 1168, n=10; $p < 0.001$; **Figure 3.8**). The IRf astrocytes were more complex when compared to NTS astrocytes ($p < 0.001$; **Figure 3.8**).

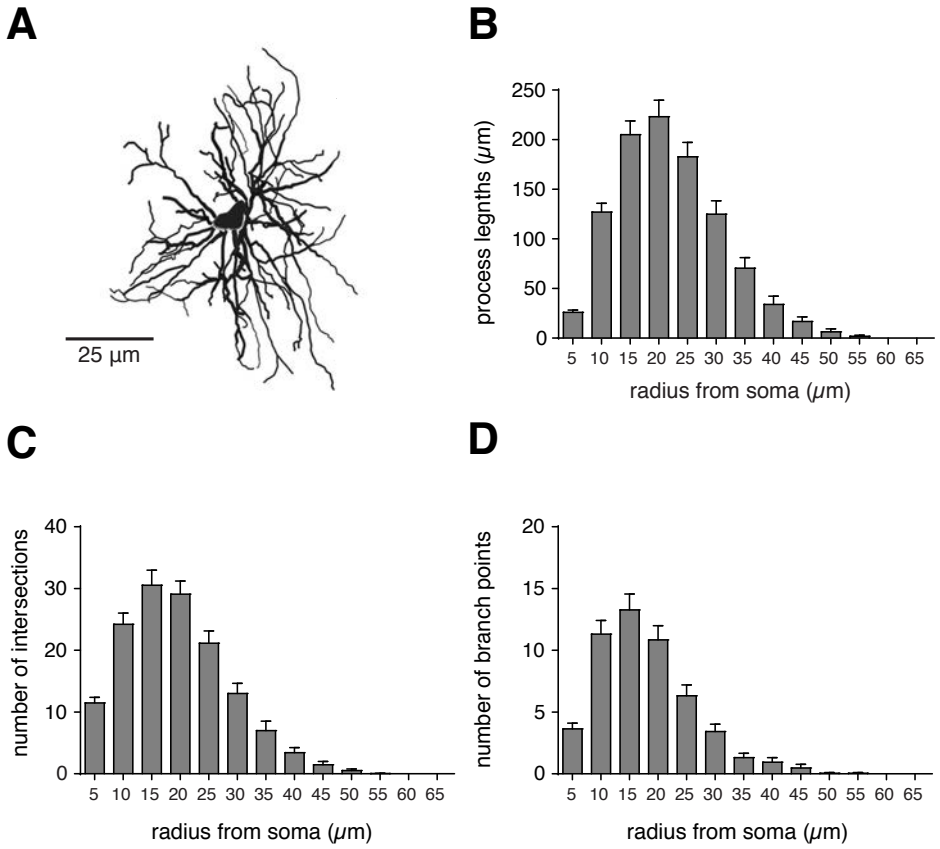

Figure 3.4| Morphometric analyses of preBötC astrocytes. A) Representative reconstruction of preBötC astrocytes. **B-D**) Summary data (see **Figure 3.3**) of process lengths, number of intersections, and number of branch points of preBotC astrocytes (n=19, from 5 different rats) from Sholl analysis. Error bars represent SEM.

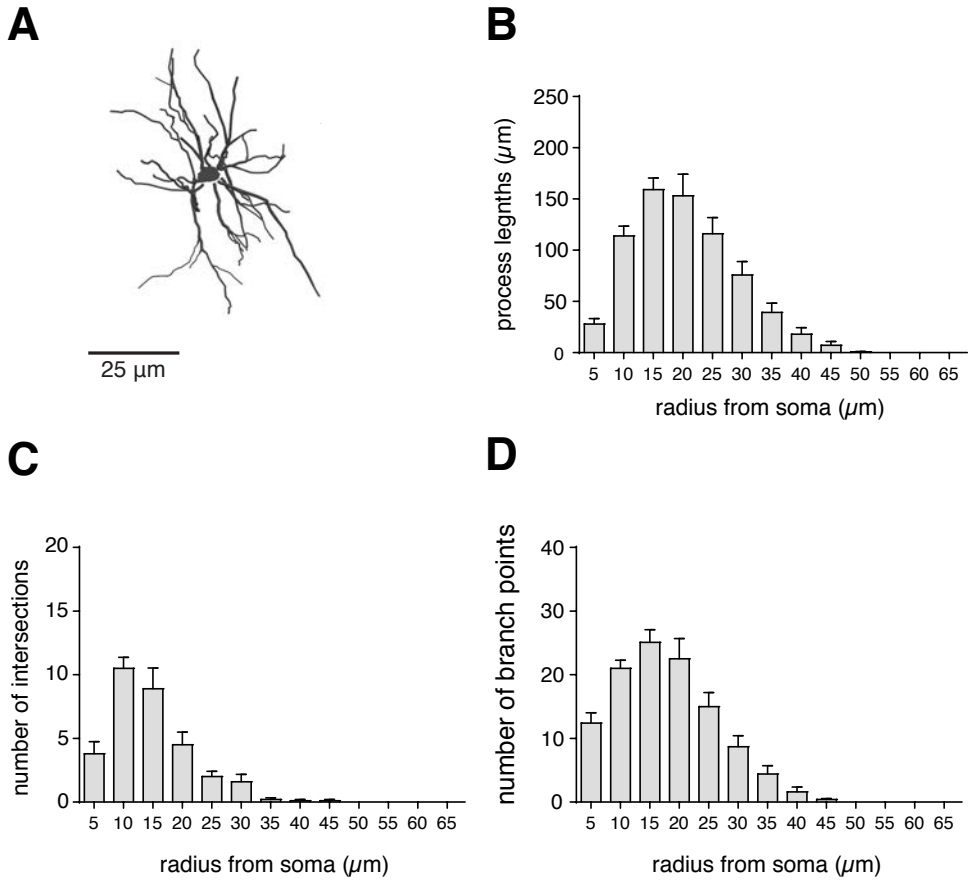

Figure 3.5| Morphometric features of IRf astrocytes. A) Representative morphological reconstruction of astrocyte in the IRf region. B-D) Summary data of Sholl analysis (see **Figure 3.3**) of IRf astrocytes (n = 10, from 5 different rats). Error bars represent SEM.

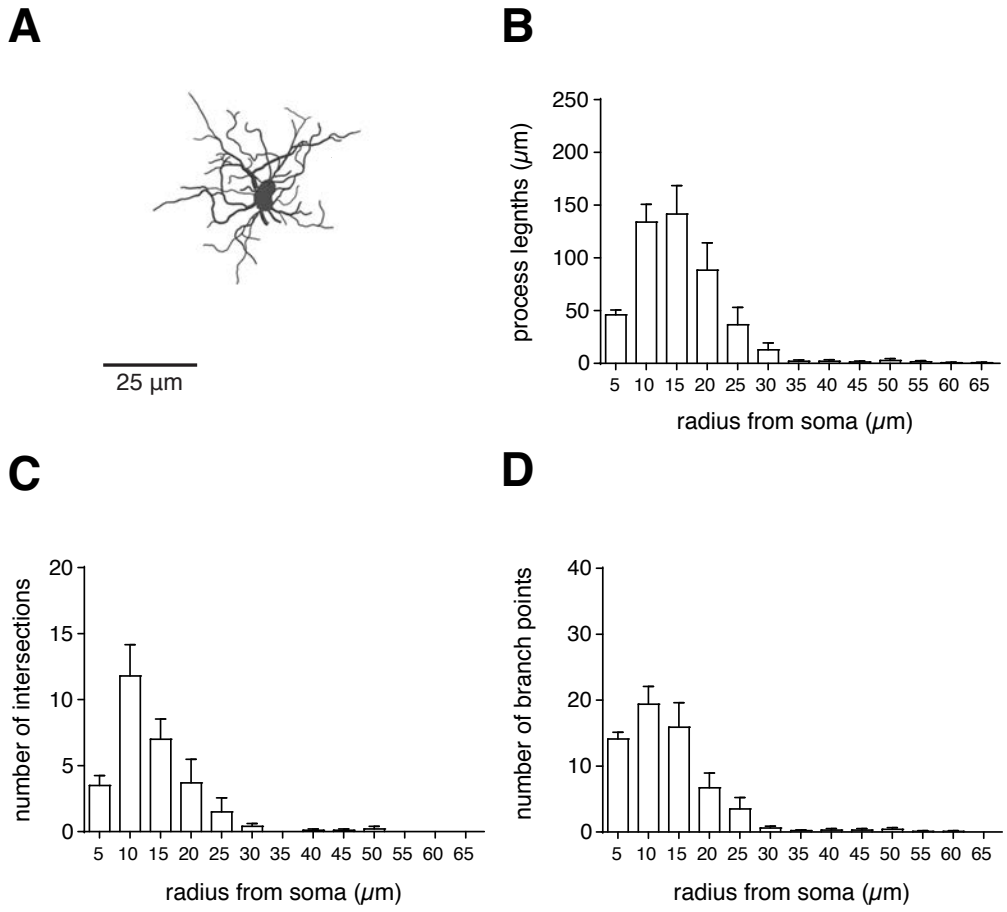

Figure 3.6| Morphometric features of NTS astrocytes. A) Reconstruction of a representative astrocyte in the NTS region. **B-D**) Summary data of Sholl analysis (see **Figure 3.3**) of NTS astrocytes (n = 10, from 5 different rats). Error bars represent SEM.

3.1.3.3. Comparison of regional blood vessel morphology

Brainstem astrocytes, similar to astrocytes residing within other brain regions, make extensive contacts with all parenchymal blood vessels (**Figure 3.9**). Differences in the morphology of astrocytes could be potentially linked to the differences in the morphological arrangements of blood vessels. Therefore, we morphometrically evaluated blood vessels in the preBötC, IRf, and NTS regions. **Figure 3.9** illustrates the 2D arrangement, represented by the maximum projection of a 3D rendered image stack, of blood vessels in the preBötC region. The average volume occupied by parenchymal blood vessels, as computed from 3D reconstructions, was similar in

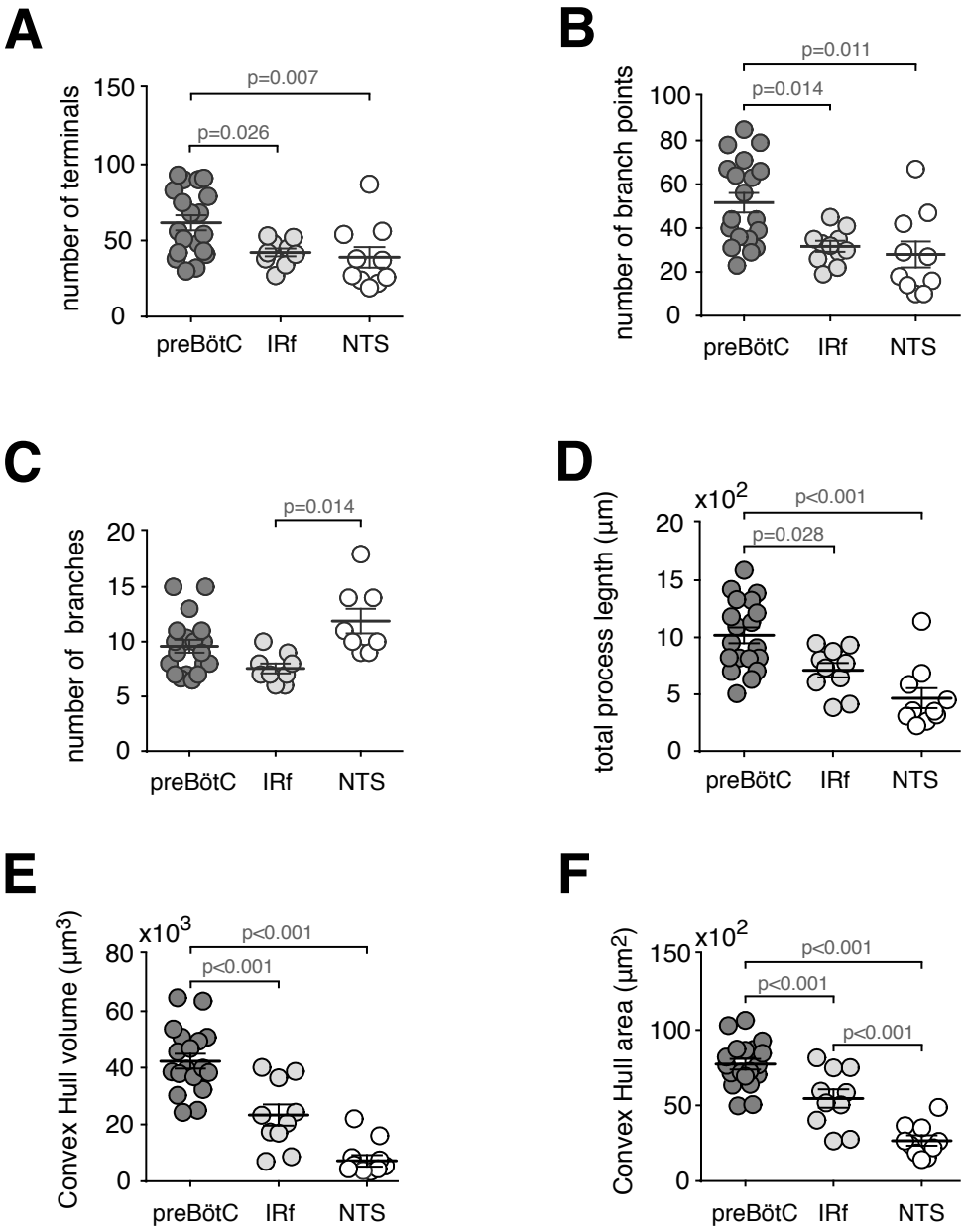

Figure 3.7| Morphometric features of astrocytes in different brainstem regions. A-D) Summary data illustrating the number of terminals (**A**), number of branch points (nodes; **B**), number of branches (**C**), and total process length (**D**) of preBötC (n = 19), IRf (n = 10), and NTS (n = 10) astrocytes. **E-F**) Summary data of the Convex-Hull volume (**E**) and surface area (**F**) of astrocytes in the preBötC, IRf, and the NTS. Overall, preBötC astrocytes have longer processes, more branch points (nodes) and terminals, and greater Convex Hull volume and surface area, compared to IRf and NTS astrocytes. Data sets without *p* values indicated are not significantly different.

the preBötC (8.9 ± 0.3 μm^3, n = 4), NTS (8.1 ± 0.6 μm^3, n = 3) and IRf (8.7 ± 0.1 μm^3, n = 3) regions (p = 0.64; **Figure 3.9E**). Similarly, the average surface area of parenchymal blood vessels in the preBötC (1.96 ± 0.02 μm^2, n = 4), NTS (1.80 ± 0.08 μm^2, n = 3) and IRf (1.92 ± 0.03 μm^2, n = 3) regions were not different from each other (p = 0.36; **Figure 3.9E**).

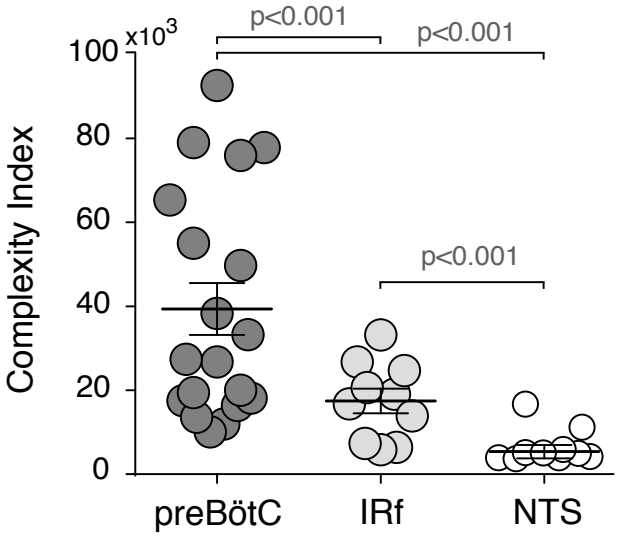

Figure 3.8| Complexity metrics of preBötC, IRf, and NTS astrocytes. Summary data comparing the measure of structural complexity of astrocytes obtained from the complexity index formula (see Material and Methods section) applied to reconstructed astrocytes from preBötC, IRf, and NTS regions. When compared to astrocytes from the other brainstem regions, preBötC astrocytes exhibit a significantly higher complexity index. Data sets without *p* values indicated are not significantly different.

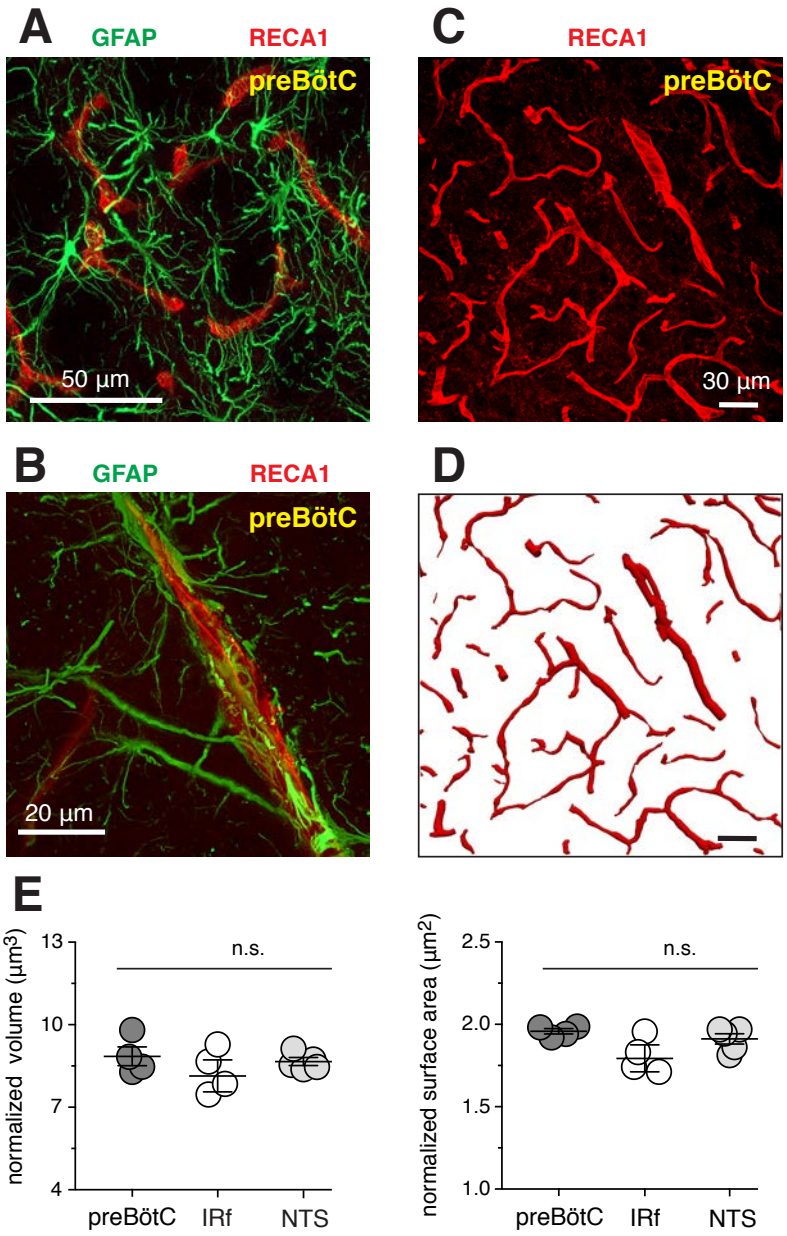

Figure 3.9| Arrangement of blood vessels in the preBötC. A&B) PreBötC astrocytes (GFAP-immunoreactivity, green) are intermingled with the parenchymal blood vessels (immune-stained with RECA1, red). **C**) Representative confocal image (merged Z-stack) of parenchymal blood vessels immuno-labeled with RECA1 in the preBötC region. **D**) Maximum projection image of 3D reconstructed blood vessels from region shown in **C**. **E**) Summary data illustrating normalized volume (*left*) and normalized surface area (*right*) of the reconstructed parenchymal blood vessels in preBötC (n = 4; from 4 different rats), IRf (n = 4; from 4 different rats), and NTS (n = 5; from 5 different rats). n.s., not significant.

3.1.4. Summary and Conclusions

Astrocytes play an important role in modulating the activities of respiratory networks, however, the morphology of brainstem astroglia was not previously

characterized. Here, in adult rats, using computer-aided reconstruction techniques, the morphology of astrocytes residing within the respiratory-related preBötC, IRf, and NTS regions has been defined and quantitatively compared. The data obtained from morphometric analyses indicate that preBötC astrocytes, inherently, have more complex morphology compared to astrocytes from within the functionally distinct neighboring brainstem region of IRf or the more distant NTS region.

Therefore, in this Chapter the following aim was addressed:

Aim 1. study the anatomical features of brainstem astrocytes and to determine whether preBötC astrocytes are morphologically different from astrocytes residing in other regions of the brainstem.

While this aim was achieved, the underlying structural/functional reasons for these regional morphological differences is presently unknown, but may reflect constraints imposed by arrangements of associated neurovascular elements and/or other local structural features of brainstem parenchyma.

Chapter 4 INVESTIGATING THE EFFECT OF ACTIVATION AND BLOCKADE OF SIGNALING PATHWAYS IN PREBÖTC ASTROCYTES ON BREATHING IN CONSCIOUS BEHAVING RATS.

4.1.1. Introduction

Astrocytes have been proposed to modulate neuronal excitability, synaptic transmission, and plasticity [1], [2]. The physiology of these electrically non-excitable cells of the brain is governed by intracellular Ca^{2+}, with increases in $[Ca^{2+}]_i$ triggering release of signaling molecules or 'gliotransmitters' (such as ATP/adenosine and D-serine). Recent studies have suggested that gliotransmitters may influence neural circuits, particularly neuromodulatory circuits affecting sleep, feeding, and chemosensing [3]–[5], yet it remains unknown whether astrocytes can regulate motor circuits and have an impact on complex behaviors *in vivo*. Experiments with rodent brainstem slices ([138], [202]) have suggested that astroglial mechanisms may play a certain role in regulating the activities of neuronal circuits producing motor rhythms, including those within the preBötC [14] in the ventrolateral medulla that generate the rhythm of breathing [203]. However, whether such modulation is functionally important for rhythmic motor behavior has not been determined.

Experiments described in this and the following Chapter focused on the astrocytes of the preBötC to test the hypothesis that they are capable of modulating local respiratory control circuit. Viral vectors were used to activate or block preBötC

astroglial signaling mechanism. This chapter first describes the detailed validation of the efficacy of the viral vectors used in this thesis, and then the effect of activation and blockade of astroglial signaling pathways (by using these viral vectors) in the preBötC on breathing behavior in conscious rats.

4.1.2. Material and Methods

In this section, in freely behaving adult rats, signaling pathways in preBötC astrocytes were activated (via viral expression of $DREADD_{Gq}$) or blocked (by viral expression of dnSNARE, TeLC, or TMAPA) and role of preBötC astrocytes in modulation of breathing was assessed when animals were challenged by hypoxia.

4.1.2.1. In vitro methods to validate viral vectors.

Total internal reflection fluorescence (TIRF) microscopy, Ca^{2+} imaging, PLC activity assay, and ATP biosensors assay were used to validate viral vectors.

4.1.2.2. Viral gene transfer and physiology experiments

Young adult male rats (250–280 g) were anesthetized and brainstem respiratory networks, including the rhythm-generating circuits of the preBötC were targeted bilaterally with microinjections of the viral vectors [LVV–Ef1α–TMPAP–EGFP, LVV–EF1–EGFP (control), AVV–sGFAP–EGFP–TeLC, AVV–sGFAP–dnSNARE–EGFP, AVV–sGFAP–$DREADD_{Gq}$–EGFP, or AVV–sGFAP–CatCh–EGFP (control)]. 5-7 days after the surgery, whole-body plethysmography was used to record respiratory activity in conscious adult rats

4.1.3. Results

4.1.3.1. Validation of dnSNARE efficacy in blocking astroglial vesicular

release mechanisms

Astrocyte-specific expression of dnSNARE was controlled by an enhanced GFAP promoter (**Figure 4.1**). To determine the efficacy of the novel dnSNARE construct, TIRF microscopy was used to monitor vesicular fusion events in cultured brainstem astrocytes transduced to express dnSNARE or a control transgene (CatCh–EGFP). In dnSNARE-expressing astrocytes, the number of juxta-membrane vesicles labeled with quinacrine (putative ATP-containing vesicles) was reduced by 67% ($p<0.001$).

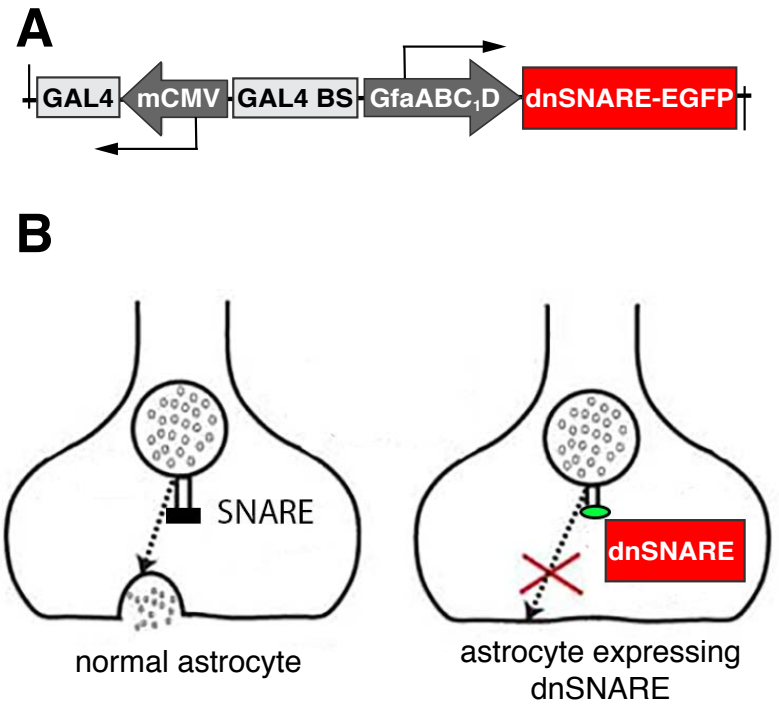

Figure 4.1| Adenoviral vector (AVV) to express dominant-negative SNARE (dnSNARE) in astrocytes. A. Schematic of AVV–sGFAP–dnSNARE–EGFP vector. B. Expression of dnSNARE in astrocytes prevents vesicular docking and release.

Previously, it has been shown that cultured astrocytes respond to application of the Ca^{2+} ionophore ionomycin or lowering PO_2 (achieved by application of the O_2 scavenger sodium dithionite) with an increased rate of exocytosis of ATP-containing vesicles [71]. Facilitated vesicular fusion induced by ionomycin or sodium dithionite, was effectively abolished in astrocytes expressing dnSNARE (**Figure 4.2**).

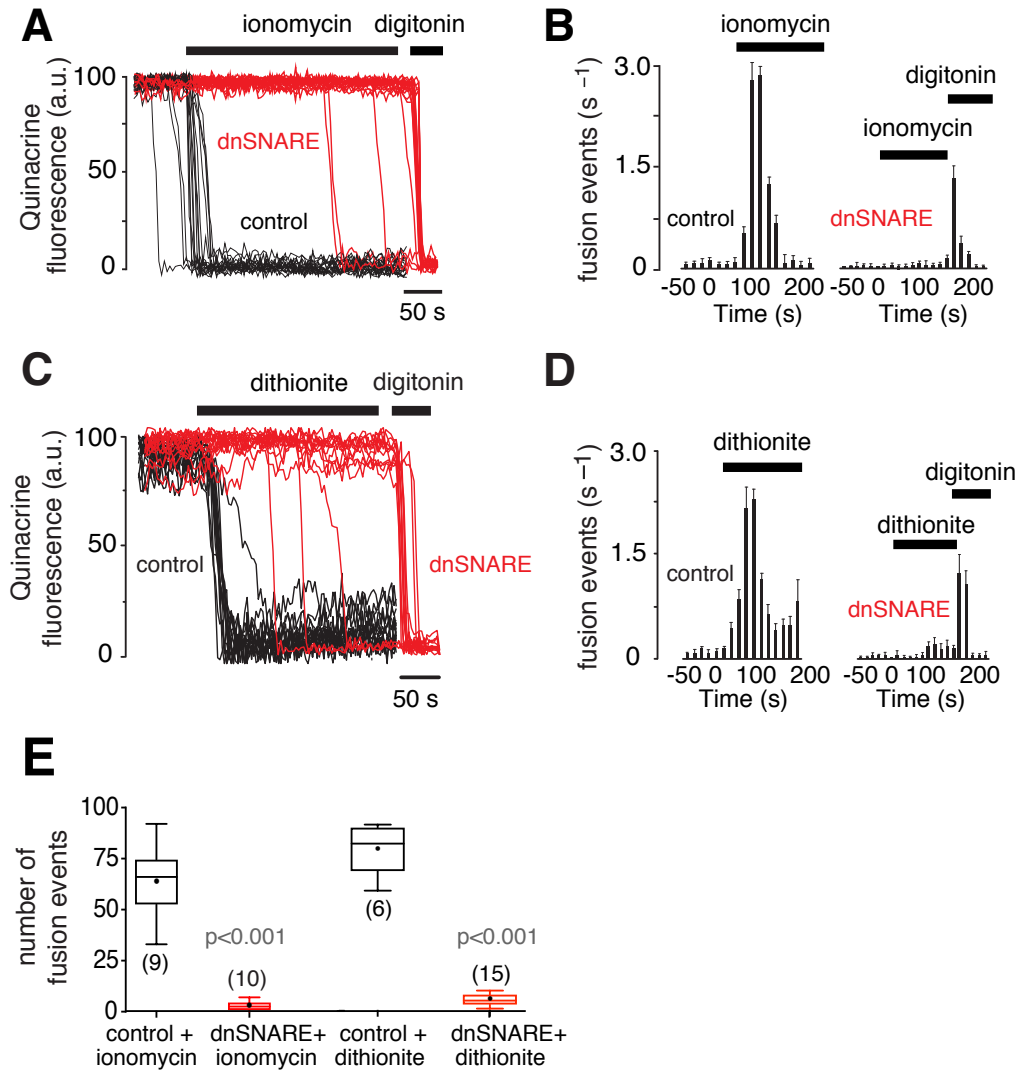

Figure 4.2| Validation of dnSNARE efficacy in blocking astroglial vesicular release mechanisms. A) Plots of TIRF intensity changes showing loss of quinacrine fluorescence from a proportion of labeled organelles in response to application of the Ca^{2+} ionophore ionomycin (1 μM) in two individual cultured astrocytes transduced to express control transgene (black traces) or dnSNARE (red traces). In cultures of astrocytes expressing dnSNARE, digitonin was applied at the end of the recording to permeabilize the membranes, resulting in a rapid loss of quinacrine fluorescence. **B**) Averaged temporal profile of ionomycin-induced vesicular fusion events detected in cultured astrocytes expressing control transgene or dnSNARE. **C**) Plots of TIRF intensity changes showing loss of quinacrine fluorescence from a proportion of labeled organelles in response to application of sodium dithionite in two individual cultured astrocytes transduced to express control transgene (black traces) or dnSNARE (red traces). In cultures of astrocytes expressing dnSNARE, digitonin was applied at the end of the recording to permeabilize the membranes, resulting in a rapid loss of quinacrine fluorescence. **D**) Averaged temporal profile of dithionite-induced vesicular fusion events detected in quinacrine-loaded cultured astrocytes expressing control transgene or dnSNARE. **E**) Total number of ionomycin- and sodium dithionite-induced vesicular fusion events detected in cultured astrocytes expressing control transgene or dnSNARE. Numbers of individual tests are indicated.

4.1.3.2. Validation of DREADD$_{Gq}$ efficacy in activating astrocytic signaling mechanisms

Release of ATP by brainstem astrocytes may occur following activation of phospholipase C (PLC) [71]. To facilitate the PLC-mediated release of gliotransmitters, we transduced preBötC astrocytes to express DREADD$_{Gq}$; **Table 2.1**) [169] (**Figure 4.3**). As expected, the DREADD designer ligand clozapine-N-oxide (CNO) triggered robust increases in $[Ca^{2+}]_i$ in brainstem astrocytes expressing DREADD$_{Gq}$ *in vitro* (**Figure 4.3**). These responses were blocked by the PLC inhibitor U73122 (**Figure 4.3**).

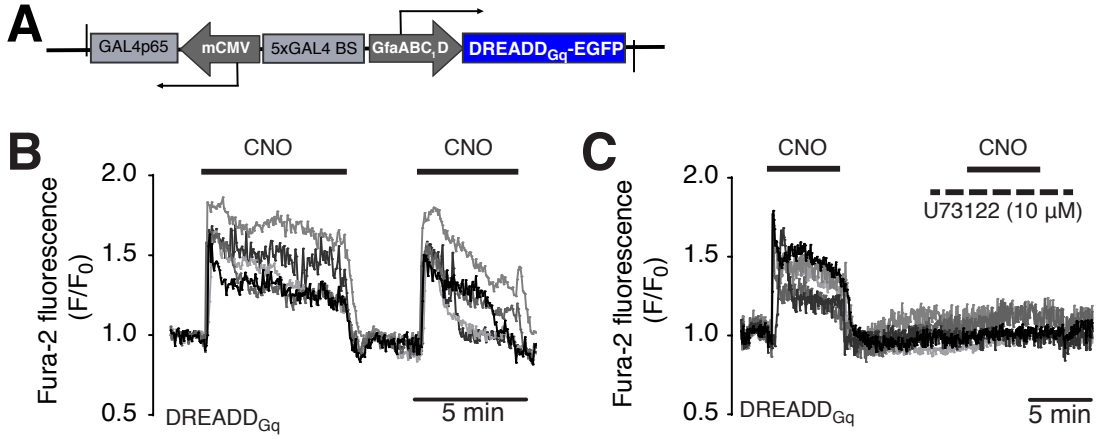

Figure 4.3| Validation of DREADD$_{Gq}$ efficacy in activating astrocytic signaling mechanisms. **A**) Schematic of AVV-sGFAP-DREADD$_{Gq}$-EGFP vector layout. **B**) Validation of AVV-sGFAP-DREADD$_{Gq}$-EGFP *in vitro*. CNO-induced $[Ca^{2+}]_i$ responses in cultured astrocytes transduced to express DREADD$_{Gq}$. **C**) The effect of CNO is blocked by the phospholipase C (PLC) inhibitor U73122.

When PLC activity was measured, it was revealed that cultured astrocytes expressing DREADD$_{Gq}$ had higher resting (i.e., in the absence of CNO) levels of inositol phosphates (**Figure 4.4**). This higher resting PLC activity in DREADD$_{Gq}$ expressing astrocytes indicated a potential constitutive activity of this receptor. Indeed, DREADD$_{Gq}$ expression was also found to be associated with higher rate of spontaneous fusion of quinacrine-labeled vesicles in cultured astrocytes (**Figure 4.5**).

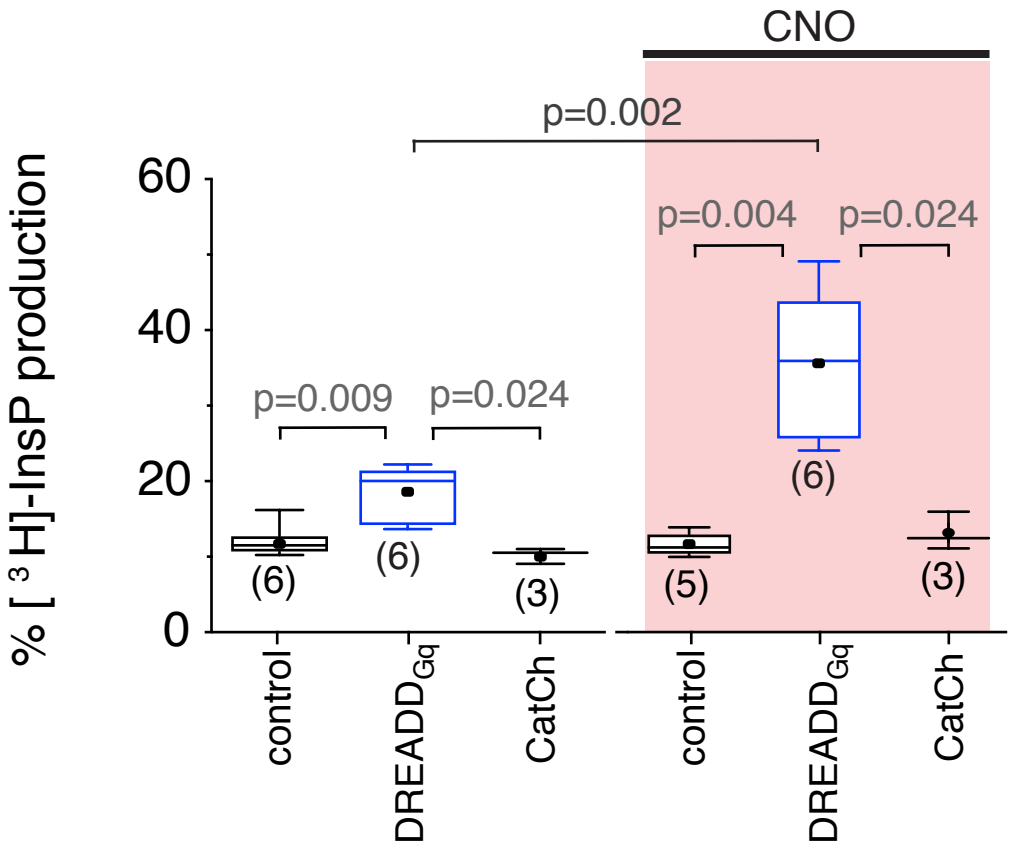

Figure 4.4| Astrocytes expressing DREADD$_{Gq}$ showed higher resting PLC activity. Summary data illustrating PLC activity in cultured brainstem astrocytes expressing DREADD$_{Gq}$ and the effects of CNO on PLC activity as assessed by measuring [^{3}H]-inositol phosphate (InsP) production relative to the total inositol lipid pool in naïve astrocytes (control) and in astrocytes transduced to express CatCh or DREADD$_{Gq}$. Higher resting InsP level in brainstem astrocytes expressing DREADD$_{Gq}$ indicate constitutive activity of the receptor.

Next, ATP tone in acute brainstem slices (from adult rats virally transduced to express DREADD$_{Gq}$ in preBötC astrocytes) was measured using microelectrode biosensors. Both sensors (null and ATP sensor) were initially placed in the recording chamber having no contact with the brainstem slice. Once a steady-state baseline was achieved, the sensors were laid flat bilaterally (ATP sensor was placed randomly on either left or right side of the slice) in direct contact with the ventral surface of the slice in equivalent positions overlaying the preBötC. The sensors were left in place to achieve stable recordings of the ATP tone and then carefully lifted from the surface of the slice to allow measurement of tonic ATP release (**Figure 4.6**). Without removing the sensors from the recording chamber, their positions on the left (expressing DREADD$_{Gq}$) and right (expressing CatCh) sides of the

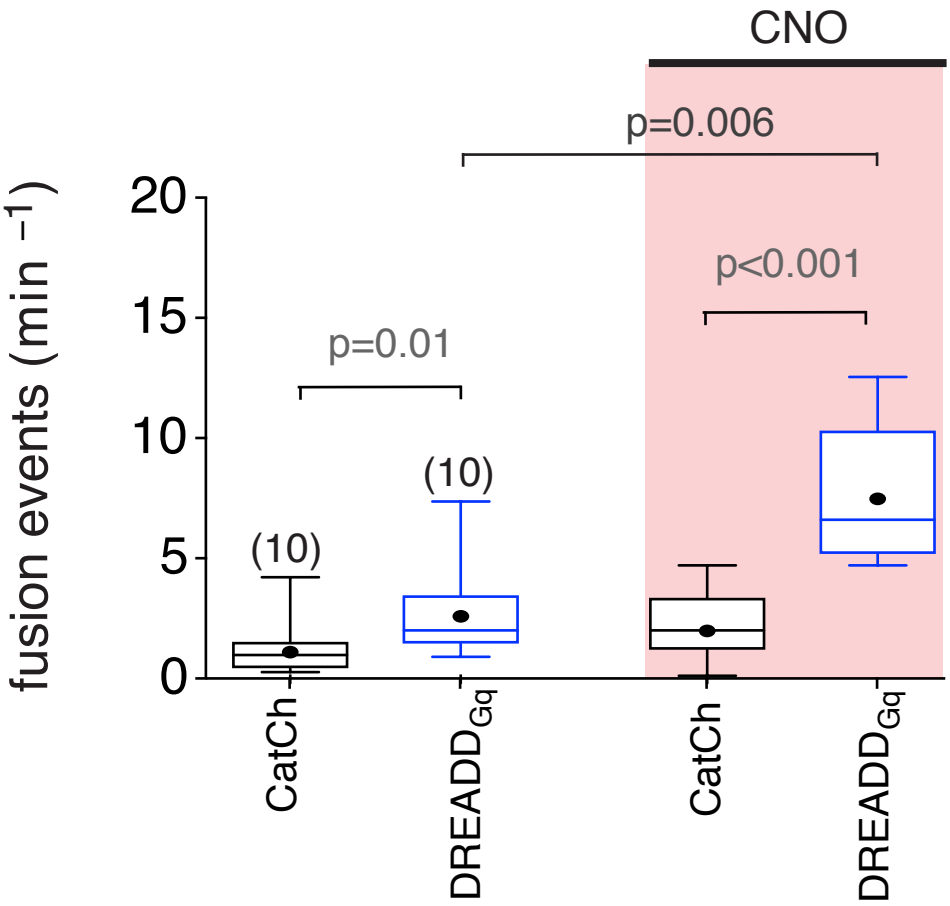

Figure 4.5| Astrocytes expressing DREADD$_{Gq}$ showed higher rate of spontaneous fusion. Summary data illustrating the rate of spontaneous and CNO-induced fusion of quinacrine-labeled vesicles in astrocytes transduced to express CatCh (n=10) or DREADD$_{Gq}$ (n=10). DREADD$_{Gq}$ expression in astrocytes is associated with a significantly higher rate of spontaneous vesicular fusion events. Numbers of individual tests from three different cultures are indicated.

brainstem slice was swapped to determine tonic ATP release from the opposite site (**Figure 4.6**). It was found that DREADD$_{Gq}$ expression was associated with facilitated release of ATP in conditions when preBötC astrocytes were transduced to express the transgene (in acute brainstem slices, **Figure 4.6**). All these data suggested that in the absence of an agonist, DREADD$_{Gq}$ is constitutively active at the level of expression provided by the viral vector used. We exploited this property of DREADD$_{Gq}$ in order to determine whether sustained PLC-mediated activation of preBötC astrocytes associated with facilitated vesicular release of ATP has an impact on the inspiratory rhythm-generating circuits in conscious rats.

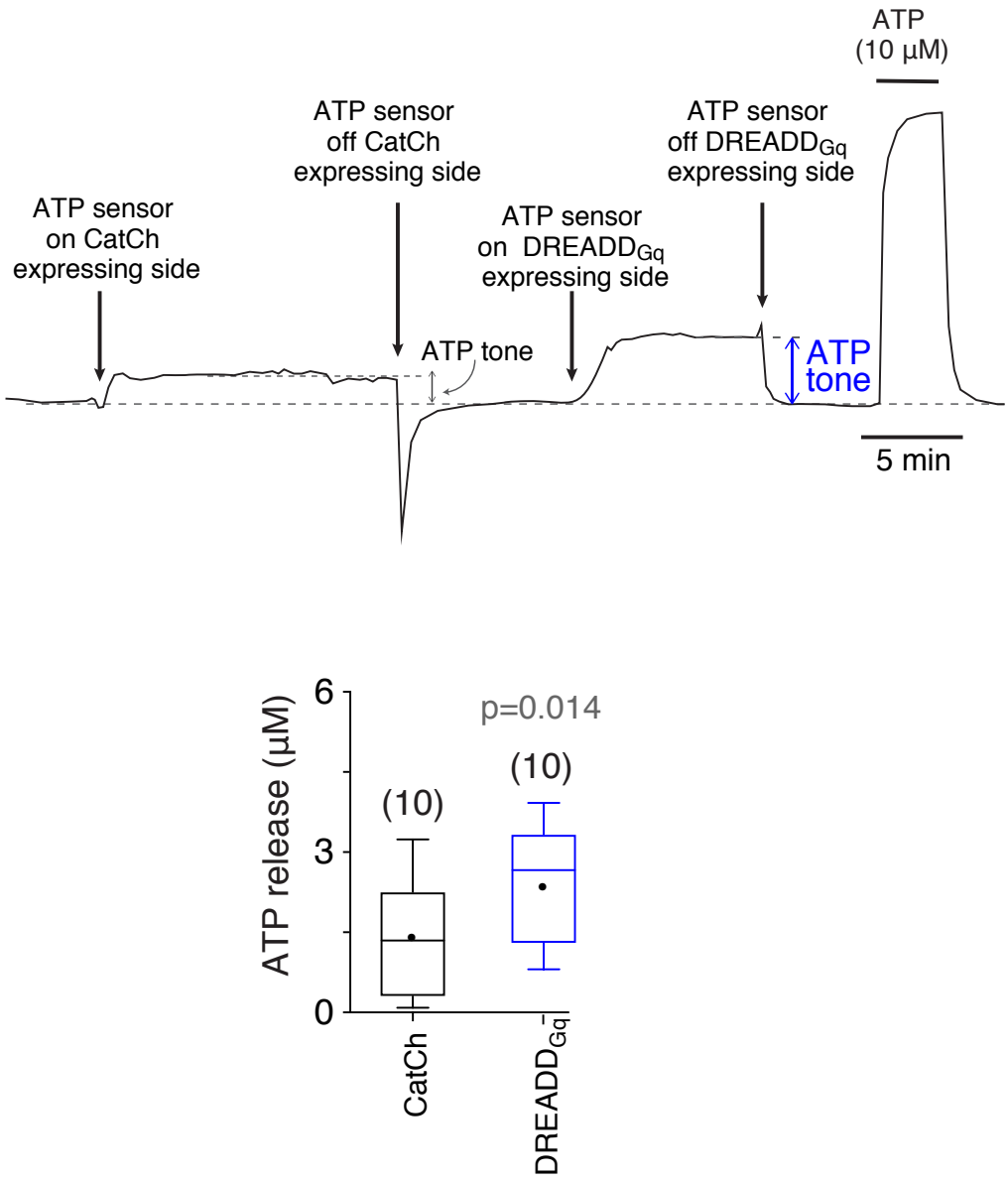

Figure 4.6| Astrocytes expressing DREADD$_{Gq}$ showed tonic release of ATP. A representative example of changes in ATP biosensor current after biosensor placement on the surface of the brainstem slice transduced to express CatCh and DREADD$_{Gq}$ in astrocytes residing in opposite preBötC areas (top). Summary data illustrating facilitated the tonic release of ATP in acute brainstem slices of adult rats transduced to express DREADD$_{Gq}$ by the preBötC astrocytes (bottom).

4.1.3.3. Activity of the respiratory rhythm-generating circuits of the preBötC is modulated by astrocytes

In conscious rats, bilateral expression of dnSNARE or TeLC in preBötC astrocytes (**Figure 4.7** – **Figure 4.8**) resulted in a significant reduction in resting breathing frequency (f_R) by 11% (94 ± 2 min^{-1} *vs* 106 ± 5 min^{-1} in controls; n=5, p=0.016) and

by 11% (92 ± 2 min^{-1} *vs* 103 ± 3 min^{-1} in controls; n = 12, p = 0.011), respectively (**Figure 4.9**). dnSNARE or TeLC expression also significantly decreased the variability of the respiratory rhythm (**Figure 4.10**).

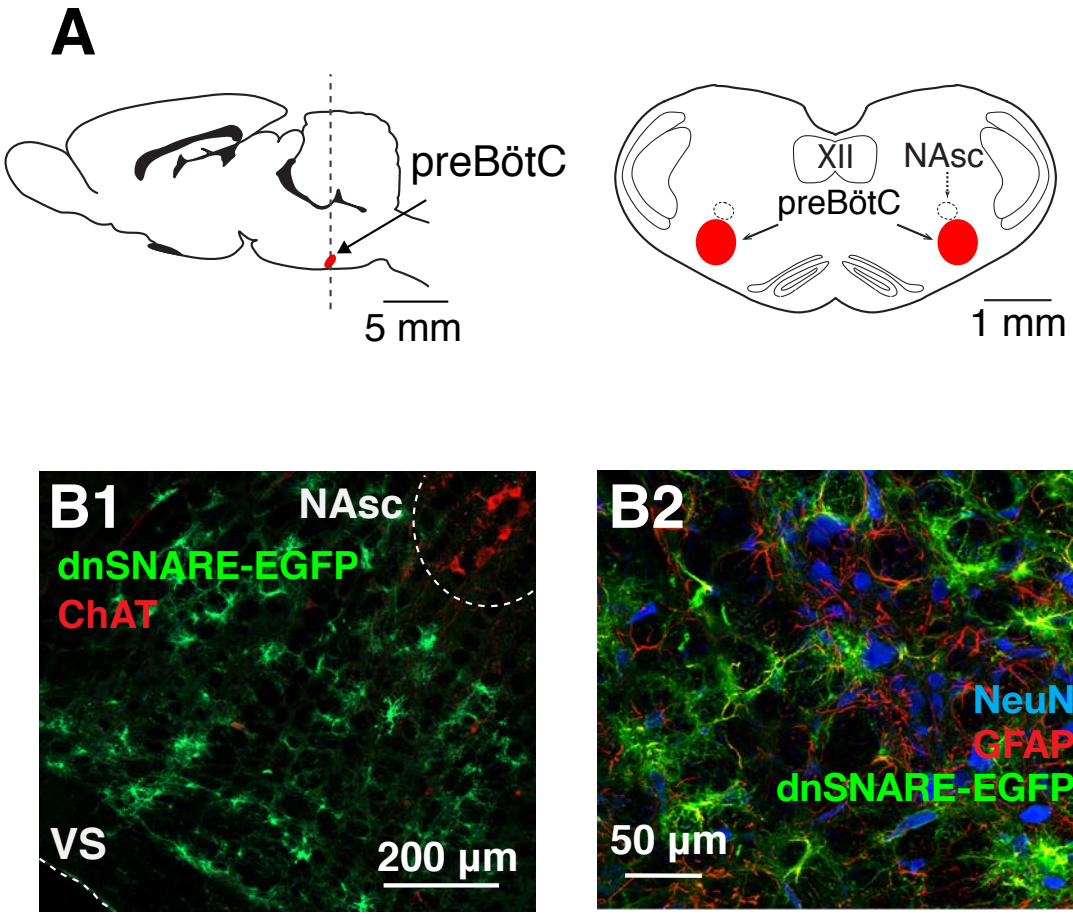

Figure 4.7| PreBötC astrocytes virally transduced to expressed dnSNARE. **A**) Schematic drawings of the rat brain in parasagittal and coronal projections illustrating the location of the preBötC. NAsc, semi-compact division of the nucleus ambiguus; XII, hypoglossal motor nucleus. **B1&B2)** Representative confocal image of dnSNARE-EGFP expression in preBötC astrocytes is shown on the left. High magnification image (right) shows expression of dnSNARE-EGFP in GFAP-positive preBötC astrocytes. NAsc neurons are identified by choline acetyltransferase (ChAT) immunoreactivity (left).

Since dnSNARE or TeLC expression in astrocytes is likely to block exocytosis of several putative gliotransmitters, the specific contribution of ATP was determined by blocking ATP-mediated signaling within the preBötC by virally-driven expression of TMPAP. It is found that bilateral expression of TMPAP in the preBötC (**Figure 4.11**) reduced resting f_R by ~11% (98 ± 3 min^{-1} *vs* 111 ±4 min^{-1} in controls, n = 7, p = 0.017; **Figure 4.11D**). Bilateral expression of DREADD$_{Gq}$ in preBötC astrocytes (**Figure 4.12**) was associated with 27% higher f_R (123 ± 5 min^{-}

^{1} *vs* 97 ± 1 min^{-1} in controls; n = 8, p < 0.001; **Figure 4.12**), and increased variability of the inspiratory rhythm (**Figure 4.10**).

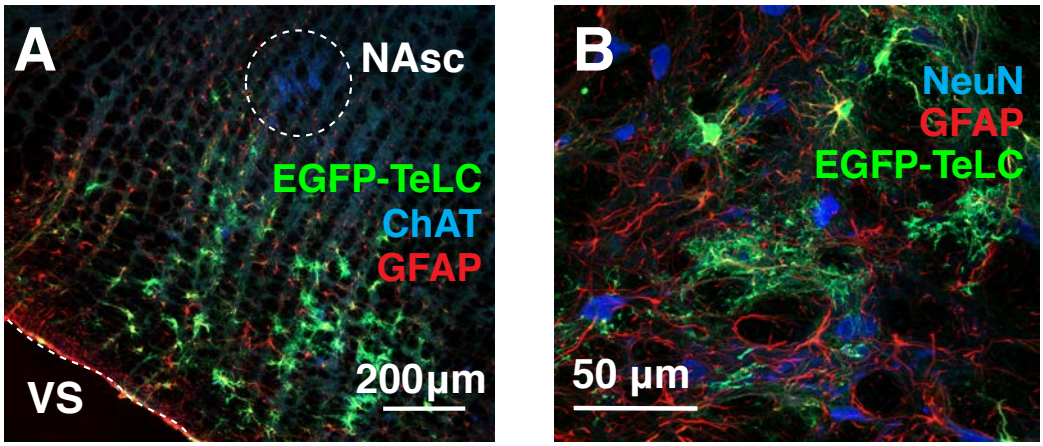

Figure 4.8| Viral targeting of preBötC astrocytes to express TeLC. A) Confocal fluorescence microscopy image illustrating EGFP-TeLC expression in a subset of preBötC astrocytes located ventral to the semi-compact division of the nucleus ambiguus (NAsc) identified by ChAT immunoreactivity. **B)** Representative higher magnification image of preBötC astrocytes targeted to express EGFP-TeLC.

4.1.3.4. PreBötC astrocytes modulate the generation of the inspiratory sighs

No significant variations across all the control groups (rats expressing control transgenes in the preBötC astrocytes) were observed when frequency of the respiratory sighs was analyzed. Therefore, the sigh frequency data obtained in representative 8 control animals transduced to express CatCh-EGFP and 7 control animals transduced to express EGFP were combined and used for the analysis. The frequency of sighs, augmented breaths generated periodically by the preBötC circuits (Li et al., 2016; Lieske et al., 2000) (**Figure 4.14**), was reduced by 27% (p < 0.001) in rats expressing dnSNARE and by 25% (p<0.001) in rats expressing TeLC in the preBötC (**Figure 4.15**). Similarly, bilateral expression of TMPAP in preBötC decreased sigh frequency by 26% (p<0.001; **Figure 4.15**). However, bilateral expression of DREADD$_{Gq}$ in preBötC astrocytes was associated with increased frequency of sighs (by 31%, n = 8, p<0.001; **Figure 4.15**).

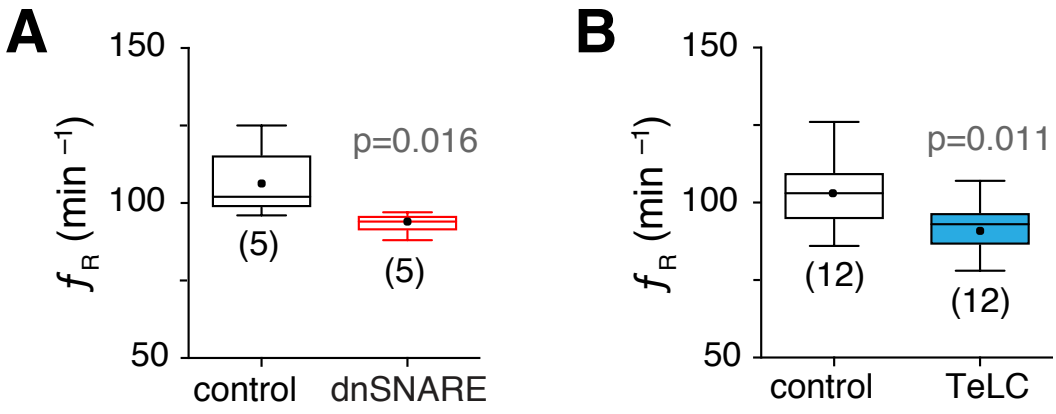

Figure 4.9| Astrocytes control the activity of the respiratory rhythm-generating circuits of the preBötC. Group data showing the effects of dnSNARE (**A**) or TeLC (**B**) expression in preBötC astrocytes on resting respiratory frequency (f_R) in conscious adult rats. In control animals, preBötC astrocytes were transduced to express CatCh-EGFP.

Hypoxia (10% O_2 in the inspired air) induces release of ATP by astrocytes [71] and increases sigh frequency [204], [205]. Therefore, the effects of dnSNARE, TeLC, TMPAP, and $DREADD_{Gq}$ expression on sigh generation during hypoxia were next evaluated. Disruption of either astroglial vesicular release (dnSNARE or TeLC expression) or ATP-mediated signaling (TMPAP expression) reduced the frequency of sighs during the hypoxic challenge by 34% (n = 5, $p<0.001$), 36% (n = 12, $p<0.001$), and 44% (n = 7, $p<0.001$), respectively (**Figure 4.16**). $DREADD_{Gq}$ expression in preBötC astrocytes had an opposite effect and increased frequency of sigh generation during hypoxia by 50% (n = 8, p = 0.003; **Figure 4.16**).

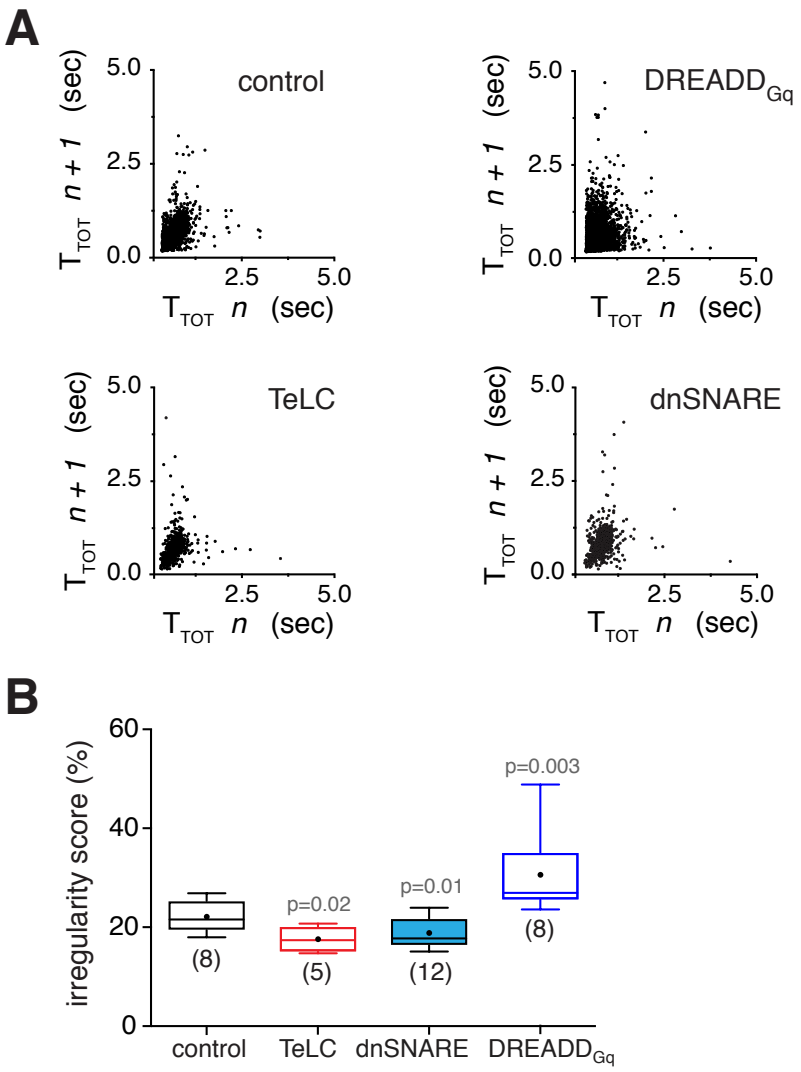

Figure 4.10| Astrocytes regulate the regularity of the respiratory rhythm-generating circuits of the preBötC. **A**) Poincaré plots of the respiratory cycle duration (T_{TOT}) for the n^{th} cycle versus T_{TOT} for the n^{th}+1 cycle in rats transduced to express the control transgene (CatCh), DREADD$_{Gq}$, TeLC or dnSNARE by the preBötC astrocytes. **B**) Summary data illustrating irregularity score of the respiratory rhythm in conscious rats transduced to express CatCh, TeLC, dnSNARE, or DREADD$_{Gq}$.

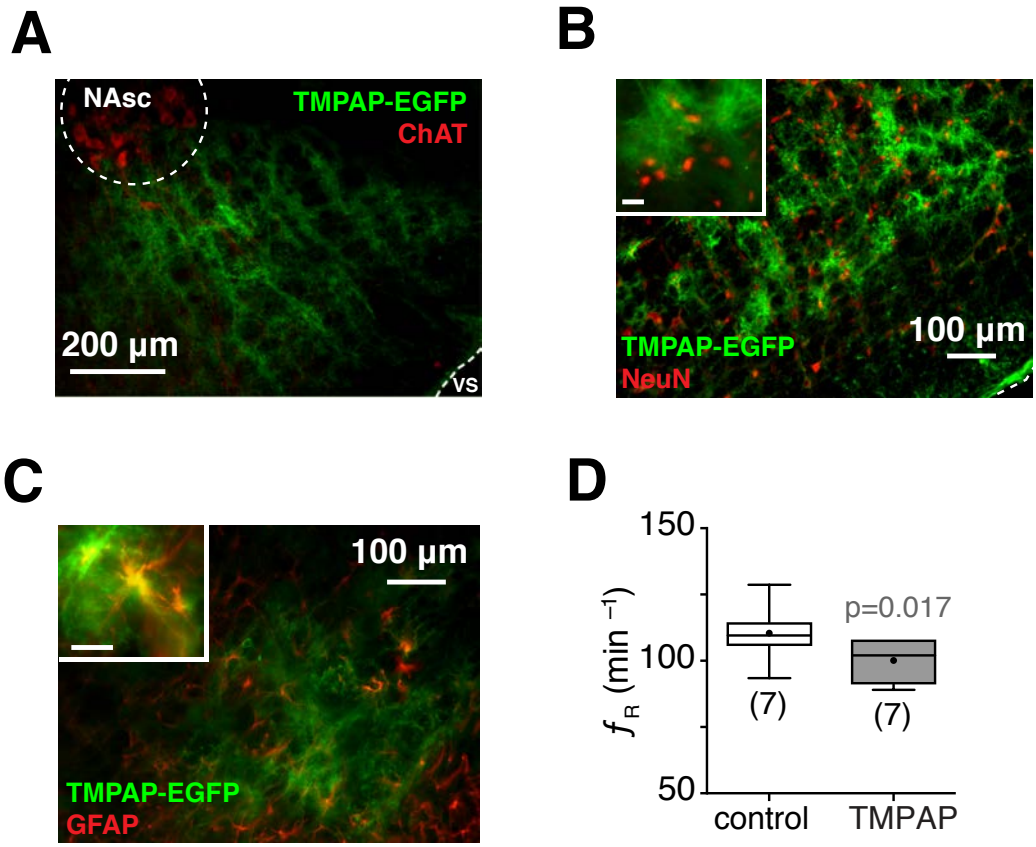

Figure 4.11| Tonic vesicular release of ATP provides excitatory drive to the respiratory rhythm-generating circuits of preBötC. A-C) Confocal fluorescence images of TMPAP-EGFP expression in the preBötC. Despite the use of the generic promoter (Ef1α), EGFP expression driven by this vector was almost exclusively confined to astroglia (see higher magnification insets in **B & C**; scale bars: 25 µm) similar to the data reported previously [167]. VS, ventral surface of the brainstem. **D**) Group data showing the effects of TMPAP expression in the preBötC region on resting f_R in conscious rats.

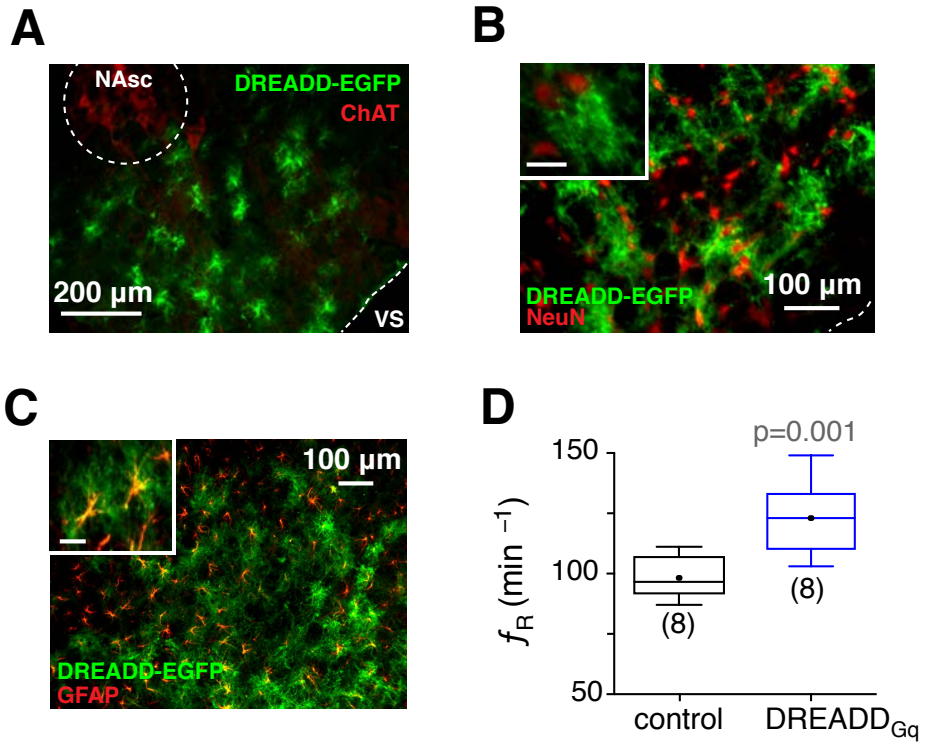

Figure 4.12| Activation of preBötC astrocytes facilitates breathing. A-C) Confocal images illustrating DREADD$_{Gq}$-EGFP expression in preBötC astrocytes. DREADD$_{Gq}$ expression is limited to astrocytes as no neurons (identified by NeuN immunoreactivity) expressed the transgene (see high magnification inset images. Scale bars = 25 µm). **D**) Group data showing the effects of DREADD$_{Gq}$ expression in preBötC astrocytes on resting f_R in conscious rats.

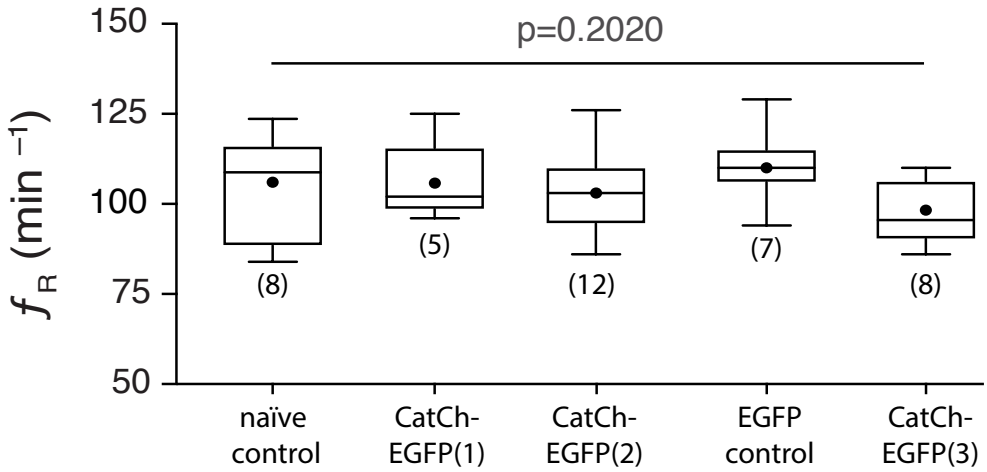

Figure 4.13| Expression of control transgenes did not affect f_R. No differences in resting respiratory activity were observed in naïve (non-transduced) rats and rats transduced to express CatCh-EGFP or EGFP in the preBötC (p=0.2). Three different groups of rats transduced to express control transgene CatCh-EGFP [CatCh-EGFP(1), CatCh- EGFP(2), and CatCh-EGFP(3)] were used as time-matched controls for the groups of animals transduced to express dnSNARE, TeLC, and DREADDGq, respectively (for details see section *Control transgenes*). Rats transduced with a lentiviral vector to express EGFP were used as controls for the experimental animals expressing TMPAP in the preBötC. *P* value – Kruskal-Wallis ANOVA by ranks followed by Dunn's *post hoc* test.

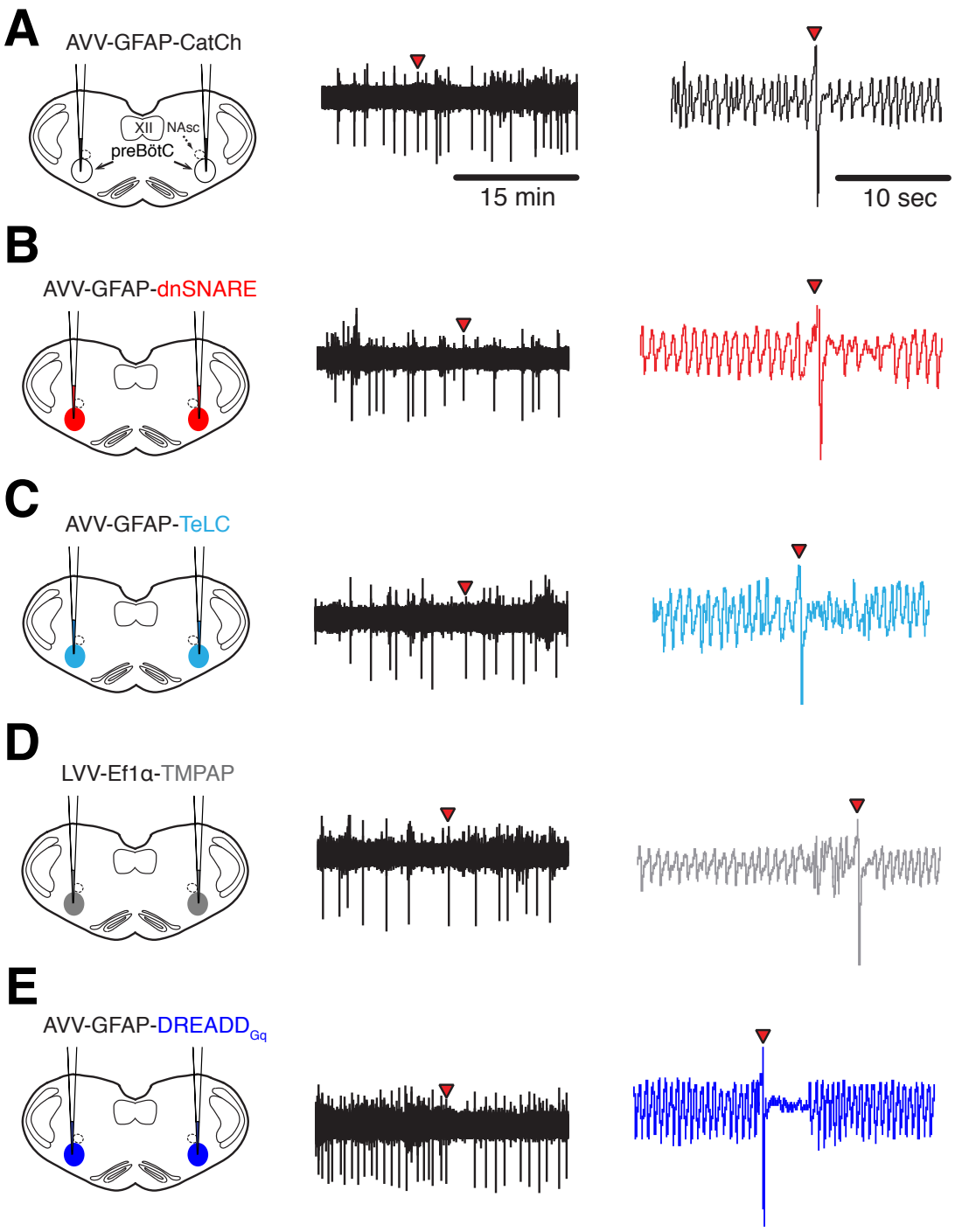

Figure 4.14| Representative whole-body plethysmography recordings obtained in conscious adult rats transduced to express CatCh (A), dnSNARE (B), TeLC (C), TMPAP (D) or DREADD$_{Gq}$ (E) by the preBötC astrocytes. Large amplitude changes in plethysmography chamber pressure [indicated by the arrowheads on the compressed (left) and expanded (right) time scale traces] are indicative of sighs that occur periodically during normal breathing.

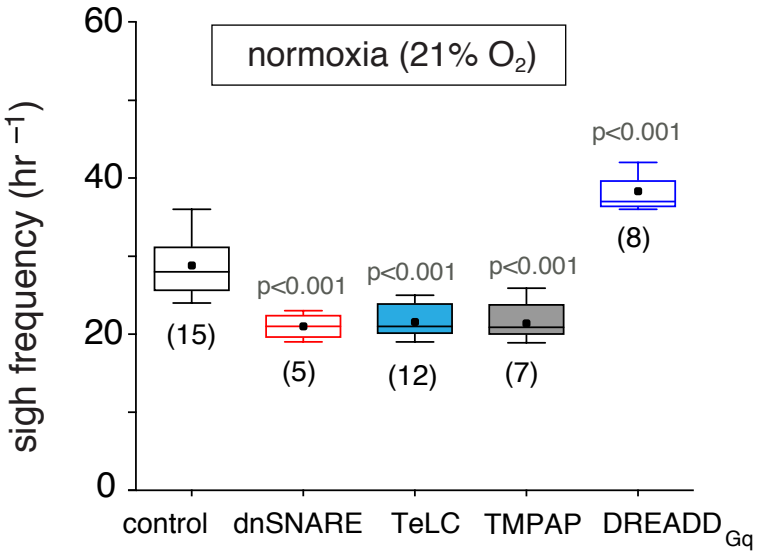

Figure 4.15| PreBötC astrocytes modulate the generation of the inspiratory sighs at rest. Summary data illustrating sigh frequency at resting conditions in conscious rats transduced to express dnSNARE, TeLC, TMPAP or $DREADD_{Gq}$ by preBötC astrocytes.

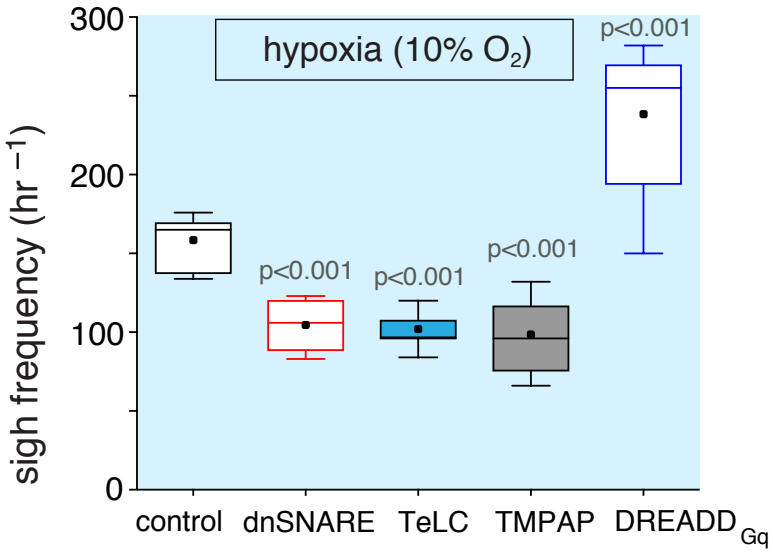

Figure 4.16| PreBötC astrocytes modulate the generation of the inspiratory sighs during systemic hypoxia. Summary data illustrating sigh frequency during systemic hypoxia in conscious rats transduced to express dnSNARE (n=5), TeLC (n=12), TMPAP (n=7) or $DREADD_{Gq}$ (n=8) by preBötC astrocytes.

4.1.4. Summary and Conclusions

Although there is some evidence that astrocytes themselves can trigger generation of rhythmic neuronal circuit activity [138], [202], it is generally believed that the

respiratory rhythm is generated by specialized neuronal populations of the preBötC. Here, we specifically targeted preBötC astrocytes to express proteins which block or enhance vesicular release mechanisms and demonstrated that astroglial release of gliotransmitters (most likely ATP) provides tonic excitatory drive to the preBötC circuits maintains regularity of breathing and underlies generation of sighs.

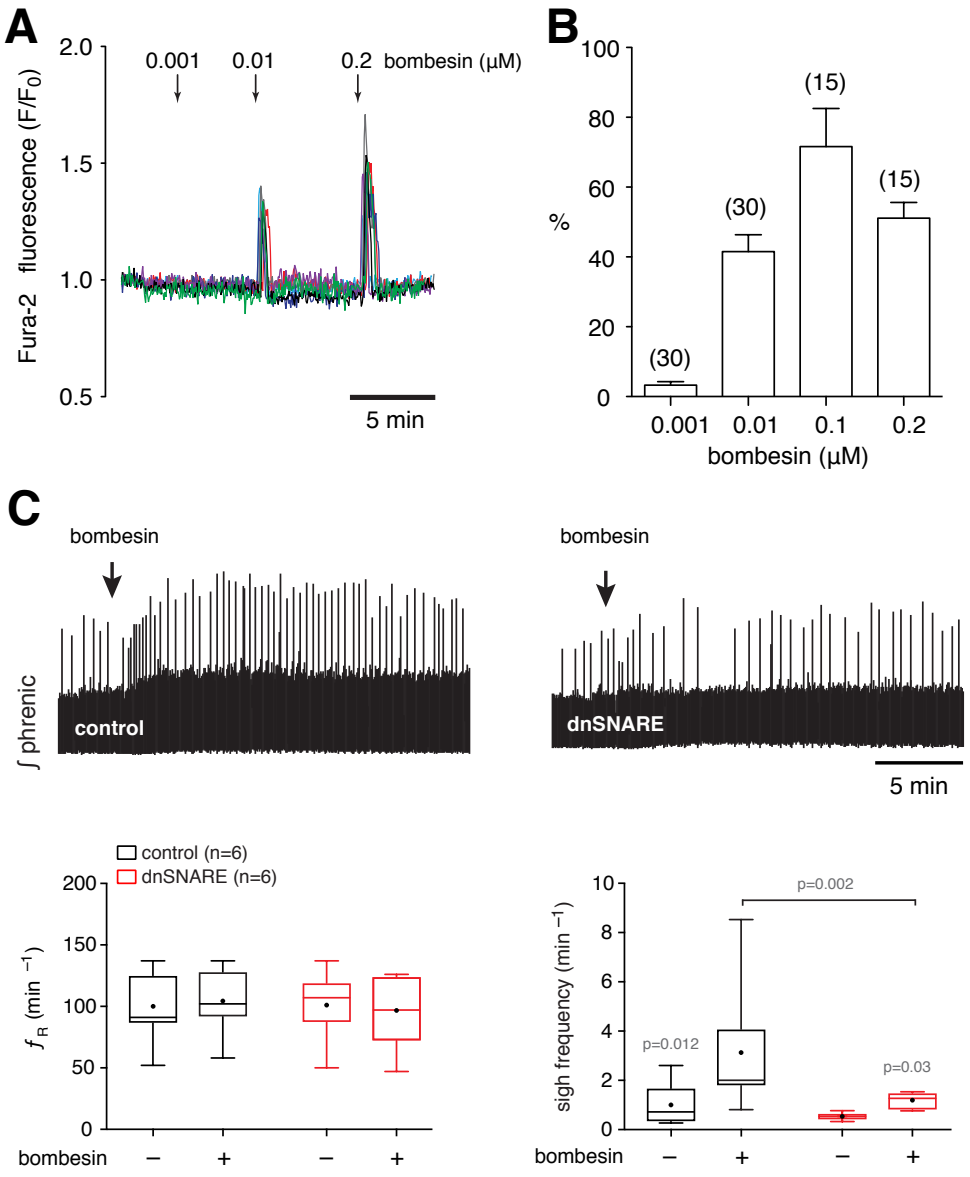

Figure 4.17| Sigh generation is modulated by signaling molecules released by preBötC astrocytes in response to locally released bombesin-like peptides. A) Representative traces illustrating the effect of bombesin on $[Ca^{2+}]_i$ in five individual brainstem astrocytes in culture (traces superimposed). **B**) Summary data illustrating the amplitudes of bombesin-induced $[Ca^{2+}]_i$ responses in cultured brainstem astrocytes. Numbers of individual astrocytes recorded in three separate experiments are indicated in parentheses. **C**) Representative recordings of phrenic nerve activity and summary data illustrating the effect of bombesin (250 μM, 50 nl) on resting respiratory rate and sigh frequency following microinjections into the preBötC where astrocytes were transduced to express control transgene or dnSNARE (anesthetized spontaneously breathing rats). Blockade of vesicular release mechanisms in preBötC astrocytes (dnSNARE expression) reduces the effect of bombesin on sigh frequency by >60%.

Therefore, experiments described in this Chapter addressed the following Aim of the thesis:

> Aim 3: To determine the effect of activation and blockade of signaling pathways in preBötC astrocytes on breathing behavior in conscious behaving rats.

The data obtained suggested that astroglial control of breathing at the level of the preBötC may become particularly important for the development of the appropriate respiratory responses to physiological metabolic challenges such as hypercapnia and hypoxia and exercise. In the experiments described in the next Chapter, I have explored the role of preBötC astrocytes in the control of breathing in conditions of increased metabolic demand.

Chapter 5 INVESTIGATING THE EFFECT OF ACTIVATION AND BLOCKADE OF SIGNALING PATHWAYS IN PREBÖTC ASTROCYTES ON BREATHING BEHAVIOR DURING HYPOXIA, HYPERCAPNIA AND EXERCISE IN CONSCIOUS RATS.

Results of the experiments described in the previous Chapter demonstrated a reduction in mean breathing frequency by ~10% after disruption of either astroglial vesicular release (dnSNARE or TeLC expression) or ATP-mediated signaling (TMPAP expression) in preBötC astrocytes. This decrease in mean breathing frequency may seem "modest," but intact chemoreceptor pathways in conscious animals would be expected to limit any significant sustained changes in the baseline respiratory activity. It was hypothesized that a full extent of astroglial modulation of the respiratory network activity might be revealed when the rhythm-generating networks are studied in isolation or when the respiratory responses to metabolic/chemosensory challenges are studied. Experiments described in this Chapter determined the role of preBötC astrocytes in the control of breathing when the animals were challenged with hypoxia, hypercapnia, and exercise. For the flow of reading, this Chapter is divided into 3 sections.

5.1. The effect of activation and blockade of signaling pathways in preBötC astrocytes on breathing behavior during systemic hypoxia in conscious rats.[1]

5.1.1. Introduction

Oxygen is essential for all complex forms of life [206], and brain function is highly vulnerable to oxygen deprivation. Specialized peripheral oxygen-sensing elements have evolved to monitor and ensure adequate oxygenation of the arterial blood supplying the brain. However, carotid body chemoreceptors are not sensitive to regional CNS differences in PO_2 that may develop as a result of variable levels of neuronal activity or significant changes in perfusion, and all mammals survive the complete loss of peripheral oxygen sensitivity.

It is generally believed that the CNS is devoid of a physiological oxygen sensor (i.e., a cell capable of sensing parenchymal PO_2 changes within the physiological range) and that no functional brain oxygen sensor is capable of stimulating breathing [76]. This view persists despite a number of previous studies reporting significant ventilatory responses to hypoxia in unanesthetized experimental animals with denervated (or silenced) peripheral oxygen chemoreceptors [70], [72]–[74]. The existence of a functional CNS oxygen sensor is also supported by the evidence showing that brainstem respiratory and cardiovascular control circuits are highly sensitive to oxygen deprivation [78], [79], [207]–[209]. Indeed, the majority of central neurons respond to hypoxia with a reduction in excitability. However, it has

[1] Key results presented in this section were reported in an article: "Functional Oxygen Sensitivity of Astrocytes. *Journal of Neuroscience*, 2015, 35(29), 10460–10473," of which I am a co-author. Results of the experimental studies, data analysis and interpretation of the results presented in this section are my contribution to that published work.

been shown that respiratory control circuits of the brainstem show increase in activity in low PO_2 conditions or in response to cytotoxic hypoxia [78], [79], [209]–[211]. There is also strong evidence that the brainstem respiratory networks, including the rhythm generating circuits of the preBötC, are potently activated by ATP [137], [145], [148]–[150], [212]. In the previous Chapter, we provided evidence that release of gliotransmitters (most likely ATP) from preBötC astrocytes regulate the normal activity of the respiratory rhythm-generating circuits at rest. Experiments described in this section determined the effect of compromised gliotransmitter (most likely ATP) release mechanisms in preBötC astrocytes on hypoxia-induced respiratory responses in conscious rats.

5.1.2. Materials and Methods

In this section, in freely behaving adult rats, signaling pathways in preBötC astrocytes were activated (via viral expression of DREADDGq) or blocked (by viral expression of dnSNARE, TeLC, or TMAPA) and role of preBötC astrocytes in the modulation of breathing was assessed when animals were challenged by hypoxia.

5.1.2.1. Viral gene transfer

Young adult male rats (250–280 g) were anesthetized and brainstem respiratory networks, including the rhythm-generating circuits of the preBötC were targeted bilaterally with microinjections of the viral vectors [LVV–Ef1α–TMPAP–EGFP, LVV–EF1–EGFP (control), AVV–sGFAP–EGFP–TeLC, AVV–sGFAP–dnSNARE–EGFP, AVV–sGFAP–$DREADD_{Gq}$–EGFP, or AVV–sGFAP–CatCh–EGFP (control)].

5.1.2.2. Ablation of the carotid body chemoreceptors (CBx)

Rats were anesthetized, and the carotid sinus nerve and its branches were cut, and the carotid bodies were removed. Sham-operated rats underwent the same surgical

procedures to expose the carotid bifurcation, but the carotid sinus nerves and the carotid bodies were left intact.

5.1.2.3. Assessment of sleep efficiency

Established behavioral criteria were used to calculate sleep efficiency score (SES) before, during, and after the hypoxic challenge with an epoch length of 2 s. The SES score was calculated according to the following formula: SES = 100 x (QS+AS) / (QS+ AS+W+IN) (see methods for more details).

5.1.2.4. Assessment of the respiratory activity

Respiratory responses to hypoxia were determined in conscious rats using whole-body plethysmography. In brief, the animal was placed in a recording chamber that was flushed continuously with humidified mixture of 79% N_2 and 21% O_2 (at 22–24°C). The animal was allowed at least 1 h to acclimatize to the chamber environment at normoxia (21% O_2, 79% N_2) before measurements of baseline ventilation were taken. Hypoxia was induced by lowering the O_2 concentration in the chamber to 10% (with the balance being N_2) for 10 min. The measurements of ventilatory responses to hypoxia were obtained during the last 5 min of the 10-min hypoxia period when breathing has stabilized.

5.1.3. Results

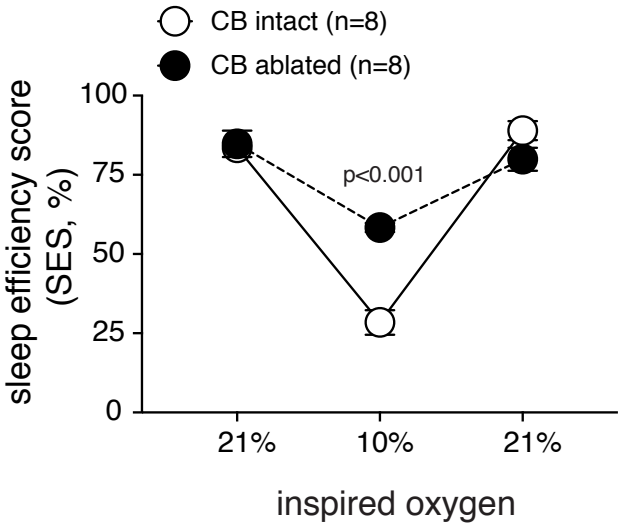

Figure 5.1| Hypoxia-induced arousal responses in rats with denervated peripheral oxygen chemoreceptors. Summary data illustrating changes in SE induced by hypoxia in the carotid body ablated and sham-operated animals (10 weeks after the surgery).

5.1.3.1. The effect of peripheral chemoreceptor denervation on the ventilatory response to systemic hypoxia.

In agreement with previous reports [70], [72]–[74], it was found that conscious rats with denervated peripheral oxygen chemoreceptors (10 weeks after carotid body ablation) displayed significant respiratory responses to hypoxia (see **Figure 5.3** and **Figure 5.5**). To confirm successful ablation of the carotid bodies, the animals were exposed to hypoxic conditions (10% oxygen in the inspired air) while asleep (during the light phase of the 24 h period), and changes in sleep efficiency were assessed. Rats that had undergone carotid body ablation displayed markedly diminished arousal responses to hypoxia (**Figure 5.1**) confirming that the sensory inputs from the peripheral oxygen chemoreceptors were absent or impaired.

5.1.3.2. The effect of general anesthesia on the hypoxic ventilatory response in peripherally chemodenervated animals.

In contrast to the non-anesthetized animals, rats with denervated peripheral

chemoreceptors failed to mount a significant respiratory response to hypoxia when anesthetized (urethane, 1.5 mg kg^{-1}) (**Figure 5.2**), suggesting that the mechanism and/or signaling pathway of central respiratory oxygen sensitivity are severely affected by general anesthesia. Thus, all subsequent experiments were performed in conscious animals.

5.1.3.3. The role of preBötC astrocytes in hypoxic ventilatory response

To specifically block astroglial vesicular release, an AVV for astrocyte-specific expression of TeLC (which cleaves certain SNARE proteins required for vesicular docking and fusion) was used. Tetanus toxin has been shown previously to inhibit ATP, glutamate and D-serine release by astrocytes [170], [213]. It was found that bilateral expression of TeLC in astrocytes residing within the respiratory rhythm generating circuits of the preBötC reduced the respiratory response to systemic hypoxia (10% oxygen in the inspired air) both in the carotid body intact (by 24%; 92 ± 2 min^{-1} *vs* 103 ± 3 min^{-1} in controls; n = 12, p=0.011; **Figure 5.3**) and peripherally chemodenervated (CBx) animals (by 35%; 92 ± 2 min^{-1} *vs* 103 ± 3 min^{-1} in controls; n = 5, p=0.006; **Figure 5.3**).

Next, an AVV for astrocyte-specific expression of dominant-negative SNARE (dnSNARE) protein was used to target preBötC astrocytes. In conscious rats, bilateral expression of dnSNARE in preBötC astrocytes attenuated the hypoxia-induced increases in f_R by 27% (159 ± 10 min^{-1} *vs* 217 ± 7 min^{-1} in controls, n = 5, p=0.008; **Figure 5.4**) and in minute ventilation by 34% (85 ± 5 a.u. *vs* 128 ± 10 a.u. in controls, n=5, p = 0.008, **Figure 5.4**)

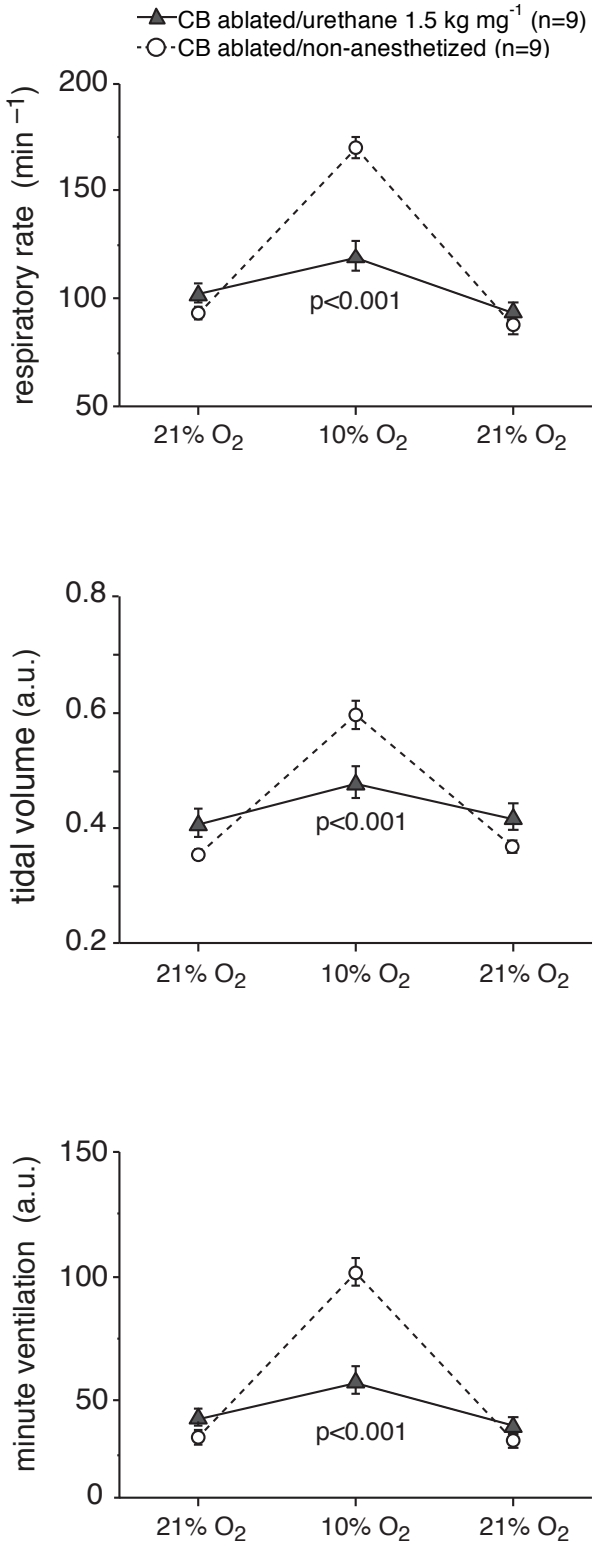

Figure 5.2| Hypoxia-induced respiratory responses in rats with denervated peripheral oxygen chemoreceptors. Summary data illustrating respiratory rate, tidal volume, and minute lung ventilation before, during, and after hypoxia in rats 10 weeks after the carotid body (CB) ablation recorded in the non-anesthetized state during quite sleeping and under general anesthesia (urethane, 1.5 mg/kg).

5.1.3.4. The role of purinergic signaling at the level of preBötC in the hypoxic ventilatory response

Since TeLC or dnSNARE expression in astrocytes is likely to block exocytosis of several putative gliotransmitters, next experiments determined the specific contribution of hypoxia-induced release of ATP to the hypoxic ventilatory response. This was achieved by blocking ATP-mediated signaling within the preBötC by virally-driven expression of a potent ectonucleotidase – transmembrane prostatic acid phosphatase (TMPAP). TMPAP expression is highly effective in preventing ATP accumulation in astroglial vesicular compartments *in vitro*, as well as in blocking extra cellular ATP actions *in vivo* [167], [168]. Bilateral expression of TMPAP within the respiratory rhythm generating circuits of the preBötC reduced the respiratory responses to systemic hypoxia both in the carotid body intact (by 25%; 166 ± 7 min^{-1} *vs* 221 ± 8 min^{-1} in controls, n=7, p=0.017; **Figure 5.5**) and peripherally chemodenervated animals (by 24%; 136 ± 5 min^{-1} *vs* 178 ± 7 min^{-1} in controls, n=7, p=0.017; **Figure 5.5**). Concomitantly, minute ventilation (V_E) was also reduced in rats expressing TMPAP in the preBötC region by 34% (94 ± 5 a.u. *vs* 142 ± 9 a.u. in controls, n=7, $p < 0.001$; **Figure 5.5)** and by 21% (80 ± 18 a.u. *vs* 101 ± 6 a.u. in controls, n=7, p=0.026; **Figure 5.5)** in rats with carotid body intact and ablated (CBx), respectively. Tidal volume was not affected by bilateral expression of TMPAP in the preBötC (**Figure 5.5**).

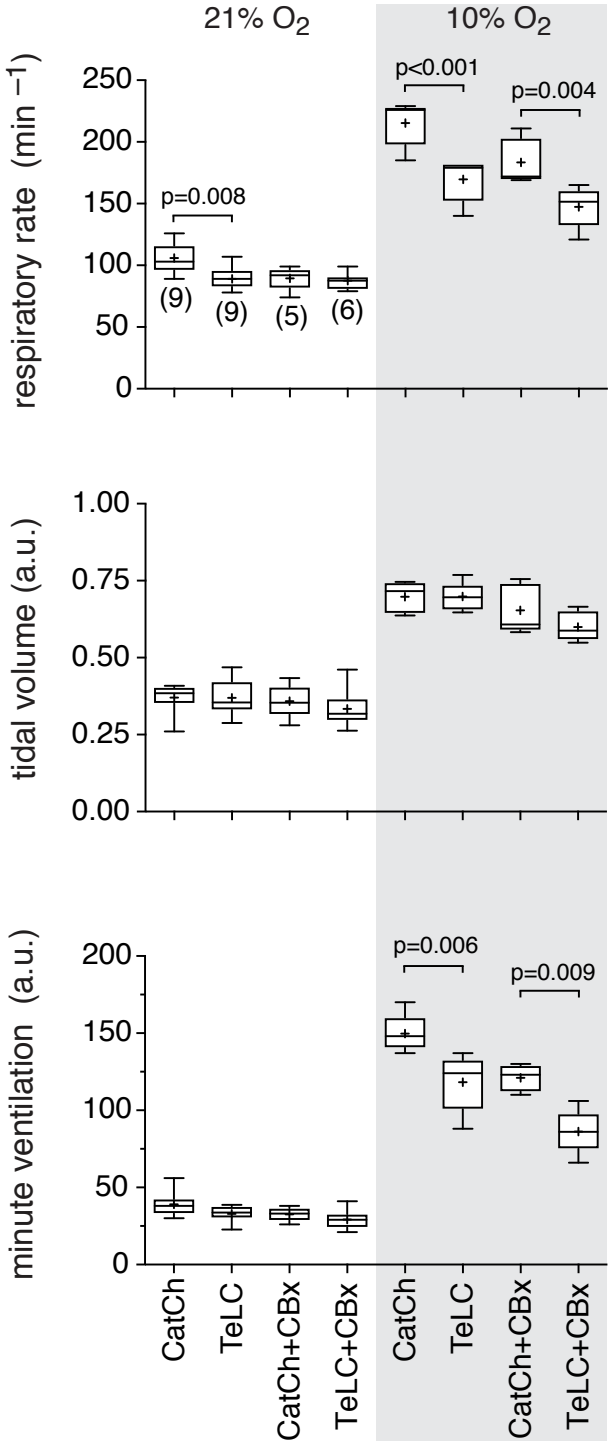

Figure 5.3| Blockade of vesicular release by TeLC in brainstem astrocytes impairs central respiratory oxygen sensitivity. Summary data illustrating hypoxia-induced changes in the respiratory rate, tidal volume, and minute lung ventilation in carotid body intact and peripherally chemodenervated (CBx; 10 weeks) conscious rats expressing either CatCh (used as a control here) or TeLC within the brainstem respiratory circuits. Data sets without *p* values indicated are not significantly different.

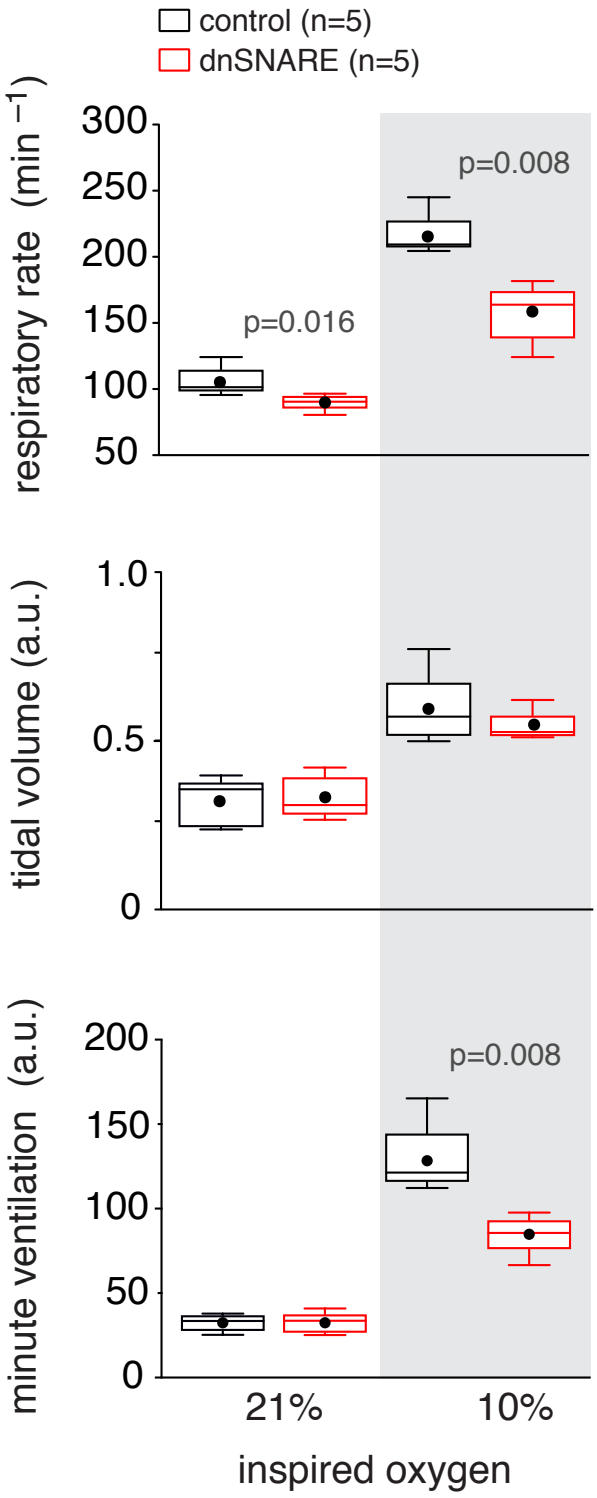

Figure 5.4| Blockade of vesicular release by dnSNARE in brainstem astrocytes impairs central respiratory oxygen sensitivity. Summary data illustrating hypoxia-induced changes in the respiratory rate, tidal volume, and minute lung ventilation in carotid body intact and peripherally chemodenervated (CBx; 10 weeks) conscious rats expressing either CatCh (used as a control here) or dnSNARE within the brainstem respiratory circuits. Data sets without *p* values indicated are not significantly different.

5.1.3.5. The effect of activation of preBötC astrocytes on the hypoxic ventilatory response.

Release of ATP by brainstem astrocytes may occur following activation of phospholipase C (PLC) [71], therefore preBötC astrocytes were next transduced to express a Gq-coupled Designer Receptor Exclusively Activated by Designer Drug ($DREADD_{Gq}$) [169] (see **Chapter 5** for $DREADD_{Gq}$ construct and validation). Results presented in the previous Chapter suggested that in the absence of an agonist (CNO), $DREADD_{Gq}$ is constitutively active at the level of expression provided by our viral vector. This property of $DREADD_{Gq}$ was then exploited in order to determine whether sustained PLC-mediated activation of preBötC astrocytes associated with facilitated vesicular release of ATP has an impact on the hypoxic ventilator response. Surprisingly, bilateral expression of $DREADD_{Gq}$ within the respiratory rhythm generating circuits of the preBötC reduced the respiratory responses (f_R) to systemic hypoxia in the carotid body intact rats (by 16%; 190 ± 3 min^{-1} *vs.* 226 ± 6 min^{-1} in controls, n = 5, p = 0.008; **Figure 5.6**). Following administration of CNO (2 mg kg^{-1}, i.p.), the respiratory responses to hypoxia were also attenuated by ~21% (176 ± 4 min^{-1} *vs* 223 ± 7 min^{-1} in controls, n = 5, p = 0.02; **Figure 5.6**). V_E was also found to be reduced in rats expressing $DREADD_{Gq}$ in preBötC astrocytes during the hypoxic challenge by 27% (114 ± 4 a.u. *vs* 156 ± 7 a.u. in controls, n = 5, p = 0.008; **Figure 5.6)** and by 25% (118 ± 3 a.u. *vs* 158 ± 8 a.u. in controls, n = 5, p=0.008; **Figure 5.6)** in the absence and presence of CNO, respectively. Tidal volume was not affected by bilateral expression of $DREADD_{Gq}$ in the preBötC area (**Figure 5.6**).

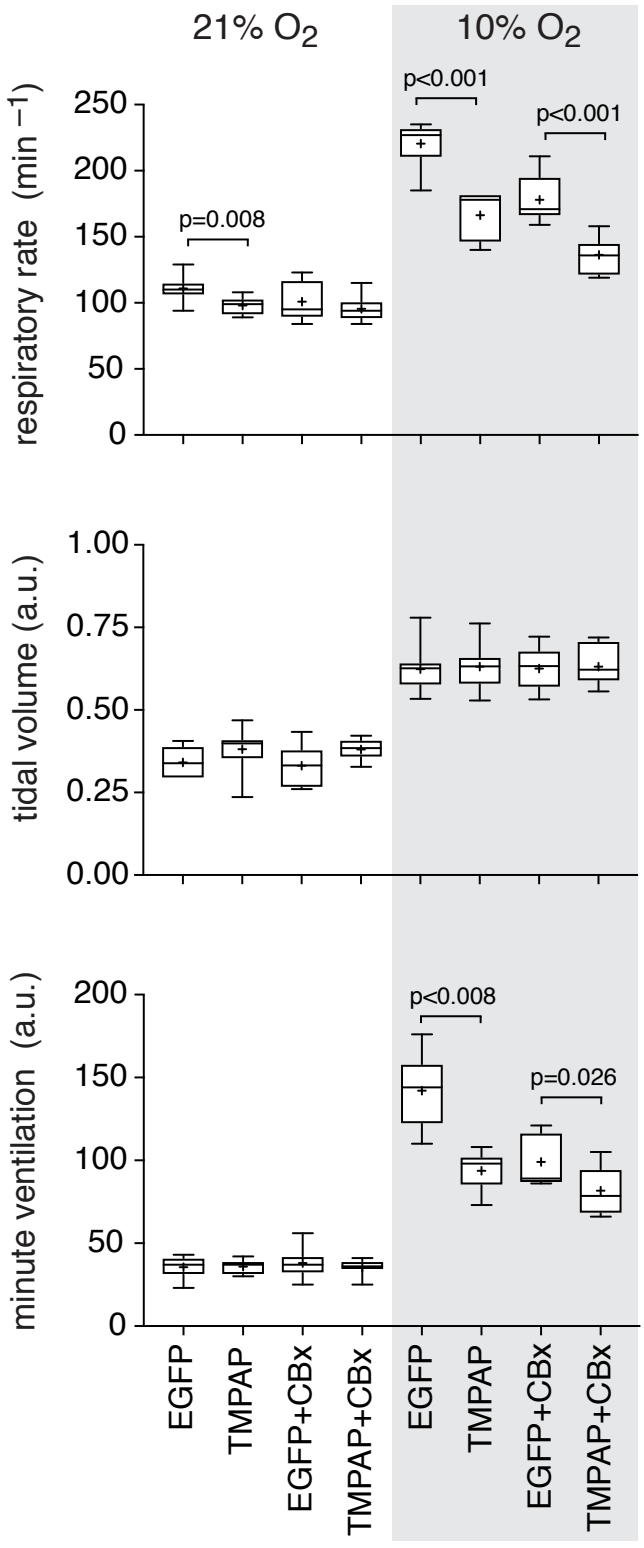

Figure 5.5| Central respiratory oxygen sensitivity is mediated by ATP actions within the brainstem respiratory circuits. Summary data illustrating changes in the respiratory rate, tidal volume, and minute lung ventilation during and after hypoxia in conscious rats expressing EGFP (control) or TMPAP–EGFP within preBötC 10 weeks after peripheral chemodenervation (CBx). Data sets without *p* values indicated are not significantly different.

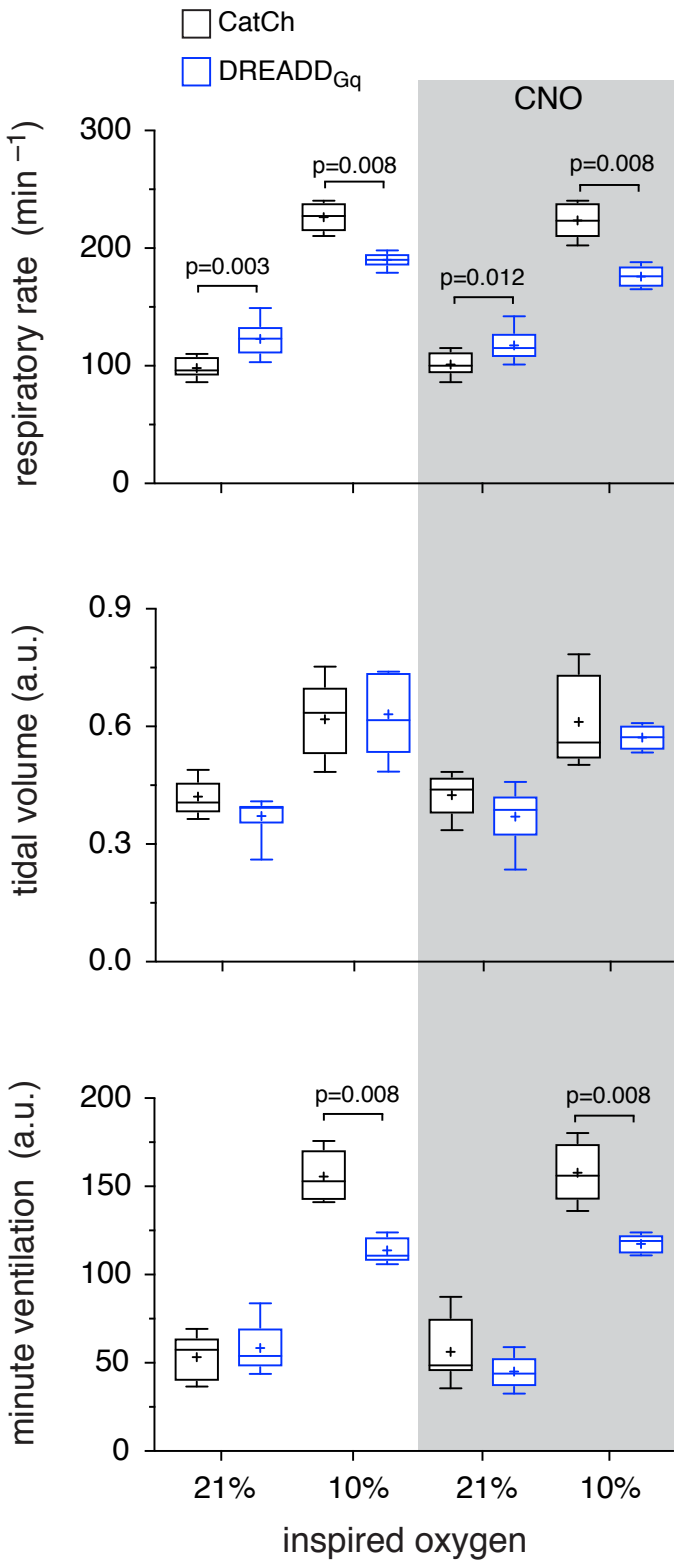

Figure 5.6| Normal astrocytic signaling within the preBötC contributes to the development of the respiratory responses to systemic hypoxia. Summary data illustrating changes in the respiratory rate, tidal volume, and minute lung ventilation at room air and after hypoxia in conscious rats expressing CatCh (control) or DREADD$_{Gq}$–EGFP within preBötC. Data sets without *p* values indicated are not significantly different.

5.1.4. Summary

Bilateral TeLC and TMPAP expression in astrocytes of the preBötC (in the carotid body intact animals) and bilateral carotid body ablation (in rats expressing control transgenes in the preBötC) resulted in quantitatively similar reductions in the magnitude of the respiratory response to hypoxia (**Figure 5.3** and**Figure 5.5**). These observations suggest that the relative contribution of the astroglial oxygen sensitive mechanism to the overall hypoxic ventilatory response is comparable to that of the specialized peripheral respiratory oxygen chemoreceptors of the carotid body. Moreover, over activation of PLC-dependent pathways in preBötC astrocytes via bilateral expression of $DREADD_{Gq}$ also attenuated the hypoxic respiratory response. These results strongly support the hypothesis that hypoxic ventilatory response is critically dependent on normal function of preBötC astrocytes.

5.2. The effect of activation and blockade of signaling pathways in preBötC astrocytes on breathing during hypercapnia in conscious rats.

5.2.1. Introduction

Breathing is controlled in accord with the arterial blood levels of partial pressure of carbon dioxide (PCO_2) as the respiratory network is not active in the absence of CO_2 and requires a threshold level of CO_2 to operate [88], [106]. Increases in PCO_2 in blood/brain are associated with decreases in pH and stimulate breathing via central [63] and peripheral chemoreceptors [61], [62]. It is believed that about 80% of the response to hypercapnia is mediated by activation of the brainstem central chemosensors [88].

Current models of central respiratory CO_2 chemosensitivity are centered at a group of pH-sensitive neurons residing in the medullary retrotrapezoid nucleus (RTN) [33] though significant prior evidence suggests that the functional respiratory chemoreceptors are also located in other brainstem areas [92], [93], [95], [98], [214] including the respiratory rhythm-generating region of preBötC [97]. Although activation of proton-activated receptor GPR4 in chemosensory neurons of RTN appears to be a distinct mechanism for modulating CO_2-activated RTN activity [108], it has been shown that extracellular ATP plays a significant role in central CO_2 chemoreception, as ATP mediates CO_2-induced respiratory responses at the RTN [5], [101], [109], [110], [146] and preBötC [95].

On the other hand, an increase in arterial PCO_2/H^+ *independently* triggers release of ATP from brainstem astrocytes [5]. Since preBötC astrocytes play an active role in central mechanisms of homeostatic control of breathing (Chapter 4 ; [71], [135], [138]–[140]), we hypothesized that they also contribute to the overall CO_2-evoked respiratory response.

5.2.2. Material and Methods

The experiments in this section were designed to assess CO_2-evoked ventilatory responses in conscious and anesthetized, mechanically ventilated adult rats in conditions of astroglial signaling blockade in the preBötC, genetic silencing of RTN neurons, and silencing/removal of the carotid bodies.

5.2.2.1. In vivo gene transfer

Adult Sprague-Dawley rats (250–280 g) received bilateral viral injections to express either TeLC or dnSNARE in preBötC astrocytes. In another set of experiments, 60–80 g male Sprague-Dawley rats were anesthetized, and the RTN area received two microinjections of AAV-hSyn-DREADD$_{Gi}$-mCitrine or control (ChR2-EGFP) viral vectors. 2-3 weeks after the first injection, rats received the second bilateral injection of either AVV-sGFAP-EGFP-TeLC or control vectors (CatCh-EGFP) targeting preBötC.

5.2.2.2. Measurements of the respiratory activity in conscious rats

Whole-body plethysmography was used to measure respiratory parameters in conscious rats. Briefly, 5-7 days after the injections of viral vectors, the experimental animal received an i.p. injection of normal saline and was placed in a Plexiglas recording chamber (~1 L) that was flushed continuously with humidified hyperoxic air (60% O_2) at a rate of 1.2 l min^{-1} (temperature 22-24°C). To take into the account circadian variations of the physiological parameters, respiratory activity in all of the animals were assessed at the same time of the day (11.00-15.00). The animals were allowed to acclimatize to the chamber environment for ~60 min before recording baseline respiratory activity. Hypercapnia was induced by stepwise increases in CO_2 concentration in the respiratory gas mixture to 3% and 6% in a hyperoxic environment (~60% O_2). Each CO_2 concentration was maintained for 5 minutes. Concentrations of O_2 and CO_2 in the chamber were monitored online with a fast-

response O_2/CO_2 analyzer (AD Instruments, ML206). The experiment was then repeated 10 minutes after injection of CNO (2 $mg \cdot kg^{-1}$; i.p.) to measure the contribution of RTN neurons to hypercapnic ventilatory response. Data were acquired using Power1401 interface and analyzed off-line using *Spike2* software (CED Limited, Cambridge).

5.2.2.3. Measurements and analysis of respiratory activity in anesthetized rats

The rats were anesthetized with urethane (1.3 g kg^{-1}; i.v.) following femoral vein cannulation under isoflurane (3%) induction. The trachea was cannulated, and the animal was ventilated artificially with oxygen−enriched air (~30% O_2, 70% N_2, <0.04% CO_2). Core temperature was kept at ~37°C using a heating blanket. The end-tidal level of CO_2 was monitored continuously using fast-response O_2/CO_2 analyzer (AD Instruments, ML206) and blood gasses were measured regularly. Phrenic nerve activity (PNA) and abdominal electromyogram (EMG_{ABD}) were recorded as indicators of central inspiratory and expiratory drives, respectively. The ventral brainstem surface was exposed as described previously [32], [101], [146]. 20 minutes after recording an *initial* response to the hypercapnic challenge (5 min, 10-12% CO_2), carotid body nerves were sectioned (CBD) bilaterally to eliminate inputs from the peripheral chemoreceptors. 20 minutes after CBD, the rat was exposed to the second hypercapnic challenge. Shortly after blood gasses returned to their normal physiological ranges, clozapine-N-oxide (CNO, $DREADD_{Gi}$ ligand) was applied (2 mg kg^{-1}, i.v.), which was followed by the 3rd hypercapnic challenge after 20 minutes (**Figure 5.7**). The CO_2-induced increases in PNA before (*initial*) and after each treatment (CBD and application of CNO) were determined as the percent change of the peak of every CO_2-evoked response with respect to the normal PNA (i.e. before hypercapnic challenge), and expressed as percent change in PNA (each CO_2-evoked ΔPNA is marked with * in **Figure 5.7**). PO_2, PCO_2, and pH of the arterial blood were measured before each hypercapnic challenge. Data were analyzed off-line using *Spike 2* software.

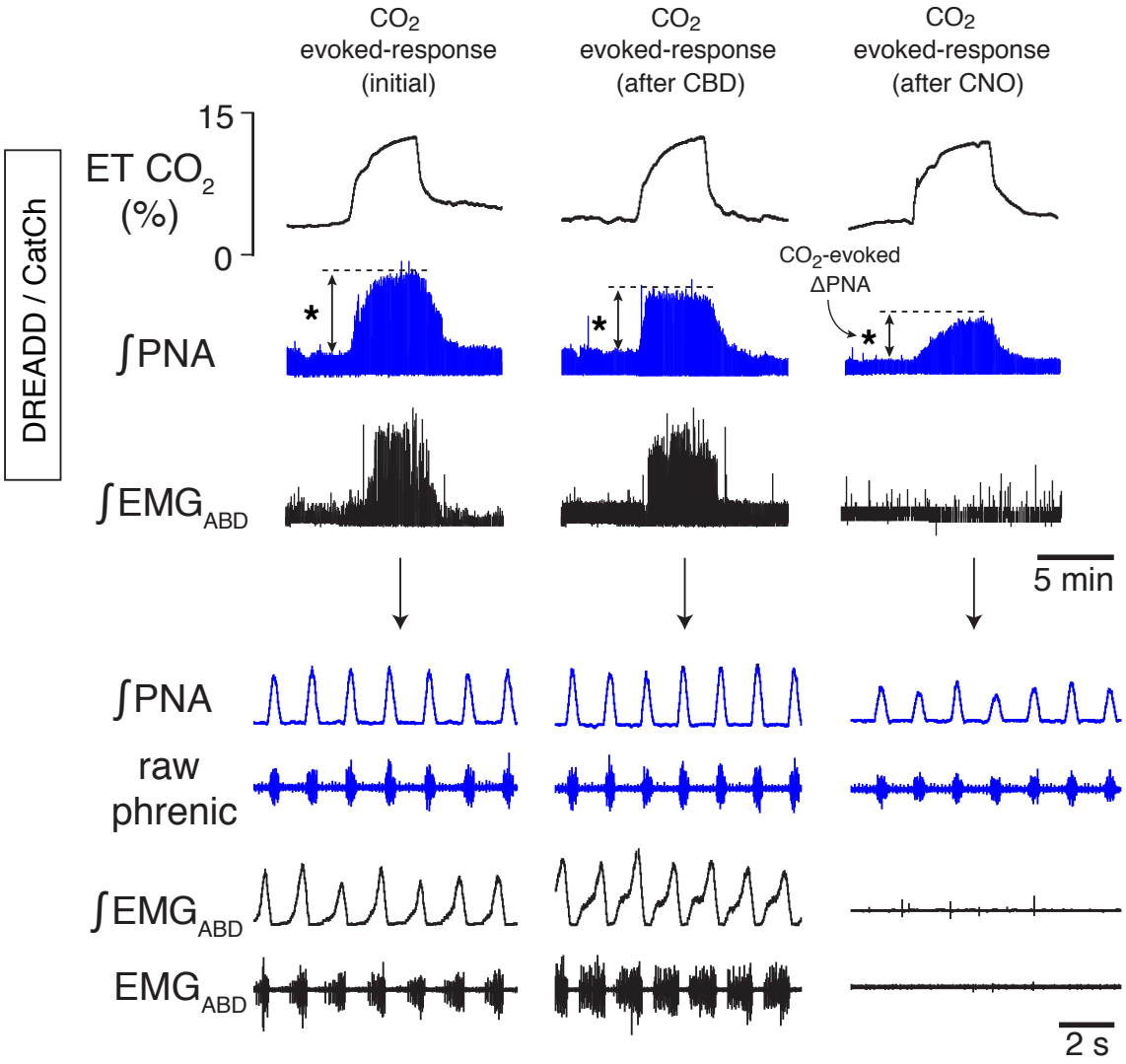

Figure 5.7| Experimental design in anesthetized, vagotomized, and artificially ventilated rats to assess CO_2-evoked ventilatory responses. Time-condensed records illustrating changes in the integrated amplitude of phrenic nerve activity (∫PNA) and abdominal EMG ($\int EMG_{ABD}$) in response to repeated hypercapnic challenges. 20 minutes after recording an *initial* response to the hypercapnic challenge (5 min, 10-12% CO_2), carotid body nerves were sectioned (CBD) bilaterally. 20 minutes after CBD, the rat was exposed to the second hypercapnic challenge (after CBD). Shortly after rat's blood gasses returned to their normal physiological ranges, CNO was applied (2 mg kg^{-1}, i.v.), which was followed by the 3rd hypercapnic challenge (20 minutes after application of CNO). The CO_2-induced increases in PNA before (*initial*) and after each treatment (CBD and application of CNO) was determined as the percent change of the peak of every CO_2-evoked response with respect to the normal PNA (i.e. PNA before each hypercapnic challenge), and expressed as percent increase in PNA (each CO_2-evoked ΔPNA is marked with *). Expanded time base recordings of PNA and EMG_{ABD} are shown below, illustrating late-expiratory abdominal activity evoked by hypercapnia and reversibly blocked by CNO application.

5.2.2.4. Immunohistochemistry

At the end of each experiment, brainstem sections were stained with chicken anti-GFP, mouse anti-TH, and/or goat anti-ChAT antibody.

5.2.3. Results

5.2.3.1. Targeting RTN neurons using AAV-hSyn-DREADD$_{Gi}$-mCitrine

The extent of virally-driven expression of DREADD$_{Gi}$ was examined by *post hoc* immunostaining. DREADD$_{Gi}$-mCitrine expression was amplified using anti-EGFP immunostaining. **Figure 5.8** shows a representative image taken from the center of the DREADD$_{Gi}$-mCitrine expression in the rostro-ventrolateral medulla oblongata. Immunostaining revealed significant expression of DREADD$_{Gi}$-mCitrine, both in the soma and processes of the neurons, in the targeted ventrolateral brainstem region that contains the RTN (**Figure 5.8**). The extent of DREADD$_{Gi}$ expression in the brainstems of all the experimental animals was histologically reconstructed (colored regions were shown) from serial coronal sections following GFP and ChAT (to visualize facial nucleus) immunostaining (**Figure 5.8**). The peak density of transduced RTN neurons expressing mCitrine was within the RTN region (extending rostro-caudally from Bregma -12.1 to -10.8 mm), with limited expression in the immediately adjacent rostral and caudal areas of the ventrolateral medullary region (**Figure 5.8**). No co-localization with TH$^+$ neurons were observed (**Figure 5.8**).

5.2.3.2. Targeting preBötC astrocytes to express TeLC or dnSNARE

In order to interfere with vesicular release mechanism, preBötC astrocytes were virally transduced to express either TeLC or dnSNARE as described in the previous chapter.

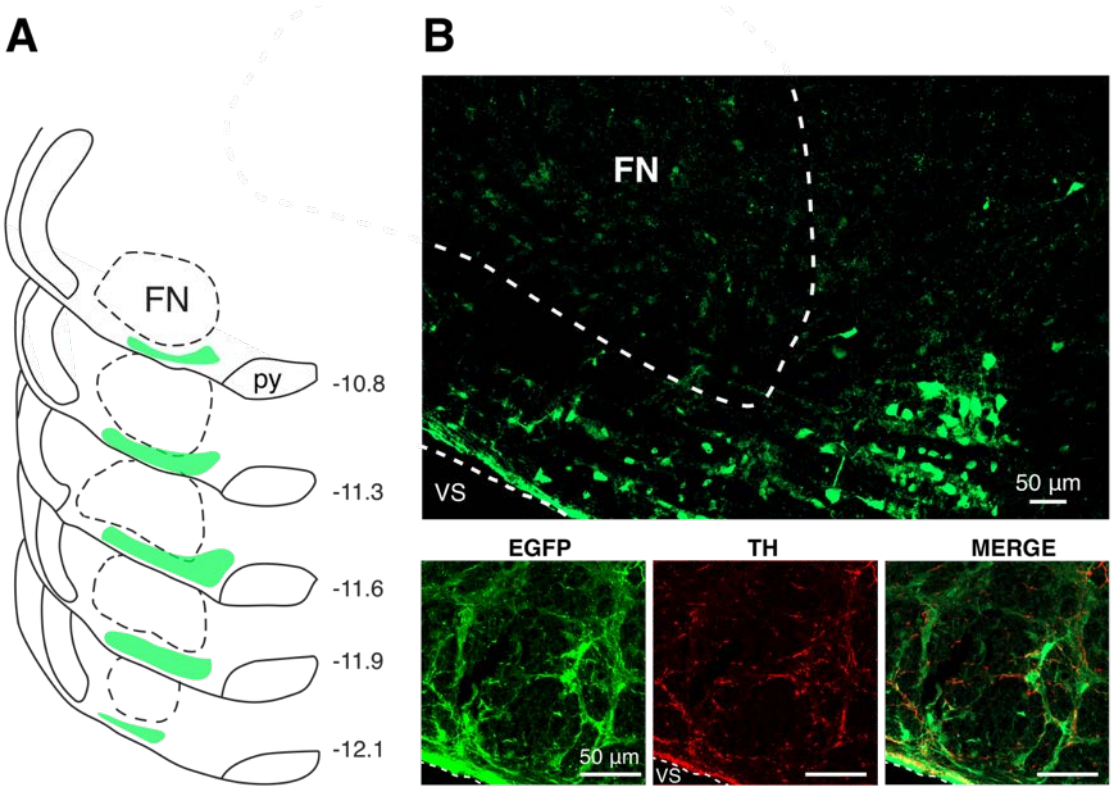

Figure 5.8| Targeting RTN neurons with an AAV to express DREADD$_{Gi}$ A) Schematic illustration of the extent of DREADD$_{Gi}$ expression following EGFP immunostaining (colored regions were shown) in the ventrolateral regions of the medulla oblongata in representative brainstems of adult rats. Adeno-associated viral vectors designed to drive the expression of DREADD$_{Gi}$-mCitrine were used to target RTN neurons bilaterally. The peak density of transduced neurons was within the RTN region (extending rostro-caudally from Bregma -10.8 to -12.1 mm), with limited expression in the immediately adjacent rostral and caudal areas of the ventrolateral medullary reticular formation. py, pyramids. FN, facial nucleus. **B**) Representative confocal images illustrating EGFP immunostaining expression corresponding to the brainstem section -11.6 mm (from Bregma). Higher magnified images illustrating neurons that are transduced to express DREADD$_{Gi}$ were not TH-positive.

5.2.3.3. The role of preBötC astrocytes in the development of CO_2-induced ventilatory response

The hypercapnic ventilatory response was assessed in conscious rats in the following groups:

1. Experimental groups: rats expressing either TeLC (n = 9) or dnSNARE (n = 5) in preBötC astrocytes
2. Control Groups: rats expressing CatCh in preBötC astrocytes

In conscious adult rats, astroglial signaling blockade in rats expressing TeLC or dnSNARE reduced baseline f_R by 12% (94 ± 3 min^{-1} vs. 107 ± 4 min^{-1} in control; n

= 9, p=0.017; **Figure 5.9**) and 17% (86 ± 3 min^{-1} vs. 104 ± 4 min^{-1} in control; n = 5, p=0.008; **Figure 5.10**), respectively, when compared with that in rats expressing control transgene (CatCh) in preBötC in hyperoxic condition (~ 60% inspired O_2). Although blockade of preBötC astrocytes signaling did not significantly affect tidal volume (V_T), the calculated values of minute ventilation ($V_E = f_R \times V_T$) in resting condition was decreased by 18% and 27% in rats expressing TeLC (p=0.019) and dnSNARE (p=0.008), respectively, when compared with that in rats expressing CatCh (**Figure 5.9** & **Figure 5.10**). Similar to normoxic condition (data presented in the previous section; **Figure 4.9**), the baseline f_R in rats expressing TeLC were also found lower when compared to the control group in a hyperoxic condition, which was used to minimize the drive from the peripheral chemoreceptors. However, in hyperoxic condition, minute ventilation at resting conditions was also significantly lower in rats expressing TeLC or dnSNARE when compared to the control group (**Figure 5.9** this chapter; **Figure 4.9** previous chapter).

Bilateral expression of TeLC in preBötC astrocytes reduced the augmentation of f_R to 3% CO_2 by 18% (121 ± 5 min^{-1} *vs* 149 ± 6 min^{-1} in controls; p=0.002) (**Figure 5.9**). There was no effect of dnSNARE expression on f_R response to 3% CO_2. Expression of either dnSNARE or TeLC transgenes did not affect CO_2-evoked augmentation of V_T (and V_E at 3% CO_2) when compared with those in rats expressing CatCh in preBötC astrocytes (**Figure 5.9** & **Figure 5.10**).

However, expression of either dnSNARE or TeLC in preBötC astrocytes

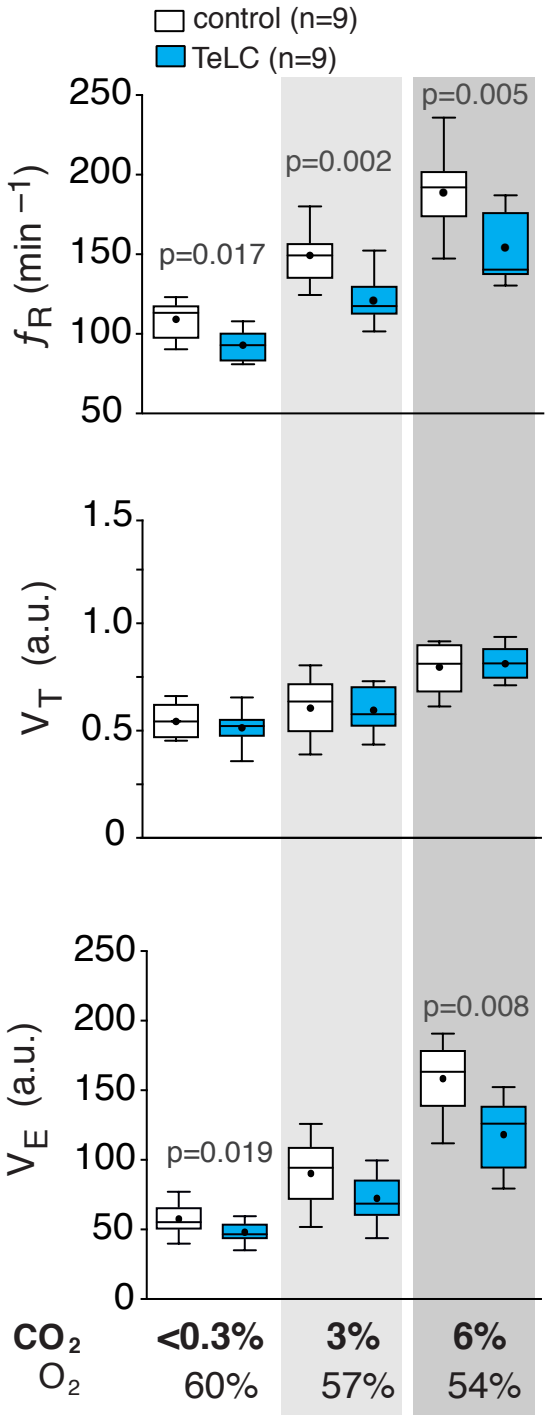

Figure 5.9| Astrocyte signaling within the preBötC contributes to the development of the respiratory responses to systemic hypercapnia. Group data illustrating the effect of TeLC expression in preBötC astrocytes on CO_2-induced increases in the f_R, V_T, and V_E in conscious rats. Data sets without *p* values indicated are not significantly different.

markedly reduced the augmentation of f_R in response to 6% CO_2 by 23% (141 ± 4 min^{-1} *vs* 182 ± 3 min^{-1} in controls; p=0.008; **Figure 5.10**) and 21% (151 ± 6 min^{-1} *vs*

190 ± 8 min^{-1} in controls; p=0.005; **Figure 5.9**), respectively, concomitantly reducing V_E (by 21%; 122 ± 7 a.u. vs. 154 ± 4 a.u. in control; p=0.008; **Figure 5.10**) and TeLC (by 23%; 119 ± 8 a.u. vs. 159 ± 9 a.u. in control; p=0.008; **Figure 5.9**), respectively. Expression of either transgene did not affect CO_2-induced increases in V_T in response to 6% CO_2 when compared with that in control groups.

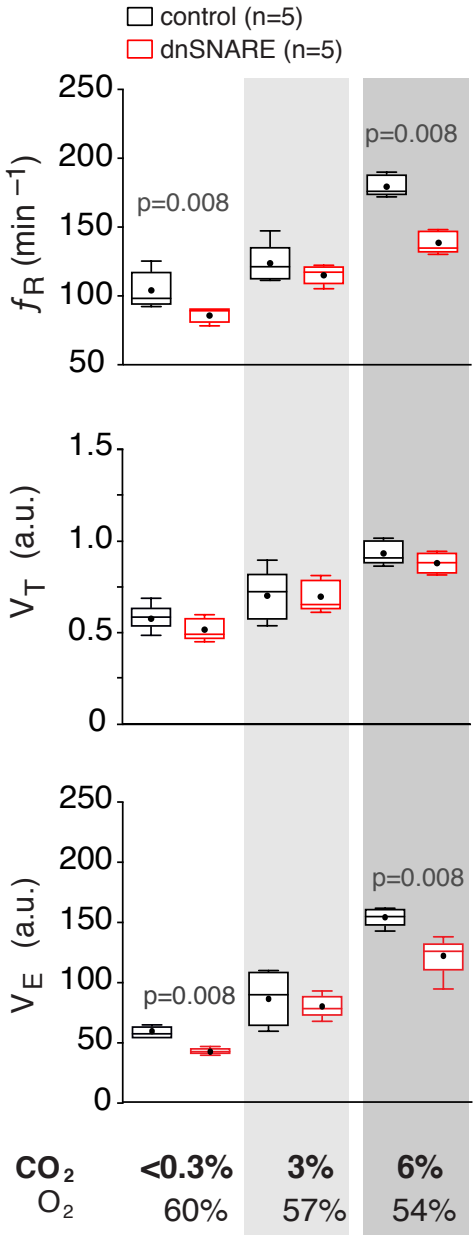

Figure 5.10| Astrocyte signaling within the preBötC contributes to the development of the respiratory responses to systemic hypercapnia. Summary data illustrating the effect of dnSNARE expression in preBötC astrocytes on CO_2-induced increases in the f_R, V_T, and V_E in conscious rats. Data sets without *p* values indicated are not significantly different.

In summary, in hyperoxic condition, interfering with preBötC astroglial signaling affected the f_R and concomitantly V_E, but not V_T, at rest and during

hypercapnic (6% inspired CO_2) challenge.

5.2.3.4. The role of RTN neurons in the development of CO_2-evoked ventilatory response

The hypercapnic ventilatory response was assessed in awake rats in the following experimental groups:

1. Control rats expressing ChR2 in RTN neurons and CatCh in preBötC astrocytes (ChR2/CatCh, n = 5).
2. Acute silencing of RTN chemoreceptors in rats expressing $DREADD_{Gi}$ in RTN neurons and control CatCh in preBötC astrocytes (DREADD/CatCh, n = 5). The difference between the hypercapnic ventilatory responses evoked following application of CNO (2 $mg \cdot kg^{-1}$; i.p.) was considered as the individual contribution of RTN neurons to the overall CO_2-evoked response.

In conscious rats virally transduced to express DREADD/CatCh, f_R, V_T, and V_E in resting condition (normocapnic/hyperoxic; no CNO) were not different from those measured in control group (**Figure 5.11**). Similarly, hypercapnia (increasing inspired CO_2 to 3% and 6%) did not affect respiratory indices (f_R, V_T, and V_E) measured in rats expressing DREADD/CatCh when compared with rats expressing ChR2/CatCh. (**Figure 5.11**).

Similarly, CNO-induced inhibition of RTN neuron had no effect on breathing in resting condition (**Figure 5.12**). However, during a moderate hypercapnic challenge (inspired 6% CO_2), inhibition of RTN neurons reduced augmentation of V_T (by 17%; 0.76 ± 0.02 a.u. vs. 0.93 ± 0.04 a.u. in control, p = 0.016; **Figure 5.12**) and concurrently V_E (by ~18%; 143 ± 5 a.u, vs. 175 ± 8 in control p = 0.016; **Figure 5.12**). In summary, inhibition of RTN neurons affected V_T (and concurrently V_E) only during the hypercapnic challenge, but not at resting condition; f_R at resting condition or during the hypercapnic challenge (**Figure 5.12**) was not affected by inhibition of RTN neurons.

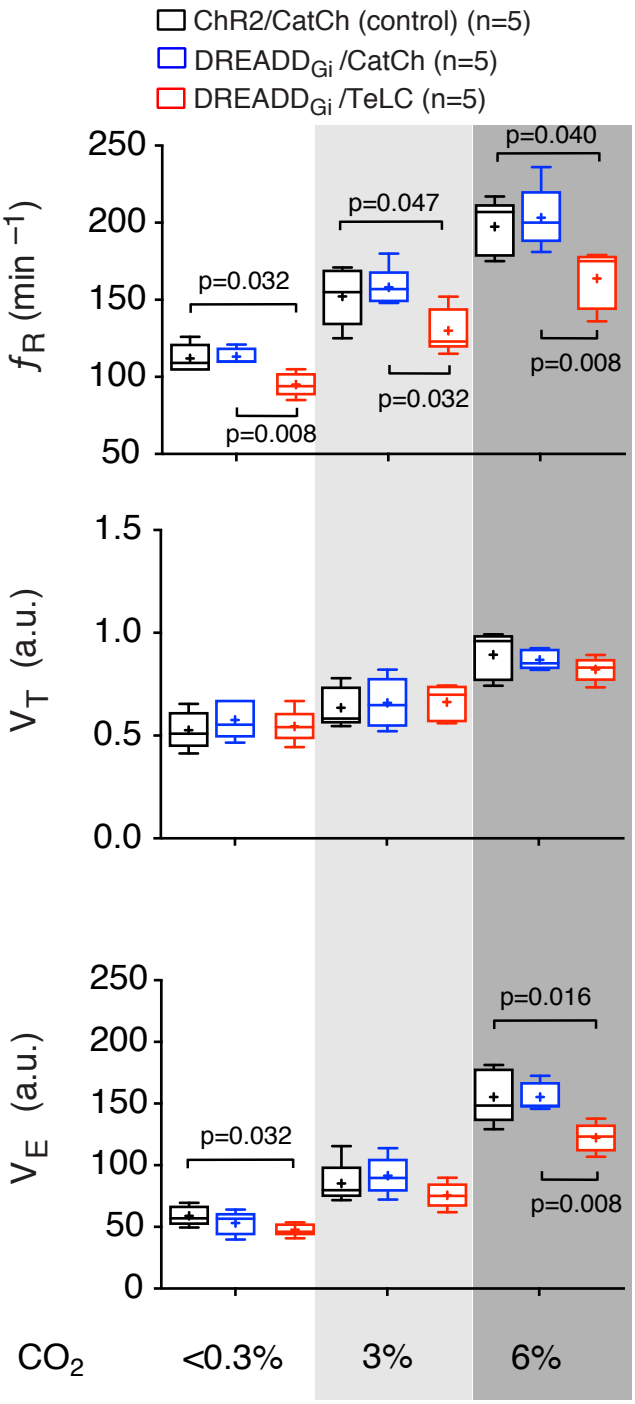

Figure 5.11| Contributions of RTN neurons and preBötC astrocytes to the development of CO_2-induced ventilatory response. Group data illustrating the effect of $DREADD_{Gi}$ expression in RTN neurons (without CNO) and TeLC expression in preBötC astrocytes on CO_2-induced increases in the f_R, V_T, and V_E in conscious rats. Data sets without *p* values indicated are not significantly different.

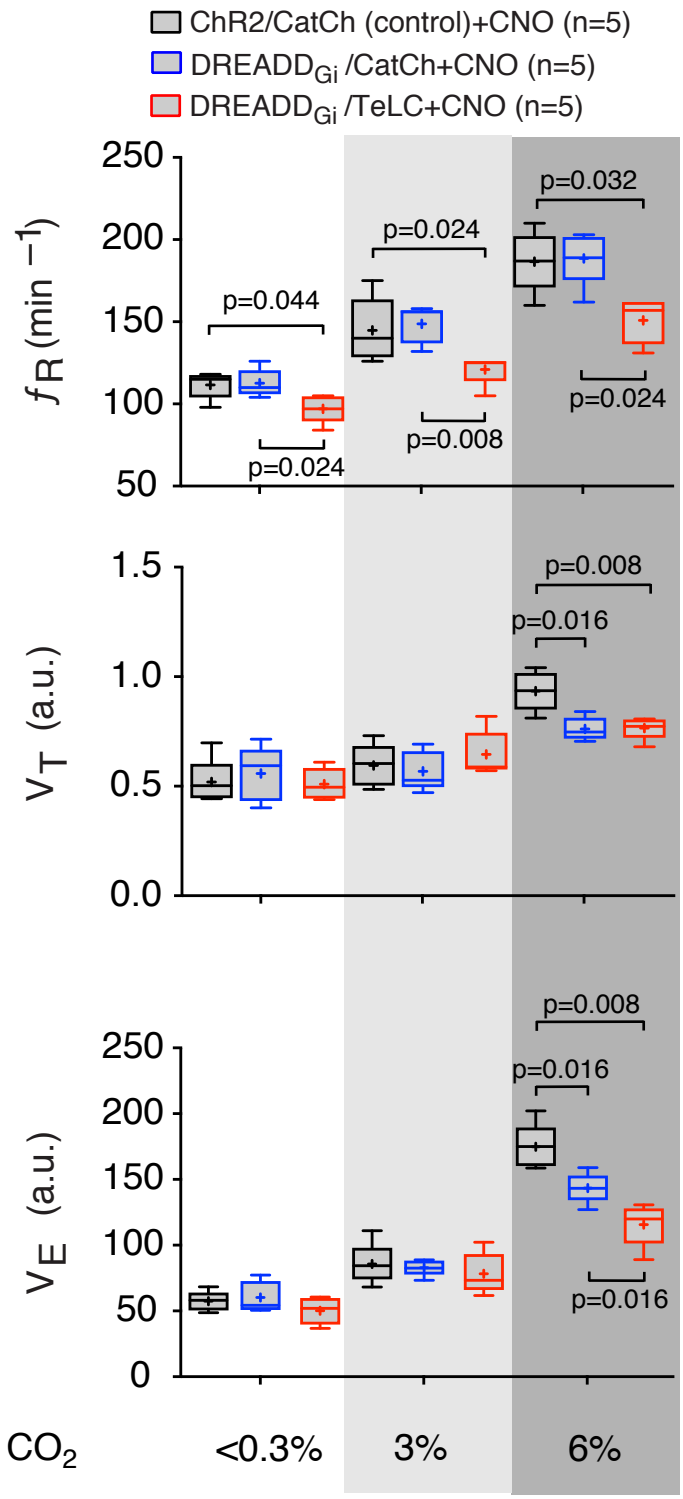

Figure 5.12| Relative contributions of RTN neurons and preBötC astrocytes to the development of CO_2-induced ventilatory response in conscious rats. Group data illustrating effects of inhibition of $DREADD_{Gi}$-expression RTN neurons (with CNO, 2 $mg \cdot kg^{-1}$; i.p.) and TeLC expression in preBötC astrocytes on CO_2-induced increases in the f_R, V_T, and V_E in conscious rats. Data sets without *p* values indicated are not significantly different.

5.2.3.5. Relative contributions of RTN neurons and preBötC astrocytes to the development of CO_2-induced ventilatory response

Data presented in sections 5.2.3.3 and 5.2.3.4 suggested that the effect of either blocking astroglial signaling in the preBötC (TeLC expression) or silencing RTN neurons (inhibiting $DREADD_{Gi}$ expressing RTN neurons) produce quantitatively similar reductions in the ventilatory response to hypercapnia in conscious rats.

Subsequent experiments determined the effect of combined blockade of preBötC astroglial signaling *and* inhibition of the RTN neurons on CO_2-induced ventilatory responses with the addition of the following experimental group to the previous DREADD/CatCh and control (ChR2/CatCh) groups:

3. Rats expressing $DREADD_{Gi}$ in RTN neurons and TeLC in preBötC astrocytes (DREADD/TeLC, n = 5) were used to test the concurrent effect of blockade of astroglial signaling in the preBötC with CNO-induced silencing RTN neurons. The reduction in the hypercapnic ventilatory response evoked following application of CNO was considered as the contribution of RTN neurons to the overall CO_2-evoked response in conditions of astroglial signaling blockade. All the following experiments were performed in the presence of CNO.

As expected, in resting condition, when compared to the control group, inhibition of RTN neurons in rats expressing DREADD/TeLC did not affect V_T. However, f_R was found to be lower in rats expressing DREADD/TeLC (by 14%; 97 ± 4 min^{-1} *vs* 112 ± 4 min^{-1} in controls; n=5, p = 0.008; **Figure 5.12**). V_E in rats expressing DREAD/TeLC was not different from the one measured in rats expressing ChR2/CatCh (p = 0.4; **Figure 5.12**).

During mild hypercapnia (inspired 3% CO_2), inhibition of RTN neurons in rats expressing DREADD/TeLC did not affect hypercapnic increased in V_T, though, f_R (121 ± 4 min^{-1}) was lower when compared with that in rats expressing ChR2/CatCh (p = 0.02) or DREADD/CatCh (p = 0.008; **Figure 5.12**). However, calculated V_E in

rats virally transduced to express DREADD/TeLC was not different when compared to the one measured in ChR2/CatCh (p = 0.4) and DREADD/CatCh (p = 0.4) (**Figure 5.12**).

At 6% inspired CO_2, f_R was found to be significantly lower in rats expressing DREADD/TeLC (151 ± 6 min^{-1}, p = 0.032) when compared to the rats expressing ChR2/CatCh (**Figure 5.12**). In a similar manner, f_R measured in rats expressing DREADD/TeLC was significantly lower when compared to that of rats expressing DREADD/CatCh (p = 0.024; **Figure 5.12**). V_T measured in rats expressing DREADD/TeLC were significantly lower when compared to that of rats expressing ChR2/CatCh (0.77 ± 0.01 a.u vs. 0.93 ± 0.04 a.u in control, p= 0.008; **Figure 5.12**). Finally, when we compared V_E in the condition of 6% CO_2 in inspired air, expression of DREADD/TeLC significantly reduced the CO_2-induced augmentation of V_E by 34% when compared with that in rats expressed control transgenes (116 ± 7 a.u. vs. 175 ± 8 a.u., p = 0.008; **Figure 5.12**). In addition, when comparing rats expressing DREAD/TeLC with rats expressing DREADD/CatCh, V_E was also found to be lower by ~ 19% (116 ± 7 a.u. vs. 143 ± 5 a.u., p = 0.016; **Figure 5.12**), indicating a possible additive effect of preBötC astrocytes characterized by a more profound reduction of the hypercapnic ventilatory response.

5.2.3.6. Contribution of the carotid bodies, RTN neurons and preBötC astrocytes to the CO_2-evoked increases in the respiratory activity

In anesthetized, vagotomized, and artificially ventilated rats expressing ChR2/CatCh, bilateral denervation of the carotid bodies (CBD) or inhibition of RTN neurons (via application of CNO, 2 $mg \cdot kg^{-1}$; i.v.) did not affect the CO_2-evoked increases in inspiratory drive (ΔPNA) or abdominal electromyogram (EMG_{ABD}) (**Figure 5.13*A* and Figure 5.14*top*)**.

While bilateral CBD in rats expressing DREADD/CatCh did not affect ΔPNA, and EMG_{ABD}, inhibition of RTN neurons abolished the CO_2-evoked increases in EMG_{ABD} (i.e. active expiration), and decreased the hypercapnic respiratory response

(percent change in PNA) by 54% (103 ± 20 % initial ΔPNA *vs.* 47 ± 7 % ΔPNA after CNO; n = 5, p = 0.023; **Figure 5.13*B* and Figure 5.14**).

Similarly, in rats transduced to express DREADD/TeLC, CBD did not affect CO_2-evoked ΔPNA (**Figure 5.13*C* and Figure 5.14**). However, application of CNO significantly reduced the CO_2-evoked increases in phrenic nerve activity (71 ± 9 % initial ΔPNA *vs.* 30 ± 5 % ΔPNA after CNO; n=5, p=0.008; **Figure 5.13*C* and Figure 5.14**).

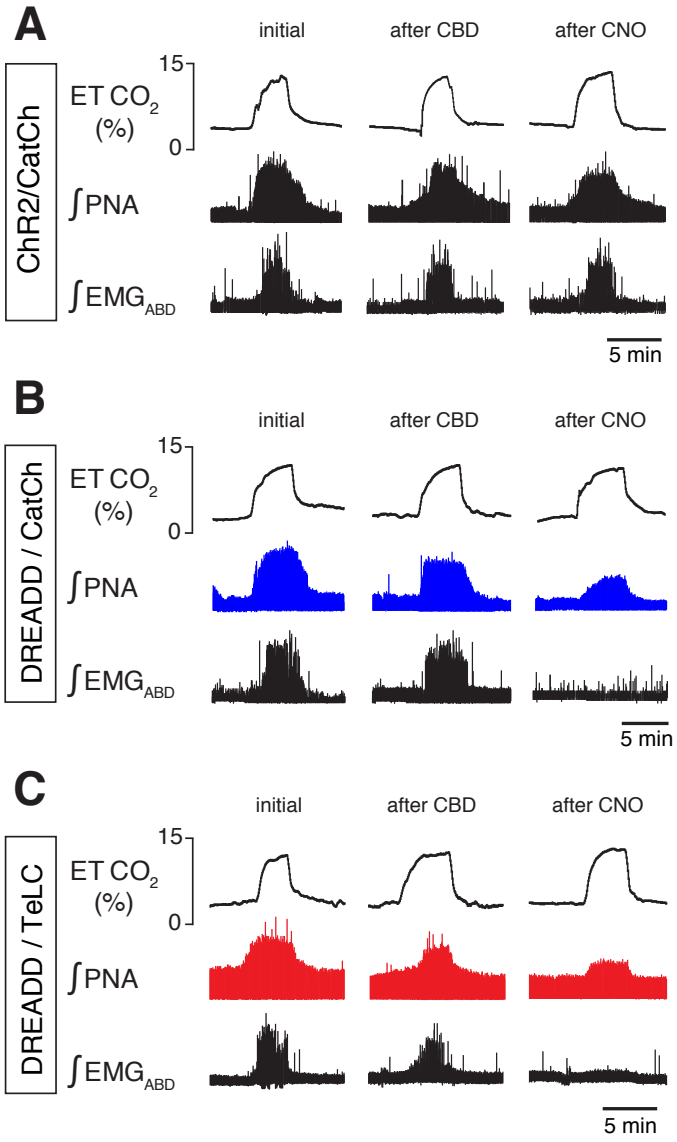

Figure 5.13| Hypercapnia fails to trigger expiratory activity following acute inhibition of DREADD$_{Gi}$-expression RTN neurons in anesthetized rats. Time-condensed records illustrating changes in integrated amplitude of phrenic nerve activity (∫PNA) and abdominal EMG (∫EMG$_{ABD}$) in response to *initial* hypercapnic challenge (initial), as well as repeated increases in the level of inspired CO_2 after CBD and in the presence of CNO (, 2 mg·kg^{-1}; i.v.) in rats transduced to express ChR2/CatCh (**A**), DREADD/CatCh (**B**), and DREADD/TeLC (**C**) (see **Figure 5.7** and Method section for details). Expanded time base recordings of PN and abdominal EMG are shown below, illustrating late-expiratory abdominal activity evoked by hypercapnia and reversibly blocked by allatostatin application to the ventral brainstem.

As mentioned above, the initial hypercapnic respiratory response was not different in rats transduced to express either transgenes (ChR2/CatCh: 103 ± 20 %; DREADD/CatCh: 114 ± 24 %; DREADD/TeLC: 71 ± 9 %; p = 0.276; **Figure 5.15A** *top*). Application of CNO (2 mg·kg^{-1}; i.v.), decreased the CO_2-evoked ΔPNA in rats expressing DREADD/CatCh and DREADD/TeLC by 51% (47 ± 7 % *vs* 95 ± 5 % in control; n = 5, p = 0.008; **Figure 5.15A** *middle*) and 68% (31 ± 6 % *vs* 98 ± 5 % in control; n = 5, p=0.008; **Figure 5.15A** *bottom*), respectively, when compared with that in rats expressing ChR2/CatCh. After bilateral denervation of the carotid bodies (CBD), the CO_2-evoked ΔPNA in rats transduced to express DREADD/TeLC was significantly lower when compared with rats expressing ChR2/CatCh (51 ± 7 % *vs* 90 ± 13 % in control; p=0.033; **Figure 5.15A** *bottom*).

In order to determine the contribution of the carotid bodies to the overall CO_2-evoked respiratory response, we have combined data obtained from hypercapnic respiratory response after CBD from ChR2/CatCh and DREADD/CatCh. Bilateral CBD reduced the CO_2-evoked increases in inspiratory drive by ~ 25% (109 ± 15 % initial ΔPNA *vs.* 82 ± 7 % ΔPNA after CBD; n = 10, p = 0.008; **Figure 5.15*B***). Blockade of vesicular release mechanisms in the preBötC astrocytes had a similar effect and reduced CO_2-induced respiratory response by 27% (71 ± 9 % initial ΔPNA in rats expressing DREADD/TeLC vs. 109 ± 15 % initial ΔPNA in rats expressing ChR2/CatCh, n = 5, p = 0.008; **Figure 5.15*B***). This decrease in ΔPNA was higher when combining CBD with either inhibition of RTN neurons [(i.e. ΔPNA response after exclusion of RTN neurons + CB), 47 ± 7 % ΔPNA after CNO in rats expressing DREADD/CatCh vs. Initial ΔPNA in control group, n = 5, p = 0.008; **Figure 5.15*B***] or blockade of vesicular release mechanisms in preBötC astrocytes [(i.e. ΔPNA response after exclusion of preBötC astrocytes + CB), 51 ± 7 % ΔPNA after CBD in rats expressing DREADD/TeLC vs. Initial ΔPNA in control group, n = 5, p = 0.008; **Figure 5.15*B***]. Lastly, in conditions of silencing RTN neurons in rats transduced to express TeLC in preBötC [(i.e. ΔPNA response after exclusion of preBötC astrocytes + RTN neurons + CB; **Figure 5.15*B***] the respiratory response

to hypercapnia was reduced by ~ 75%. [30 ± 5 % ΔPNA after CNO in rats expressing DREADD/TeLC vs. Initial ΔPNA in control group, n=5, p=0.008).

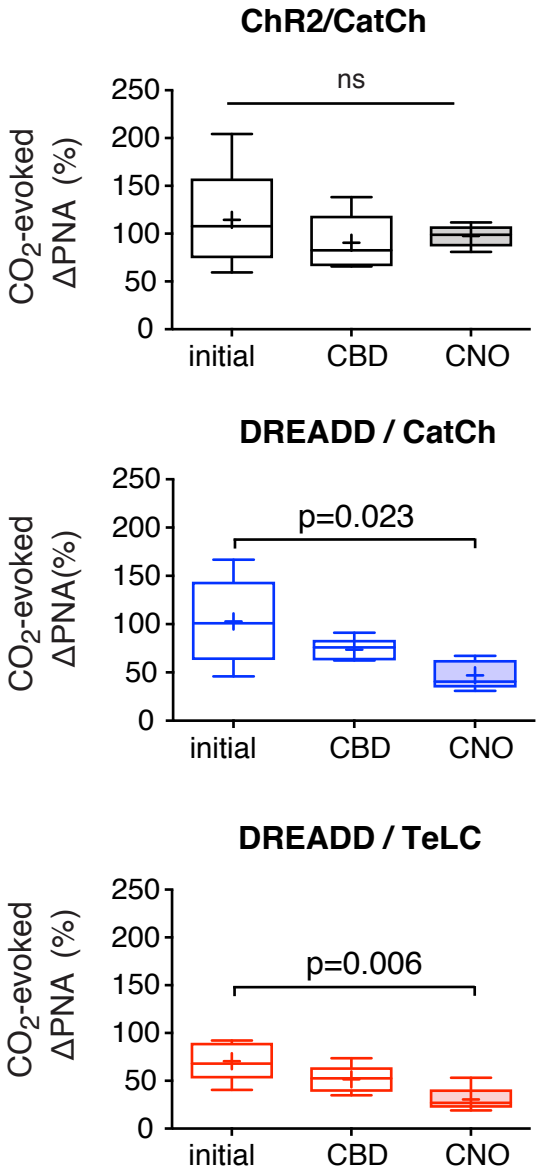

Figure 5.14| Relative contributions of RTN neurons and preBötC astrocytes to the development of CO_2-induced ventilatory response in anesthetized rats. Group data illustrating effects of inhibition of $DREADD_{Gi}$-expression RTN neurons (with CNO, 2 $mg \cdot kg^{-1}$; i.v.) and/or TeLC expression in preBötC astrocytes on CO_2-evoked increases in PNA (CO_2-evoked ΔPNA) in rats transduced to express ChR2/CatCh (*top*), DREADD/CatCh (*middle*), and DREADD/TeLC (*bottom*) (see **Figure 5.7**, **Figure 5.13** and Method section for details). Data sets without *p* values indicated are not significantly different. ns, not significant.

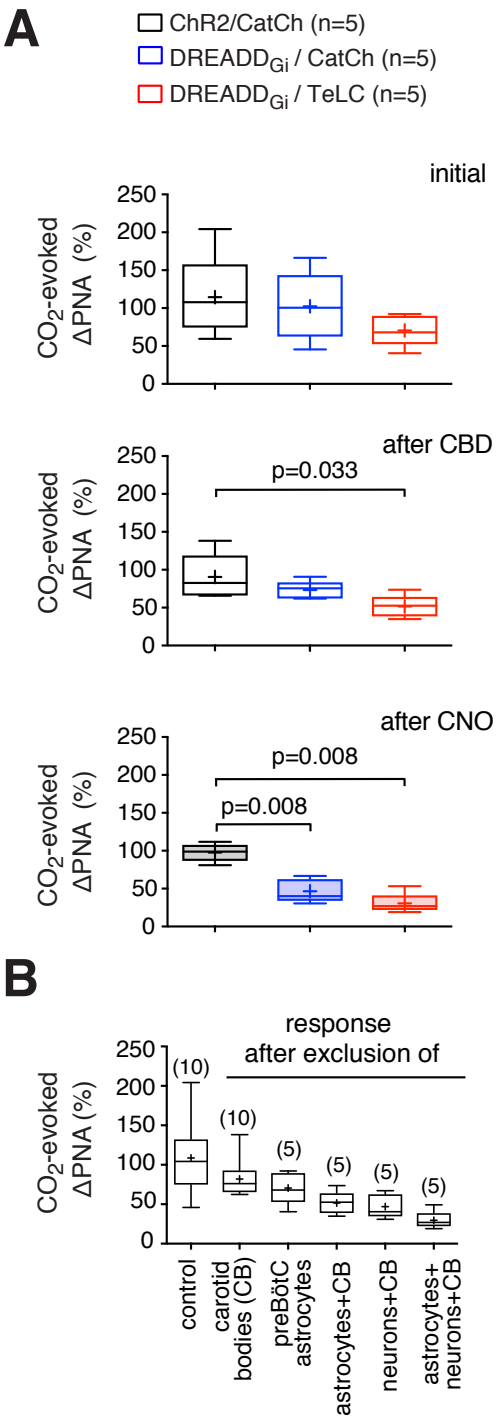

Figure 5.15| Relative contributions of carotid bodies, RTN neurons, preBötC astrocytes to the development of CO_2-induced ventilatory response in anesthetized rats. A) Summary data illustrating effects of denervation of carotid bodies (CBD) and inhibition of $DREADD_{Gi}$-expression RTN neurons (with CNO, 2 $mg \cdot kg^{-1}$; i.v.) on CO_2-evoked increases in PNA (CO_2-evoked ΔPNA) in rats transduced to express ChR2/CatCh, DREADD/CatCh, and DREADD/TeLC (see **Figure 5.7**, **Figure 5.13** and Method section for details). **B**) relative contribution of carotid bodies, preBötC astrocytes and RTN neurons the overall CO_2-evoked ventilatory response in anesthetized rats. Data sets without *p* values indicated are not significantly different.

*5.2.3.7. **Summary***

Our data confirmed the previous report [88] that the relative contribution of carotid bodies to the total CO_2-evoked ventilatory response is about 25%. In addition, we have provided evidence for the important role of preBötC astrocytes in CO_2-evoked increases in ventilation. Moreover, our data also suggest that, quantitatively, the relative contribution of these astrocytes to the overall central CO_2 chemosensitivity is equal to that of RTN neurons. In addition, we further provide evidences that a separate component of the CO_2 drive (~ 25%) should arrive from the chemosensitive cells located in other parts of the brainstem [214], [215], though we cannot exclude contributions from RTN neurons that were not transduced to express $DREADD_{Gi}$ or preBötC astrocytes that were not expressing TeLC.

5.3. The effect of blockade of signaling pathways in preBötC astrocytes on exercise capacity.

5.3.1. Introduction

The respiratory system rapidly adapts to ever-changing behavioral and environmental conditions to ensure an appropriate supply of metabolic substrates to, and removal of metabolic waste products from, all tissues of the body. To match O_2 and glucose delivery to increased metabolic demands during exercise, ventilation and cardiac output are controlled by several physiological feedforward and feedback mechanisms. In response to moderate exercise (constant work-load), cardiorespiratory changes develop in 3 distinct phases (**Figure 5.16).** Phase 1- an initial rapid increase in cardiorespiratory output that precedes increases in oxygen demand: Phase 2- a gradual increase in ventilation and cardiac output: Phase 3 - a plateau phase of elevated cardiorespiratory output, as steady state exercise is reached [6], [216], [217]. The rapid increase in cardiorespiratory output (Phase 1) occurs too soon after the onset of exercise to involve metabolic feedback, and can even occur prior to exercise [217]–[219]. During Phase 1, descending cortical feed-forward and/or muscle reflex mechanisms increase ventilation and cardiac output in anticipation of, and during the initial phases of, exercise [220]–[223]. Feedback signals from muscle stretch/metabolic receptors and possibly central and peripheral chemoreceptors are responsible for the gradual increases in (Phase 2), and maintenance of (Phase 3), enhanced cardiorespiratory activity during continued exercise ([224], [225]. During steady state exercise (Phase 3), the rise in ventilation (V_E) in proportional to O_2 uptake and CO_2 excretion, however, in heavy exercise, V_E continues to increase until exhaustion [226]. The mechanisms responsible for increases in V_E proportionally to the increase in metabolic rate during exercise are not fully known.

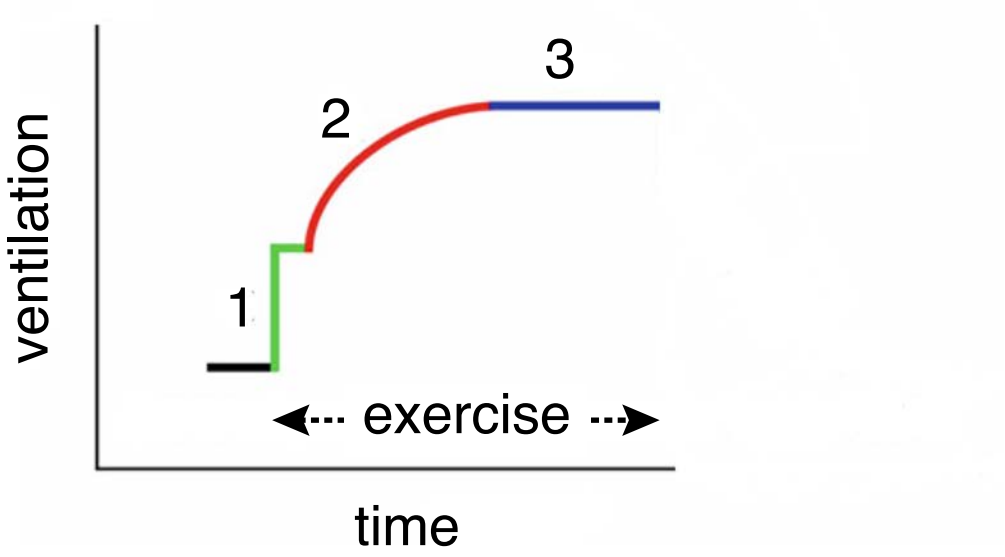

Figure 5.16| Time course of the ventilatory response during moderate exercise. Phase 1 (green) represents the rapid initial increase in ventilation. Phase 2 (red) represents the gradual increase into steady-state levels of ventilation that are achieved in phase 3 (blue) [Adapted from [6]].

Putative chemosensitive neurons of RTN play an important role in the mechanisms of central respiratory response to CO_2 [32], [33]. There is also evidence that the RTN is critically important for the control of expiratory activity [31], [53], [55], and that these neurons are activated during exercise [227]. Thus, one of the aims of the experiments described in this chapter was to define the role of the RTN neurons in determining the exercise capacity. In addition, results presented in sections 5.1 and 5.2 also suggested that astroglial control of breathing at the level of the preBötC may become particularly important when higher metabolic demand (such as during physical activity and exercise) must be supported by enhanced respiratory effort. To test these hypotheses, preBötC astrocytes were targeted to express either TeLC or dnSNARE, and RTN neurons were targeted to express the $DREADD_{Gi}$ receptor. The effects of blocking vesicular release mechanisms in preBötC astrocytes and/or inhibiting RTN neurons on exercise capacity were determined.

5.3.2. Material and Methods

5.3.2.1. In vivo gene transfer

60–80 g male Sprague-Dawley rats were anesthetized, and the RTN area received microinjections of the $DREADD_{Gi}$-mCitrine or control (ChR2-EGFP) viral vectors. 2-3 weeks after the first injection, rats received a second bilateral injection of AVV-sGFAP-EGFP-TeLC or control vector (AVV-sGFAP-CatCh-EGFP) targeting preBötC. In some experiments, adult rats (250–280 g) just received bilateral viral injections to express either TeLC or dnSNARE in preBötC astrocytes.

5.3.2.2. Measurements of exercise capacity

Exercise capacity of experimental rats was determined in a forced exercise experimental paradigm using a single lane rodent treadmill. The distance covered by the animal was recorded, and exercise capacity was expressed as work done in Joules (kg m^{-2} s^{-2}). Biotelemetry was used to record the systemic arterial blood pressure and heart rate in exercising animals.

5.3.3. Results

5.3.3.1. Measurements of exercise capacity

Bilateral expression of dnSNARE or TeLC in preBötC astrocytes resulted in a marked reduction of exercise capacity by 57% (0.5 ± 0.1 KJ *vs* 1.1 ± 0.2 KJ in controls; n = 5, p=0.016) and 42% (0.7 ± 0.1 KJ *vs* 1.2 ± 0.1 KJ in rats expressing CatCh (controls); n=9, p<0.001), respectively (**Figure 5.17**). $DREADD_{Gi}$ expression in the RTN/preBötC *per se* had no effect on exercise capacity (1.26 ± 0.12 KJ vs. 1.24 ± 0.09 KJ in rats expressing ChR2/CatCh (control), n = 5 per group, p = 0.99). Inhibition of RTN neurons by application of CNO (2 $mg \cdot kg^{-1}$; i.p.) in rats

expressing $DREADD_{Gi}$/CatCh decreased exercise capacity by 58% (0.50 ± 0.08 KJ vs. 1.19 ± 0.08 KJ in control, n = 5 per group, p <0.001) (**Figure 5.18**). Inhibition of RTN neurons with CNO in rats expressing TeLC in preBötC astrocytes (DREADD/TeLC) resulted in a dramatic reduction of exercise capacity by ~ 78% (0.28 ± 0.03 KJ vs 1.25 ± 0.09 KJ in control, n = 5 per group, p = 0.004; **Figure 5.19**)

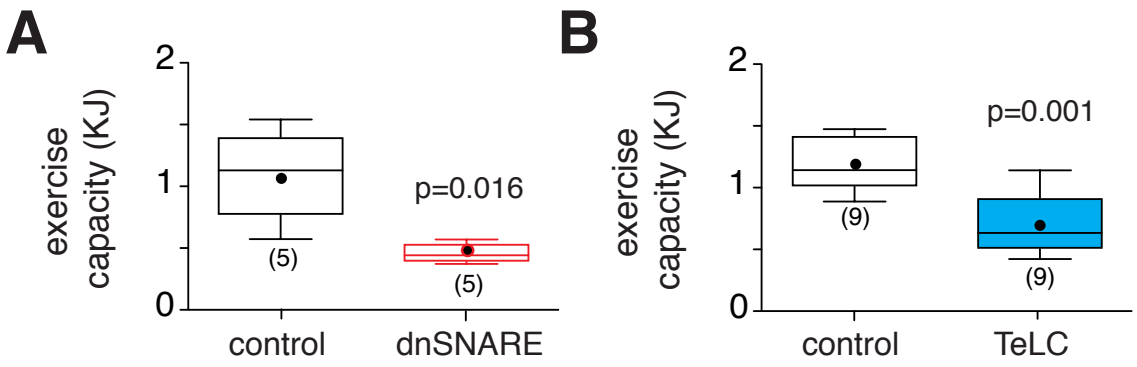

Figure 5.17| Astrocyte signaling within the preBötC preBötC determines exercise capacity. Summary data illustrating the effects of dnSNARE (**A**) or TeLC (**B**) expression in preBötC astrocytes on exercise capacity.

5.3.3.2. Measurements of cardiovascular response to exercise

Since major sources of central sympathetic drive that are critically important for cardiovascular control (C1 neurons) and breathing (preBötC neurons) are anatomically close to each other in the brainstem, using biotelemetry, we measured increases in heart rate and systemic arterial blood pressure during exercise in rats expressing TeLC or CatCh (control) in preBötC astrocytes. It was found that cardiovascular responses to exercise were not affected by TeLC expression (**Figure 5.20**), suggesting that the impaired exercise capacity is due to the respiratory, not a circulatory deficit.

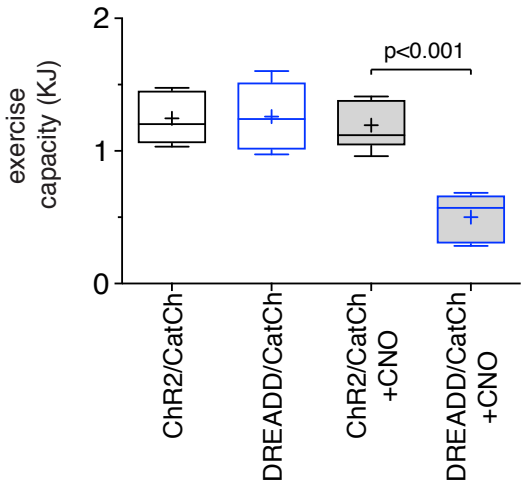

Figure 5.18| Inhibition of RTN neurons reduced exercise capacity in rats. Exercise capacity is unaffected by CNO in rats transduced to express ChR2/CatCh (control; n=5). However, application of CNO (2 mg.Kg^{-1}, i.p.) markedly reduced exercise capacity in rats transduced to express DREADD$_{Gi}$ by the RTN neurons (DREADD/CatCh; n=5).

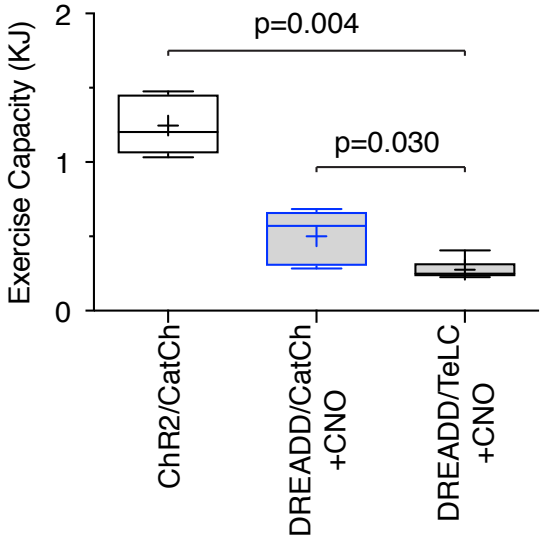

Figure 5.19| Relative contributions of RTN neurons and preBötC astrocytes to the overall exercise capacity in rats. Application of CNO (2 mg.Kg^{-1}, i.p.) further reduced exercise capacity in rats transduced to express DREADD/TeLC when compared to rats expressing ChR2/CatCh (n=5) or DREADD/CatCh (n=5).

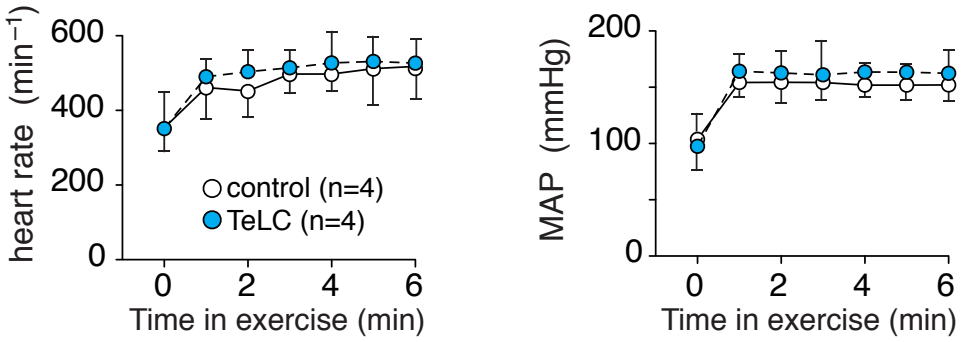

Figure 5.20| TeLC expression in preBötC astrocytes had no effect on the cardiovascular responses to exercise. MAP – mean arterial blood pressure.

5.3.4. Summary

The results presented in this chapter suggest that preBötC astrocytes are functionally specialized CNS chemosensors, critically contributing to the development of the respiratory responses to systemic hypoxia and hypercapnia. PreBötC astrocytes contribute to the overall respiratory response to hypoxia to ensure appropriate oxygenation of the arterial blood. Quantitatively, their contribution to the magnitude of the respiratory response to hypoxia appears to be similar to the contribution of the carotid body chemoreceptors. PreBötC astrocytes also contribute to the respiratory response to systemic hypercapnia. Their relative contribution to the overall hypercapnic inspiratory (phrenic) response appears to be similar to that of RTN neurons. Blockade of vesicular release mechanisms in preBötC astrocytes and inhibition of the RTN neurons are associated with similar reductions in exercise capacity.

Therefore, experiments described in this Chapter addressed the following Aim of the thesis:

> Aim 4. To determine the effect of activation and blockade of signaling pathways in preBötC astrocytes on breathing behavior during hypoxia, hypercapnia, and exercise in conscious rats.

Collectively, the data obtained indicate that astrocytes are able to control the activities of vital rhythmic motor circuits with a significant impact on motor behavior *in vivo*. The role of preBötC astrocytes becomes especially important in conditions of enhanced metabolic demand such as systemic hypoxia, hypercapnia, and exercise when homeostatic adjustments of breathing are critical to support physiological and behavioral demands of the body

Chapter 6 **DISCUSSION**

In mammals (and most other land animals.), breathing is generally defined as the movement of the air in and out of the lungs, to maintain the arterial PO_2, PCO_2, and pH within physiological ranges. This apparently simple rhythmic movement is a complex behavior, involving repeating cycles of inspiration and expiration. The current theory of how the basic rhythm and pattern of breathing are generated is centered around functionally distinct neuronal cell groups in the medulla oblongata and pons that drive and modulate rhythmic breathing [12], [37].

It is now accepted that the inspiratory rhythm is generated endogenously by the preBötC [12], [14], located bilaterally in the ventrolateral medulla oblongata. The essential preBötC neurons implicated in the generation of normal breathing are functionally (and likely molecularly) heterogeneous [12], [42], as there are subpopulations of excitatory and inhibitory neurons with electrophysiological characteristics that have distinct functions during breathing cycles [18].

In vitro experiments with rodent brainstem tissue slices [138], [202] have suggested that astrocytic signaling may drive the activity of circuits producing motor rhythms including those within the preBötC [138]. Yet it remains unknown whether preBötC astrocytes can directly control motor circuits and whether such control is functionally important for normal rhythmic motor behavior *in vivo*. The morphological features of astrocytes in this critical brainstem region are also unknown. In this dissertation, we have investigated the role of preBötC astrocytes in the control of breathing. We also employed computer-based reconstruction of GFAP-immunoreactive astrocytes in several brainstem regions associated with the respiratory function of adult rats to characterize astrocyte morphology.

6.1.1. Morphometric analysis of astrocytes in brainstem respiratory regions

Astrocytes have been proposed to modulate activities of autonomic and respiratory circuits in several regions of the brainstem via release of gliotransmitters including in the preBötC [71], [138], [139], [197], RTN [5], [143], [144], [228], [229], and NTS [139], [230], however, the morphological features of astrocytes in respiratory-related brainstem regions were not been examined. We have shown that, morphologically, preBötC astrocytes are more complex compared to the neighboring astrocytes residing within other distinct functional regions of the NTS and IRf. Specifically, cellular processes of preBötC astrocytes are longer and have more branches compared to that of astrocytes residing within the other medullary regions. PreBötC astrocytes are found to be larger, i.e., they have greater volume and surface area when compared to astrocytes residing within NTS and IRf. The morphological differences that were observed, despite the similar distribution of blood vessels in the abovementioned regions, suggest that astrocytes in the brainstem have intrinsic regional specificities.

6.1.1.1. Immunohistochemical labelling and reconstruction of regional astrocyte morphology

We employed GFAP immuno-labeling to delineate features of astrocytic morphology for reconstruction. GFAP belongs to the family of intermediate filament proteins that are mainly expressed in protoplasmic and specialized CNS astrocytes [231], [232]. This structural protein is one of the fundamental components of the astroglial cytoskeleton and plays a critical role in the formation of the complex processes of astroglia [233]–[236].

Other astroglial markers such as S100β, vimentin, glutamine synthetase, and glutamate transporters (such as GLAST or GLT) have been used to study astroglial properties [237]. However, S100β and glutamine synthetase immunostaining is mainly localized to the cytoplasm of astrocytes, and may weakly label cellular processes [238]. Moreover, glutamine synthetase is expressed in oligodendrocytes and neurons as well as astrocytes [239], [240]. Although vimentin is also a good

marker for analyzing the morphology of astrocytes, it is primarily expressed in developing (i.e., immature) glia cells [241], [242]. GLAST or GLT immunostaining is also not suitable for morphometric analysis of astrocytic processes [243], since only low-quality images can be acquired [244]. SOX9 is another astrocytic specific marker that can be used to identify astrocytes in the adult brain [245], but SOX9 labels the nucleus and provides no information about projected processes. Additionally, a previous report stated that quantifying the morphology of hippocampal astrocytes when either filled with lipophilic dyes (which uncover the fine cellular processes) or immunostained with anti-GFAP antibody (which does not reveal fine processes of astrocytes), there were no significant differences observed between measurements of dye-filled or GFAP-stained astrocytes *in vitro* [246]. Therefore, GFAP immunostaining of astrocytes is considered to be a reliable method to identify the major cellular processes of mature astrocytes. As a control to show that the GFAP antibody is equally effective in staining GFAP in different astrocytes, I randomly used two different anti-GFAP antibodies, namely a polyclonal rabbit anti-GFAP antibody and a cy3-conjugated monoclonal mouse anti-GFAP antibody. There were no differences in morphometric analysis of astrocytes immunostained with either of these antibodies. Also, for comparative analyses of GFAP-positive astrocytes, the brains used were fixed with the identical protocol and solutions, processed at the same time, and developed in the identical immunostaining solution for the same period of time to standardize labeling. In addition, images used for morphological reconstruction were acquired for the different regions of interest from *a single brainstem section* to assure standardized conditions for immunostaining and image acquisition.

It has been estimated that GFAP-positive processes occupy about 15% of the total volume of the astrocyte, and many of the smaller astrocytic processes are GFAP-negative [124], [189], [247], which is a potential limitation of our approach. Thus, in order to estimate the total volume occupied by the reconstructed astrocyte processes, a 3D Convex Hull analysis was performed to provide a metric of the volume occupied by the astrocytic process fields, which presumably would encase much of the field of fine processes not stained by GFAP.

6.1.1.2. Astrocyte morphometric properties

The data presented here suggest that morphologically, preBötC astrocytes have larger (have higher Convex Hull volume) and are structurally more complex (higher Complexity Index) than astrocytes residing within the other functionally distinct neighboring brainstem regions of IRf, or the more distant NTS region. Specifically, preBötC astrocytes have longer processes, more branch points, and more nodes, when compared to the NTS or IRf astrocytes.

The underlying structural/functional reasons for these regional morphological differences is presently unclear, but morphological features could reflect constraints imposed by arrangements of associated neurons and/or blood vessels. We have not analyzed the regional somato-dendritic morphology of neurons in relation to astrocyte morphology, but we analyzed the morphology of local vasculature since it is well known that astrocytes are intimately associated with brain parenchymal blood vessels. Thus, the morphological differences between the brainstem astrocytes could reflect architectural features of the local vasculature. We found, however, that the arrangement of blood vessels in terms of their average volume and surface area in the brainstem regions studied was not different (see **Figure 3.9**).

6.1.2. Physiological experiments in preBötC astrocytes *in vivo*

In conscious adult rats, genetic targeting preBötC astrocytes with adenoviral vectors to express either TeLC or dnSNARE effectively blocked the mechanisms of vesicular release in transduced astrocytes. Bilateral expression of either TeLC or dnSNARE in preBötC astrocytes reduced the resting respiratory rate (f_R) and made the inspiratory rhythm more regular. Moreover, the frequency of functionally important augmented breaths (sighs), produced by increased inspiratory effort was also reduced in rats transduced to express TeLC or dnSNARE in preBötC astrocytes. Bilateral expression of either transgene in preBötC astrocytes also decreased the breathing frequency responses to systemic hypoxia and hypercapnia. Since TeLC or dnSNARE expression in astrocytes likely compromises exocytosis of several putative gliotransmitters including ATP, we then determined the specific

contribution of ATP-mediated signaling by facilitating the extracellular breakdown of ATP within the preBötC by virally-driven expression of a potent ectonucleotidase, transmembrane prostatic acid phosphatase (TMPAP). We showed that bilateral expression of TMPAP in the preBötC significantly reduced resting f_R, sigh frequency, and hypoxic ventilatory response in conscious rats. We also hypothesized that stimulation of preBötC astrocytes *in vivo* [through facilitated Ca^{2+}-dependent release of ATP (possibly via recruitment of phospholipase C pathway)] may increases the activity of the inspiratory rhythm-generating circuits. To test this hypothesis, preBötC astrocytes were transduced to express a Gq-coupled Designer Receptor Exclusively Activated by Designer Drug ($DREADD_{Gq}$), which exhibit a clear level of constitutive activity (i.e., in the absence of ligand). Bilateral expression of $DREADD_{Gq}$ in the preBötC significantly increased resting f_R and sigh frequency in conscious rats.

6.1.2.1. The Effect of Activation and Blockade of Signaling Pathways in PreBötC Astrocytes on Breathing in Conscious Behaving Rats.

6.1.2.1.1. Specificity of viral vectors with enhanced GFAP promoter

Here viral vectors with enhanced GFAP promoter were used to drive the expression of the genes of interest in the brainstem astrocytes of adult rats. In the brainstem, GFAP expression is always very strong implying high activity of GFAP promoter in this region, which helped us to effectively drive viral transgene expression under the control of this promoter. The specificity of viral constructs based on the use of enhanced GFAP promoter was described in Chapter 2 . Moreover, here, adenoviral vectors were used to deliver the genes of interest, and even in the adeno-associated virus (AAV) backbone (which has a heavily biased gene expression toward neurons as the AAV transduction efficiency of neurons is many times greater than that of glia), GFAP promoter provided expression specificity in the brainstem astrocytes of >95% [164].

6.1.2.1.2. TMPAP expression was almost exclusively confined to astroglial

The pattern of TMPAP expression in the brainstem confirmed previous observation that this construct preferentially targets astrocytes [167]. Although the primary hypothesis is that vesicular release of ATP from astrocytes provides tonic activation of the inspiratory rhythm-generating circuits of the preBötC, the data obtained cannot discriminate the cellular origin of ATP, as it can be released by neurons, astrocytes, microglia and potentially pericytes [248]–[250].

6.1.2.1.3. Regulation of brainstem respiratory rhythm-generating circuits by astrocytes

All three approaches (expression of dnSNARE in astrocytes, expression of TeLC in astrocytes, and TMPAP expression in the preBötC region) resulted in quantitatively similar changes in resting respiratory activity. On the other hand, bilateral expression of $DREADD_{Gq}$ (which exhibit some level of constitutive activity) in preBötC astrocytes was associated with a higher f_R and increased irregularity of inspiratory rhythm. These data strongly suggesting that tonic vesicular release of ATP by brainstem astrocytes provides excitatory drive to the respiratory rhythm-generating circuits.

6.1.2.1.4. Role of preBötC astrocytes in modulation of sigh generation

There is recent evidence that generation of sighs is facilitated by the actions of bombesin-like peptides [251] and inhibited when astroglial function is compromised [252], suggesting that sigh generation may be modulated by signaling molecules released by preBötC astrocytes in response to various stimuli, including locally released bombesin-like peptides. In fact, we found that bombesin triggers robust $[Ca^{2+}]_i$ responses in cultured brainstem astrocytes. Bilateral expression of TeLC or dnSNARE in the preBötC significantly reduced sigh frequency in conscious rats. On the other hand, in conscious rats, bilateral expression of $DREADD_{Gq}$ in preBötC

astrocytes was associated with an increase in sigh frequency. Together these data suggest that at rest, vesicular release of gliotransmitters(s) (most likely ATP) by preBötC astrocytes modulates the generation of sighs (functionally important augmented breaths). In addition, blockade of vesicular release mechanisms in preBötC astrocytes (dnSNARE expression), in anesthetized adult rat, reduces the effect of bombesin on sigh frequency by >60% (**Figure 4.17**). These data support the hypothesis that the actions of bombesin-like peptides within the preBötC [251] are (at least in part) mediated by astrocytes.

6.1.2.2. activation and blockade of signaling pathways in preBötC astrocytes on breathing behavior during systemic hypoxia in conscious rats.

Decreased PO_2 activates astrocytes that is associated with increased exocytosis of putative ATP-containing vesicles [71]. Hypoxia-induced fusion of these vesicles in astrocytes appears to recruit SNARE proteins sensitive to cleavage by tetanus toxin [71]. In section 5.1, to determine the physiological significance of this mechanism of astroglial O_2 sensitivity, two different strategies were employed to interfere with astroglial signaling pathways. First, to block the mechanisms of vesicular exocytosis, astrocytes were targeted to express either TeLC or dnSNARE. Second, to promote the rapid breakdown of the vesicular and released ATP in the preBötC, an LVV was used to drive the expression of a potent ectonucleotidase TMPAP [166]. We found that the central stimulatory effect of hypoxia on breathing appears to be largely mediated by astroglial ATP release, which acts within a restricted region of the brainstem that embraces the respiratory rhythm-generating circuits. It is also possible that direct sensitivity of the respiratory neurons to the decreases in PO_2 contributes to the hypoxic ventilatory response. Indeed, a number of studies performed using *in vitro*, *in situ*, and in anesthetized animal models reported that the brainstem respiratory and cardiovascular control circuits are sensitive and activated in response to oxygen deprivation [78], [79], [207]–[209]. Despite this significant evidence, the existence of a functional CNS oxygen sensor capable of stimulating breathing is not accepted universally, perhaps reflecting questions about the physiological relevance of the hypoxia-evoked responses observed in the reduced

preparations and the results obtained in anesthetized animal models. Indeed, in section 5.1, we confirmed that the respiratory responses to hypoxia in peripherally chemodenervated rats are reduced dramatically when the animals are anesthetized, suggesting that the mechanism(s) and/or signaling pathway(s) of central respiratory oxygen sensitivity are very sensitive to general anesthesia.

Previous studies performed in non-anesthetized mammals (but not humans) showed significant hypoxic ventilatory responses after denervation (or silencing) of the peripheral oxygen chemoreceptors [70], [72]–[74] and support the existence of a functional central oxygen sensor capable of stimulating breathing [for recent review see [76]]. Data presented in Chapter 4 (and the recent publications [71], [141]) point toward an important role of preBötC astrocytes in central O_2 sensitivity as well as the hypoxic ventilatory response. PreBötC astrocytes sense hypoxia (in a mitochondrial-dependent sensing mechanism [71]), release ATP (involving exocytotic vesicular release mechanism [71]), and excite the respiratory network (most likely via activation of $P2Y_1$ receptors [141]).

We also found that the hypoxic ventilatory response was lower in rats transduced to express $DREADD_{Gq}$ in preBötC astrocytes when compared to the control group. It is possible that over activation in PLC pathways preBötC astrocytes (via expression of $DREADD_{Gq}$) leads to depletion of ATP vesicles that normally are used during hypoxia, which may lead to an impaired augmentation of breathing during hypoxic challenge. Application of CNO did not change the decreased hypoxic ventilatory response in rats transduced to express $DREADD_{Gq}$ in preBötC astrocytes, which suggests that the activity of transmitter release mechanisms is already saturated in these astrocytes by constitutive activity of the $DREADD_{Gq}$.

6.1.2.3. <u>The effect of activation and blockade of signaling pathways in preBötC astrocytes on breathing during hypercapnia in conscious rats.</u>

In Chapter 5, by removing inputs from the peripheral (carotid body) and putative central CO_2 chemoreceptors (RTN), we determined the role of preBötC astrocytes in the development of the respiratory response to hypercapnia. The data obtained

suggest that preBötC astrocytes play an important role in the CO_2 chemosensory control of breathing in adult rats, as interfering with vesicular release mechanisms in preBötC astrocytes led to decrease in augmentation of CO_2-evoked f_R, but not CO_2-evoked V_T.

It also was found that in conscious rats, inhibition of $DREADD_{Gi}$-expressing neurons in the RTN had no effect on respiratory activity at rest (**Figure 5.12**), but significantly decreased the respiratory response to increases in the level of inspired CO_2 by decreasing the tidal volume (V_T), as reported before [32], [55], [253]. However,

Post hoc immunostaining of the brainstems transduced to express $DREADD_{Gi}$-mCitrine in the RTN showed that ~1500 neurons expressed the transgene in the ventrolateral brainstem, including the RTN. Although we amplified the viral expression by immunohistochemical detection of mCitrine, it is possible, that still we may have underestimated the actual transduced neurons. However, since application of CNO almost completely abolished active expirations [measured by abdominal electromyogram (EMG_{ABD}, **Figure 5.7**)], this physiological evidence suggests that a critical number of key RTN neurons were clearly transduced.

Analysis of the distribution of the EGFP-positive neurons revealed that the majority of the transduced neurons are located near the ventral surface at the medial RTN/pFRG region [59] and display anatomical features of the chemosensitive RTN neurons [86]. Some GFP-labeled neurons were also found caudal to the facial nucleus in the ventrolateral medulla, where catecholaminergic C1 neurons are distributed [254]. However, immunohistochemical staining of tyrosine hydroxylase–positive (C1) neurons revealed no co-labeling of GFP^+ and TH^+ cells, which is consistent with the data reported previously that AAV2 vectors have a lower affinity towards TH neurons in the rat's brainstem [38]. It has been also shown that hSyn promoters are less active in catecholaminergic neurons of substantia nigra [255]. In this context, even if a small number of TH^+ neurons are transduced to express $DREADD_{Gi}$ transgene and concomitantly inhibited by CNO, their contributions to the CO_2-evoked expiratory activities are small since the inspiratory responses elicited by the RTN neurons are not dependent on the activity of C1 neurons [32], [256], [257]. Moreover, it has been reported that C1 neurons in RTN

are important in transmitting some of the acute respiratory response produced by stimulation of carotid body [257]. However, in our experimental protocol, we have inhibited $DREADD_{Gi}$ expressing RTN neurons after minimizing effects of the carotid bodies (i.e. placing conscious animals in 60% O_2 to decrease the drive from the peripheral chemoreceptors or bilateral denervation of the carotid bodies in anesthetized preparations), thus the deficit in CO_2-evoked respiratory response after inhibition $DREADD_{Gi}$ expressing neurons with CNO is most likely due to inhibition of RTN neurons, rather than C1 neurons.

In vagotomized, carotid body-denervated urethane-anesthetized rats *in vivo*, we have shown that inhibition of RTN neurons decreased inspiratory drive in hypercapnia (decrease in ΔPNA) by ~ 50% – similar to the effect of blocking vesicular release mechanisms from preBötC astrocyte. Based on these data, it is possible that the RTN neurons and the preBötC astrocytes employ separate pathways to augment the ventilatory response during hypercapnia. Although, preBötC has neuronal H^+/CO_2 sensing mechanisms [96], [97], results presented in this section suggested that preBötC astrocytes are important for the development of the appropriate respiratory responses to hypercapnia.

The provided evidence show that preBötC astrocytes are critically involved in the CO_2-evoked augmentation of breathing, in which this contribution is quantitatively similar to the effect of RTN neurons. In ventilatory response to hypercapnia, as opposed to RTN neurons that contribute to augmentation of tidal volume, preBötC astrocytes affect the breathing rate – maybe by altering the excitability of the preBötC network or recruiting more respiratory neurons to participate in the hypercapnic ventilatory response. Earlier studies suggested a role for astroglial in CO_2/pH detection and central chemosensitivity [5], [100], [142], [144], [147], [229] in the RTN and NTS [111], [143], [258], [259]. These scattered CO_2-sensitive astrocytes and neurons [260] in RTN, NTS, and preBötC provide further evidence for the idea of the widely distribution of chemoreception in the medulla (Nattie, 1999, 2000, 2001; Thomas and Spyer, 2000; Nattie and Li, 2009).

6.1.2.4. <u>The effect of blockade of signaling pathways in preBötC astrocytes on</u>

exercise capacity.

Together data presented in Chapter 4 and Chapter 5 indicate that astrocytic signaling provides ongoing excitation of preBötC respiratory circuits that regulates the inspiratory rhythm, underlies generation of sighs, and shapes respiratory responses to physiological challenges such as hypercapnia and hypoxia. Based on these results, we hypothesized that astroglial control of breathing might become particularly significant during physical activity when increased oxygen demand requires augmented respiratory effort. Accordingly, we determined whether compromised vesicular release mechanisms in preBötC astrocytes in adult rats impairs the ability to exercise in an experimental model of forced treadmill exercise. Bilateral transduction of preBötC astrocytes with TeLC or dnSNARE resulted in premature fatigue, and dramatically reduces exercise capacity. Cardiovascular responses to exercise (increases in heart rate and systemic arterial blood pressure) were not affected by TeLC expression in preBötC astrocytes, suggesting that the impaired exercise capacity is due to a respiratory, not a circulatory, deficit.

Physical exertion is essential for the survival of all animals, whether it be to avoid predators, escape natural disasters, or any other circumstances that require explosive power or endurance. Large increases in metabolic demand associated with surges in muscular effort, require an increase in the delivery of oxygen and metabolic substrates and removal of waste products, e.g., CO_2 and lactate. Mammals have developed several physiological feedforward and feedback mechanisms to ensure that metabolic demands of working muscles are met. Here, we tested the hypothesis that RTN neurons and preBötC astrocytes are critically involved in defining exercise capacity.

We found that in rats, acute silencing of RTN neurons is associated with a dramatic (~ 60%) reduction in exercise capacity. Since our viral injections did not transduce catecholaminergic C1 neurons (no co-localization of $DREADD_{Gi}^{+}$ and TH^{+} cells were observed; section 5.3), it is possible that this reduction in exercise capacity was due to inability to mount an appropriate respiratory response. Critical involvement of RTN neurons in defining exercise capacity is in line with the proposed role of RTN neurons in respiratory control system, in which they provide a powerful drive during active breathing [55], [59], [253], during systemic

hypercapnia [32], [86], [108], [144], or when brain lactate concentration increases [261]. RTN neurons receives inputs from the peripheral respiratory chemoreceptors, other respiratory groups of the brainstem [21], and may function as an integrative center of respiration [100], [262] to increase breathing rate during *heavy exercise*.

Similarly, disruption of vesicular release mechanisms in preBötC astrocytes remarkably decreased the exercise capacity by ~ 60%. The mechanism by which preBötC astrocytes affect exercise capacity is not known. During heavy exercise, V_E increases disproportionally to O_2 uptake, which leads to increase in PO_2 and decrease in PCO_2 from their values at rest. This increase in PO_2 might generally reduce the tonic activity and responsivity of carotid bodies [217], [263], and as we have shown in the previous section, the role of preBötC astrocytes in modulation of V_E become more important when peripheral input from carotid bodies are decreased (**Figure 5.3**).

Maximal exercise leads to an increase in concentration of adenosine, norepinephrine (NE), extracellular $[K^+]$, and maybe other chemicals in the brain [217], [219], [264], [265]; NE, K^+, and adenosine can activate astrocytes [120], [266]–[269]. Thus, it is possible that interfering with vesicular releasing mechanisms of preBötC astrocytes leads to inappropriate respiratory response during exhausting exercise. Moreover, recent data indicated that ATP level is maintained constant during heavy exercise [270], and since astrocytes are the main source for extracellular ATP, it is plausible that by blocking release mechanisms in preBötC astrocytes (by expressing TeLC or dnSNARE), the local concentration of ATP is decreased. In Chapter 4 , we showed that activity of the preBötC respiratory circuits are modulated by release of ATP from local astrocytes; thus, blocking this release (by expressing TeLC or dnSNARE) may markedly decrease the exercise capacity of these rats.

Moreover, to meet metabolic demands of preBötC neurons, it is also possible that preBötC astrocytes locally release lactate during heavy exercise. In fact, it has been shown that despite the protection of brain from lactate by the blood brain barrier [271], CNS lactate level increases in heavy exercise [270]. In the brain, astrocytes provide lactate as an energy source to neurons to maintain their functions. Thus, it is likely that disruption of the normal function of preBötC astrocyte by

expressing dnSNARE or TeLC, might have some effect on providing energy resource (lactate) to preBötC neurons. More experiments are required to explain how preBötC astrocytes affect exercise capacity.

On the treadmill, all rats were able to begin running. However, interfering with vesicular release mechanisms in preBötC astrocytes or inhibiting RTN neurons markedly affects sustain physical activity. Thus, the RTN neurons and preBötC astrocytes do not appear to receive process feedforward inputs responsible for rapid increases in respiratory activity at the onset of physical exertion. The importance of the RTN neurons and preBötC astrocytes only became apparent when the maintenance of enhanced respiratory effort became contingent on feedback mechanisms [222], [223]. We have also provided evidence that disrupting vesicular release mechanism of gliotransmitters in preBötC astrocytes and silencing RTN neurons resulted in quantitatively similar reductions in the magnitude of exercise capacity (**Figure 5.17**and **Figure 5.18**). In addition, interfering with *both* astrocytic release mechanisms and activity of RTN neurons further decreased the exercise capacity by ~ 80% (**Figure 5.19**), which suggests that preBötC astrocytes and RTN neurons may act in parallel in terms of their role in defining exercise capacity.

6.1.3. Conclusions and Future directions

Deciphering the functional and structural properties of the mammalian respiratory control circuits is a longstanding problem [12]. The fact that the respiratory system is ancient and primal, and other body systems cannot exist without it, makes the CNS extremely vigilant about homeostatic control of breathing. Homeostatic regulation of O_2, CO_2, and pH is a dynamic process, in which the respiratory system (in accordance with other systems) should adjust rhythm and pattern of breathing in response to internal or external metabolic demands in order to maintain a steady-state condition. Thus, it is vital for the brain to maintain rate and depth of breathing normally stable and be able to flexibly increases or decreases these variables to react to environmental stimuli or physiological demand of the body.

We have provided evidence that preBötC astrocytes are capable of regulating

the activities of the respiratory rhythm-generating circuits, and the normal function of these astroglial cells is critical for the optimum function of the respiratory system. It is suggested that variabilities in breathing ensures respiratory system sensitivity [272], [273]. In fact, disruption of either astroglial vesicular release (TeLC or dnSNARE expression) or ATP-mediated signaling (TMPAP expression) reduced breathing irregularity (i.e. decreased breathing variability). Rats exhibiting this somehow "regular breathing" were not able to mount appropriate responses to arising challenge or body demand (such as hypoxia or exercise). On the other hand, activation of preBötC astrocytes via expression of $DREADD_{Gq}$ increased the variability of breathing, and rats showing this "irregular breathing" were also not able to optimally react to a physiological challenge (hypoxia). This capacity of astrocytes to maintain an appropriate level of variability in the respiratory system seems critical for adaptability of breathing to face challenges. More experiments are needed to further explore this idea in the future.

Recent data showed that a small subpopulation of preBötC neurons appear to be dedicated to the generation of sighs in a manner associated with bombesin-related peptides [251]. Our data suggests that sigh generation may be modulated by signaling molecules released by preBötC astrocytes in response to various stimuli, including locally released bombesin-like peptides, though it is possible that astrocytes can independently regulate the sigh-generating neurons of the preBötC.

Moreover, it has been shown that a small molecularly-defined subpopulation of preBötC neurons can regulate higher order brain function (i.e., arousal state) without roles in eupneic rhythm generation, sighs, or mediating chemosensory-related adjustments of breathing pattern in freely behaving mice [274]. Therefore, it is possible that preBötC astrocytes intermingled with these neurons can also modulate this "gateway" circuit, affecting brain arousal state. Consequently, future experiments will be designed to investigate breathing behavioral changes related to arousal in rats following interfering with gliogtransmitter release mechanisms in preBötC astrocytes. Specifically, I hypothesize that expression of TeLC in preBötC astrocytes shift breathing rates toward slower breathing frequencies associated with mild arousal conditions during the acclimatization period.

In this thesis, in multifaceted experimental paradigm, contemporary chemogenetics methods, viral gene transfer, and pharmacological approaches were used to manipulate astroglial signaling mechanisms residing within respiratory rhythm generating circuits of the preBötC. Experiments presented in this thesis addressed several questions which are relevant to the current understating of the role of astrocytes in controlling rhythm-generating circuits of the preBötC at rest and during increased metabolic demand. More experiments are needed to further investigate the signaling molecules that mediate the bidirectional communication between astrocytes and neurons residing within the preBötC region, possibly by employing optogenetics and chemogenetics methods in transgenic animals.

References

[1] A. Araque, G. Carmignoto, P. G. Haydon, S. H. R. Oliet, R. Robitaille, and A. Volterra, “Gliotransmitters travel in time and space.,” *Neuron*, vol. 81, no. 4, pp. 728–739, Feb. 2014.

[2] V. Gundersen, J. Storm-Mathisen, and L. H. Bergersen, “Neuroglial Transmission.,” *Physiol Rev*, vol. 95, no. 3, pp. 695–726, Jul. 2015.

[3] N. Chen, H. Sugihara, J. Kim, Z. Fu, B. Barak, M. Sur, G. Feng, and W. Han, “Direct modulation of GFAP-expressing glia in the arcuate nucleus bi-directionally regulates feeding.,” *elife*, vol. 5, Oct. 2016.

[4] M. M. Halassa, C. Florian, T. Fellin, J. R. Munoz, S.-Y. Lee, T. Abel, P. G. Haydon, and M. G. Frank, “Astrocytic modulation of sleep homeostasis and cognitive consequences of sleep loss.,” *Neuron*, vol. 61, no. 2, pp. 213–219, Jan. 2009.

[5] A. V. Gourine, V. Kasymov, N. Marina, F. Tang, M. F. Figueiredo, S. Lane, A. G. Teschemacher, K. M. Spyer, K. Deisseroth, and S. Kasparov, “Astrocytes control breathing through pH-dependent release of ATP.,” *Science*, vol. 329, no. 5991, pp. 571–575, Jul. 2010.

[6] J. J. Greer and G. D. Funk, “Respiration,” in *Neuroscience in the 21st Century*, D. W. Pfaff, Ed. New York, NY: Springer New York, 2013, pp. 1423–1462.

[7] D. E. Weese-Mayer, E. M. Berry-Kravis, and M. L. Marazita, “In pursuit (and discovery) of a genetic basis for congenital central hypoventilation syndrome.,” *Respir Physiol Neurobiol*, vol. 149, no. 1–3, pp. 73–82, Nov. 2005.

[8] N. N. Finer, R. Higgins, J. Kattwinkel, and R. J. Martin, “Summary proceedings from the apnea-of-prematurity group.,” *Pediatrics*, vol. 117, no. 3 Pt 2, pp. S47–51, Mar. 2006.

[9] D. T. Mage and M. Donner, “A Unifying Theory for SIDS.,” *Int J Pediatr*, vol. 2009, p. 368270, Oct. 2009.

[10] J. C. Smith, A. P. L. Abdala, H. Koizumi, I. A. Rybak, and J. F. R. Paton, “Spatial and functional architecture of the mammalian brain stem respiratory network: a hierarchy of three oscillatory mechanisms.,” *J Neurophysiol*, vol. 98, no. 6, pp. 3370–3387, Dec. 2007.

[11] A. L. Bianchi, M. Denavit-Saubié, and J. Champagnat, “Central control of breathing in mammals: neuronal circuitry, membrane properties, and neurotransmitters.,” *Physiol Rev*, vol. 75, no. 1, pp. 1–45, Jan. 1995.

[12] J. L. Feldman, C. A. Del Negro, and P. A. Gray, “Understanding the rhythm of breathing: so near, yet so far.,” *Annu Rev Physiol*, vol. 75, pp. 423–452, 2013.

[13] D. W. Richter and K. M. Spyer, “Studying rhythmogenesis of breathing: comparison of in vivo and in vitro models.,” *Trends Neurosci*, vol. 24, no. 8, pp. 464–472, Aug. 2001.

[14] J. C. Smith, H. H. Ellenberger, K. Ballanyi, D. W. Richter, and J. L. Feldman, “Pre-Bötzinger complex: a brainstem region that may generate respiratory rhythm in mammals.,” *Science*, vol. 254, no. 5032, pp. 726–729, Nov. 1991.

[15] H. Koizumi, N. Koshiya, J. X. Chia, F. Cao, J. Nugent, R. Zhang, and J. C. Smith, “Structural-functional properties of identified excitatory and inhibitory interneurons within pre-Botzinger complex respiratory

microcircuits.," *J Neurosci*, vol. 33, no. 7, pp. 2994–3009, Feb. 2013.

[16] B. M. Gajda, A. Y. Fong, and W. K. Milsom, "Species differences in respiratory rhythm generation in rodents.," *Am J Physiol Regul Integr Comp Physiol*, vol. 298, no. 4, pp. R887–98, Apr. 2010.

[17] G. D. Funk and J. J. Greer, "The rhythmic, transverse medullary slice preparation in respiratory neurobiology: contributions and caveats.," *Respir Physiol Neurobiol*, vol. 186, no. 2, pp. 236–253, Apr. 2013.

[18] D. W. Richter and J. C. Smith, "Respiratory rhythm generation in vivo.," *Physiology (Bethesda)*, vol. 29, no. 1, pp. 58–71, Jan. 2014.

[19] M. Dutschmann and T. E. Dick, "Pontine mechanisms of respiratory control.," *Compr Physiol*, vol. 2, no. 4, pp. 2443–2469, Oct. 2012.

[20] A. C. T. Takakura, T. S. Moreira, E. Colombari, G. H. West, R. L. Stornetta, and P. G. Guyenet, "Peripheral chemoreceptor inputs to retrotrapezoid nucleus (RTN) CO2-sensitive neurons in rats.," *J Physiol (Lond)*, vol. 572, no. Pt 2, pp. 503–523, Apr. 2006.

[21] D. L. Rosin, D. A. Chang, and P. G. Guyenet, "Afferent and efferent connections of the rat retrotrapezoid nucleus.," *J Comp Neurol*, vol. 499, no. 1, pp. 64–89, Nov. 2006.

[22] H. Herbert, M. M. Moga, and C. B. Saper, "Connections of the parabrachial nucleus with the nucleus of the solitary tract and the medullary reticular formation in the rat.," *J Comp Neurol*, vol. 293, no. 4, pp. 540–580, Mar. 1990.

[23] A. Mizusawa, H. Ogawa, Y. Kikuchi, W. Hida, and K. Shirato, "Role of the parabrachial nucleus in ventilatory responses of awake rats.," *J Physiol*

(Lond), vol. 489 (Pt 3), pp. 877–884, Dec. 1995.

[24] W. M. St John and S. C. Wang, "Integration of chemoreceptor stimuli by caudal pontile and rostral medullary sites.," *J Appl Physiol*, vol. 41, no. 5 Pt. 1, pp. 612–622, Nov. 1976.

[25] J. C. Finley and D. M. Katz, "The central organization of carotid body afferent projections to the brainstem of the rat.," *Brain Res*, vol. 572, no. 1–2, pp. 108–116, Feb. 1992.

[26] E. N. Bruce, J. Mitra, and N. S. Cherniack, "Central and peripheral chemoreceptor inputs to phrenic and hypoglossal motoneurons.," *J Appl Physiol*, vol. 53, no. 6, pp. 1504–1511, Dec. 1982.

[27] J. F. Paton, J. Deuchars, Y. W. Li, and S. Kasparov, "Properties of solitary tract neurones responding to peripheral arterial chemoreceptors.," *Neuroscience*, vol. 105, no. 1, pp. 231–248, 2001.

[28] N. Koshiya, D. Huangfu, and P. G. Guyenet, "Ventrolateral medulla and sympathetic chemoreflex in the rat.," *Brain Res*, vol. 609, no. 1–2, pp. 174–184, Apr. 1993.

[29] G. F. Alheid, W. Jiao, and D. R. McCrimmon, "Caudal nuclei of the rat nucleus of the solitary tract differentially innervate respiratory compartments within the ventrolateral medulla.," *Neuroscience*, vol. 190, pp. 207–227, Sep. 2011.

[30] J. C. Smith, D. E. Morrison, H. H. Ellenberger, M. R. Otto, and J. L. Feldman, "Brainstem projections to the major respiratory neuron populations in the medulla of the cat.," *J Comp Neurol*, vol. 281, no. 1, pp. 69–96, Mar. 1989.

[31] S. Pagliardini, W. A. Janczewski, W. Tan, C. T. Dickson, K. Deisseroth, and J. L. Feldman, “Active expiration induced by excitation of ventral medulla in adult anesthetized rats.,” *J Neurosci*, vol. 31, no. 8, pp. 2895–2905, Feb. 2011.

[32] N. Marina, A. P. Abdala, S. Trapp, A. Li, E. E. Nattie, J. Hewinson, J. C. Smith, J. F. R. Paton, and A. V. Gourine, “Essential role of Phox2b-expressing ventrolateral brainstem neurons in the chemosensory control of inspiration and expiration.,” *J Neurosci*, vol. 30, no. 37, pp. 12466–12473, Sep. 2010.

[33] P. G. Guyenet, “Regulation of breathing and autonomic outflows by chemoreceptors.,” *Compr Physiol*, vol. 4, no. 4, pp. 1511–1562, Oct. 2014.

[34] G. F. Tian, J. H. Peever, and J. Duffin, “Bötzinger-complex, bulbospinal expiratory neurones monosynaptically inhibit ventral-group respiratory neurones in the decerebrate rat.,” *Exp Brain Res*, vol. 124, no. 2, pp. 173–180, Jan. 1999.

[35] K. Ezure, “Synaptic connections between medullary respiratory neurons and considerations on the genesis of respiratory rhythm.,” *Prog Neurobiol*, vol. 35, no. 6, pp. 429–450, 1990.

[36] K. Ezure, I. Tanaka, and M. Kondo, “Glycine is used as a transmitter by decrementing expiratory neurons of the ventrolateral medulla in the rat.,” *J Neurosci*, vol. 23, no. 26, pp. 8941–8948, Oct. 2003.

[37] J. C. Smith, A. P. L. Abdala, A. Borgmann, I. A. Rybak, and J. F. R. Paton, “Brainstem respiratory networks: building blocks and microcircuits.,” *Trends Neurosci*, vol. 36, no. 3, pp. 152–162, Mar. 2013.

[38] W. Tan, S. Pagliardini, P. Yang, W. A. Janczewski, and J. L. Feldman,

"Projections of preBötzinger complex neurons in adult rats.," *J Comp Neurol*, vol. 518, no. 10, pp. 1862–1878, May 2010.

[39] S. W. Schwarzacher, J. C. Smith, and D. W. Richter, "Pre-Bötzinger complex in the cat.," *J Neurophysiol*, vol. 73, no. 4, pp. 1452–1461, Apr. 1995.

[40] S. W. Schwarzacher, U. Rüb, and T. Deller, "Neuroanatomical characteristics of the human pre-Bötzinger complex and its involvement in neurodegenerative brainstem diseases.," *Brain*, vol. 134, no. Pt 1, pp. 24–35, Jan. 2011.

[41] A. M. Lavezzi and L. Matturri, "Functional neuroanatomy of the human pre-Bötzinger complex with particular reference to sudden unexplained perinatal and infant death.," *Neuropathology*, vol. 28, no. 1, pp. 10–16, Feb. 2008.

[42] P. A. Gray, J. A. Hayes, G. Y. Ling, I. Llona, S. Tupal, M. C. D. Picardo, S. E. Ross, T. Hirata, J. G. Corbin, J. Eugenín, and C. A. Del Negro, "Developmental origin of preBötzinger complex respiratory neurons.," *J Neurosci*, vol. 30, no. 44, pp. 14883–14895, Nov. 2010.

[43] J. Bouvier, M. Thoby-Brisson, N. Renier, V. Dubreuil, J. Ericson, J. Champagnat, A. Pierani, A. Chédotal, and G. Fortin, "Hindbrain interneurons and axon guidance signaling critical for breathing.," *Nat Neurosci*, vol. 13, no. 9, pp. 1066–1074, Sep. 2010.

[44] A. Ruangkittisakul, A. Kottick, M. C. D. Picardo, K. Ballanyi, and C. A. Del Negro, "Identification of the pre-Bötzinger complex inspiratory center in calibrated 'sandwich' slices from newborn mice with fluorescent Dbx1 interneurons.," *Physiol Rep*, vol. 2, no. 8, Aug. 2014.

[45] X. Wang, J. A. Hayes, M. C. D. Picardo, and C. A. Del Negro, “Automated cell-specific laser detection and ablation of neural circuits in neonatal brain tissue.,” *J Physiol (Lond)*, vol. 591, no. 10, pp. 2393–2401, May 2013.

[46] G. F. Alheid and D. R. McCrimmon, “The chemical neuroanatomy of breathing.,” *Respir Physiol Neurobiol*, vol. 164, no. 1–2, pp. 3–11, Dec. 2008.

[47] V. C. Chitravanshi and H. N. Sapru, “Phrenic nerve responses to chemical stimulation of the subregions of ventral medullary respiratory neuronal group in the rat.,” *Brain Res*, vol. 821, no. 2, pp. 443–460, Mar. 1999.

[48] S. Iscoe, “Control of abdominal muscles.,” *Prog Neurobiol*, vol. 56, no. 4, pp. 433–506, Nov. 1998.

[49] E. Cinelli, F. Bongianni, T. Pantaleo, and D. Mutolo, “Modulation of the cough reflex by GABA(A) receptors in the caudal ventral respiratory group of the rabbit.,” *Front Physiol*, vol. 3, p. 403, Oct. 2012.

[50] D. W. Richter, “Generation and maintenance of the respiratory rhythm.,” *J Exp Biol*, vol. 100, pp. 93–107, Oct. 1982.

[51] L. Fedorko and E. G. Merrill, “Axonal projections from the rostral expiratory neurones of the Bötzinger complex to medulla and spinal cord in the cat.,” *J Physiol (Lond)*, vol. 350, pp. 487–496, May 1984.

[52] C. Jiang and J. Lipski, “Extensive monosynaptic inhibition of ventral respiratory group neurons by augmenting neurons in the Bötzinger complex in the cat.,” *Exp Brain Res*, vol. 81, no. 3, pp. 639–648, 1990.

[53] W. A. Janczewski and J. L. Feldman, “Distinct rhythm generators for inspiration and expiration in the juvenile rat.,” *J Physiol (Lond)*, vol. 570,

no. Pt 2, pp. 407–420, Jan. 2006.

[54] W. A. Janczewski, A. Tashima, P. Hsu, Y. Cui, and J. L. Feldman, “Role of inhibition in respiratory pattern generation.,” *J Neurosci*, vol. 33, no. 13, pp. 5454–5465, Mar. 2013.

[55] R. T. R. Huckstepp, K. P. Cardoza, L. E. Henderson, and J. L. Feldman, “Role of parafacial nuclei in control of breathing in adult rats.,” *J Neurosci*, vol. 35, no. 3, pp. 1052–1067, Jan. 2015.

[56] T. M. Anderson, A. J. Garcia, N. A. Baertsch, J. Pollak, J. C. Bloom, A. D. Wei, K. G. Rai, and J.-M. Ramirez, “A novel excitatory network for the control of breathing.,” *Nature*, vol. 536, no. 7614, pp. 76–80, Aug. 2016.

[57] M. Dutschmann and H. Herbert, “The Kölliker-Fuse nucleus gates the postinspiratory phase of the respiratory cycle to control inspiratory off-switch and upper airway resistance in rat.,” *Eur J Neurosci*, vol. 24, no. 4, pp. 1071–1084, Aug. 2006.

[58] M. Mörschel and M. Dutschmann, “Pontine respiratory activity involved in inspiratory/expiratory phase transition.,” *Philos Trans R Soc Lond, B, Biol Sci*, vol. 364, no. 1529, pp. 2517–2526, Sep. 2009.

[59] R. T. Huckstepp, L. E. Henderson, K. P. Cardoza, and J. L. Feldman, “Interactions between respiratory oscillators in adult rats.,” *elife*, vol. 5, Jun. 2016.

[60] J. M. Ramirez, A. Doi, A. J. Garcia, F. P. Elsen, H. Koch, and A. D. Wei, “The cellular building blocks of breathing.,” *Compr Physiol*, vol. 2, no. 4, pp. 2683–2731, Oct. 2012.

[61] C. Heymans and J. J. Bouckaert, “Sinus caroticus and respiratory reflexes,”

J Physiol (Lond), vol. 69, no. 2, pp. 254–266, Apr. 1930.

[62] C. Heymans and E. Neil, "Reflexogenic Areas of the Cardiovascular System," *British Journal of surgery*, vol. 46, no. 195, pp. 92–92, Jul. 1958.

[63] R. G. O'Regan and S. Majcherczyk, "Role of peripheral chemoreceptors and central chemosensitivity in the regulation of respiration and circulation.," *J Exp Biol*, vol. 100, pp. 23–40, Oct. 1982.

[64] H. V. Forster, "Plasticity in Respiratory Motor Control," *J Appl Physiol*, 2003.

[65] H. V. Forster, L. G. Pan, T. F. Lowry, A. Serra, J. Wenninger, and P. Martino, "Important role of carotid chemoreceptor afferents in control of breathing of adult and neonatal mammals.," *Respir Physiol*, vol. 119, no. 2–3, pp. 199–208, Feb. 2000.

[66] P. B. Persson, H. Ehmke, and H. R. Kirchheim, "Blood pressure control in arterial- and cardiopulmonary receptor denervated dogs.," *Acta Physiol Scand*, vol. 142, no. 2, pp. 221–228, Jun. 1991.

[67] P. B. Persson and H. R. Kirchheim, *Baroreceptor reflexes: integrative functions and clinical aspects*. 2013.

[68] S. Andronikou, M. Shirahata, A. Mokashi, and S. Lahiri, "Carotid body chemoreceptor and ventilatory responses to sustained hypoxia and hypercapnia in the cat.," *Respir Physiol*, vol. 72, no. 3, pp. 361–374, Jun. 1988.

[69] Z.-Y. Tan, Y. Lu, C. A. Whiteis, C. J. Benson, M. W. Chapleau, and F. M. Abboud, "Acid-sensing ion channels contribute to transduction of extracellular acidosis in rat carotid body glomus cells.," *Circ Res*, vol. 101,

no. 10, pp. 1009–1019, Nov. 2007.

[70] G. E. Bisgard, H. V. Forster, and J. P. Klein, “Recovery of peripheral chemoreceptor function after denervation in ponies.,” *J Appl Physiol*, vol. 49, no. 6, pp. 964–970, Dec. 1980.

[71] P. R. Angelova, V. Kasymov, I. Christie, S. Sheikhbahaei, E. Turovsky, N. Marina, A. Korsak, J. Zwicker, A. G. Teschemacher, G. L. Ackland, G. D. Funk, S. Kasparov, A. Y. Abramov, and A. V. Gourine, “Functional Oxygen Sensitivity of Astrocytes.,” *J Neurosci*, vol. 35, no. 29, pp. 10460–10473, Jul. 2015.

[72] H. W. Davenport and G. Brewer, “The respiratory responses to anoxemia of unanesthetized dogs with chronically denervated aortic and carotid chemoreceptors and their causes.,” *Am J Physiol*, vol. 148, no. 2, pp. 406–416, Feb. 1947.

[73] M. J. Miller and S. M. Tenney, “Hypoxia-induced tachypnea in carotid-deafferented cats.,” *Respir Physiol*, vol. 23, no. 1, pp. 31–39, Jan. 1975.

[74] E. B. Olson, E. H. Vidruk, and J. A. Dempsey, “Carotid body excision significantly changes ventilatory control in awake rats.,” *J Appl Physiol*, vol. 64, no. 2, pp. 666–671, Feb. 1988.

[75] N. J. Marcus, R. Del Rio, E. P. Schultz, X.-H. Xia, and H. D. Schultz, “Carotid body denervation improves autonomic and cardiac function and attenuates disordered breathing in congestive heart failure.,” *J Physiol (Lond)*, vol. 592, no. 2, pp. 391–408, Jan. 2014.

[76] A. V. Gourine and G. D. Funk, “On the existence of a central respiratory oxygen sensor.,” *J Appl Physiol*, p. jap.00194.2017, May 2017.

[77] G. D. Funk, “Neuromodulation: purinergic signaling in respiratory control.,” *Compr Physiol*, vol. 3, no. 1, pp. 331–363, Jan. 2013.

[78] I. C. Solomon, N. H. Edelman, and J. A. Neubauer, “Pre-Bötzinger complex functions as a central hypoxia chemosensor for respiration in vivo.,” *J Neurophysiol*, vol. 83, no. 5, pp. 2854–2868, May 2000.

[79] J. a Neubauer and J. Sunderram, “Oxygen Sensing in Health and Disease Oxygen-sensing neurons in the central nervous system,” 2004.

[80] R. Del Rio, N. J. Marcus, and H. D. Schultz, “Carotid chemoreceptor ablation improves survival in heart failure: rescuing autonomic control of cardiorespiratory function.,” *J Am Coll Cardiol*, vol. 62, no. 25, pp. 2422–2430, Dec. 2013.

[81] J. Soliz, V. Joseph, C. Soulage, C. Becskei, J. Vogel, J. M. Pequignot, O. Ogunshola, and M. Gassmann, “Erythropoietin regulates hypoxic ventilation in mice by interacting with brainstem and carotid bodies.,” *J Physiol (Lond)*, vol. 568, no. Pt 2, pp. 559–571, Oct. 2005.

[82] A. J. Chang, F. E. Ortega, J. Riegler, D. V. Madison, and M. A. Krasnow, “Oxygen regulation of breathing through an olfactory receptor activated by lactate.,” *Nature*, vol. 527, no. 7577, pp. 240–244, Nov. 2015.

[83] J. M. Bissonnette and S. J. Knopp, “Developmental changes in the hypoxic ventilatory response in C57BL/6 mice.,” *Respir Physiol*, vol. 128, no. 2, pp. 179–186, Nov. 2001.

[84] D. M. Robinson, H. Kwok, B. M. Adams, K. C. Peebles, and G. D. Funk, “Development of the ventilatory response to hypoxia in Swiss CD-1 mice.,” *J Appl Physiol*, vol. 88, no. 5, pp. 1907–1914, May 2000.

[85] H. H. Loeschcke, “Central chemosensitivity and the reaction theory.,” *J Physiol (Lond)*, vol. 332, pp. 1–24, Nov. 1982.

[86] D. K. Mulkey, R. L. Stornetta, M. C. Weston, J. R. Simmons, A. Parker, D. A. Bayliss, and P. G. Guyenet, “Respiratory control by ventral surface chemoreceptor neurons in rats.,” *Nat Neurosci*, vol. 7, no. 12, pp. 1360–1369, Dec. 2004.

[87] H. V. Forster, P. Martino, M. Hodges, K. Krause, J. Bonis, S. Davis, and L. Pan, “The carotid chemoreceptors are a major determinant of ventilatory CO2 sensitivity and of PaCO2 during eupneic breathing.,” *Adv Exp Med Biol*, vol. 605, pp. 322–326, 2008.

[88] J. Heeringa, A. Berkenbosch, J. de Goede, and C. N. Olievier, “Relative contribution of central and peripheral chemoreceptors to the ventilatory response to CO2 during hyperoxia.,” *Respir Physiol*, vol. 37, no. 3, pp. 365–379, Aug. 1979.

[89] L. G. Pan, H. V. Forster, P. Martino, P. J. Strecker, J. Beales, A. Serra, T. F. Lowry, M. M. Forster, A. L. Forster, J. R. Miller, S. Neumueller, C. Muere, S. Olesiak, L. Pan, J. D. Bukowy, A. O. Daghistany, M. R. Hodges, H. V. Forster, M. Fiamma, E. T. O. Connor, A. Roy, I. Zuna, and R. J. A. Wilson, “Important role of carotid afferents in control of breathing carotid sinus nerves on respiratory motor control Important role of carotid afferents in control of breathing,” *J Appl Physiol*, 1998.

[90] G. E. Bisgard, H. V. Forster, J. A. Orr, D. D. Buss, C. A. Rawlings, and B. Rasmussen, “Hypoventilation in ponies after carotid body denervation.,” *J Appl Physiol*, vol. 40, no. 2, pp. 184–190, Feb. 1976.

[91] A. Dahan, E. Sarton, and L. Teppema, “Plasticity in the brain: influence of bilateral carotid body resection (bCBR) on central CO2 sensitivity.,” *Adv*

Exp Med Biol, vol. 605, pp. 312–316, 2008.

[92] E. E. Nattie, "Central chemosensitivity, sleep, and wakefulness.," *Respir Physiol*, vol. 129, no. 1–2, pp. 257–268, Dec. 2001.

[93] E. Nattie and A. Li, "Central chemoreception in wakefulness and sleep: evidence for a distributed network and a role for orexin.," *J Appl Physiol*, vol. 108, no. 5, pp. 1417–1424, May 2010.

[94] E. Nattie and A. Li, "Central chemoreceptors: locations and functions.," *Compr Physiol*, vol. 2, no. 1, pp. 221–254, Jan. 2012.

[95] T. Thomas and K. M. Spyer, "ATP as a mediator of mammalian central CO2 chemoreception.," *J Physiol (Lond)*, vol. 523 Pt 2, pp. 441–447, Mar. 2000.

[96] I. C. Solomon, N. H. Edelman, M. H. O. N. Iii, M. M. Ott, S. C. Nuding, L. S. Segers, R. O. Connor, K. F. Morris, B. G. Lindsey, R. T. R. Huckstepp, N. Dale, J. A. Physiol, H. Koizumi, S. E. Smerin, T. Yamanishi, B. R. Moorjani, R. Zhang, and J. C. Smith, "CO 2 / H + chemoreception in the cat pre-Bötzinger complex in vivo understanding of mechanism CO 2 / H ƨ chemoreception in the cat pre-Bo ¨ tzinger complex in vivo," *J Appl Physiol*, 2000.

[97] H. Koizumi, S. E. Smerin, T. Yamanishi, B. R. Moorjani, R. Zhang, and J. C. Smith, "TASK channels contribute to the K+-dominated leak current regulating respiratory rhythm generation in vitro.," *J Neurosci*, vol. 30, no. 12, pp. 4273–4284, Mar. 2010.

[98] K. M. Spyer and T. Thomas, "Sensing arterial CO(2) levels: a role for medullary P2X receptors.," *J Auton Nerv Syst*, vol. 81, no. 1–3, pp. 228–235, Jul. 2000.

[99] F. A. Teran, C. A. Massey, and G. B. Richerson, “Serotonin neurons and central respiratory chemoreception: where are we now?,” *Prog Brain Res*, vol. 209, pp. 207–233, 2014.

[100] R. T. R. Huckstepp and N. Dale, “Redefining the components of central CO2 chemosensitivity--towards a better understanding of mechanism.,” *J Physiol (Lond)*, vol. 589, no. Pt 23, pp. 5561–5579, Dec. 2011.

[101] A. V. Gourine, E. Llaudet, N. Dale, and K. M. Spyer, “Release of ATP in the ventral medulla during hypoxia in rats: role in hypoxic ventilatory response.,” *J Neurosci*, vol. 25, no. 5, pp. 1211–1218, Feb. 2005.

[102] V. Dubreuil, N. Ramanantsoa, D. Trochet, V. Vaubourg, J. Amiel, J. Gallego, J.-F. Brunet, and C. Goridis, “A human mutation in Phox2b causes lack of CO2 chemosensitivity, fatal central apnea, and specific loss of parafacial neurons.,” *Proc Natl Acad Sci U S A*, vol. 105, no. 3, pp. 1067–1072, Jan. 2008.

[103] N. Ramanantsoa, M.-R. Hirsch, M. Thoby-Brisson, V. Dubreuil, J. Bouvier, P.-L. Ruffault, B. Matrot, G. Fortin, J.-F. Brunet, J. Gallego, and C. Goridis, “Breathing without CO(2) chemosensitivity in conditional Phox2b mutants.,” *J Neurosci*, vol. 31, no. 36, pp. 12880–12888, Sep. 2011.

[104] P. G. Guyenet, D. A. Bayliss, R. L. Stornetta, M. G. Fortuna, S. B. G. Abbott, and S. D. DePuy, “Retrotrapezoid nucleus, respiratory chemosensitivity and breathing automaticity.,” *Respir Physiol Neurobiol*, vol. 168, no. 1–2, pp. 59–68, Aug. 2009.

[105] P. G. Guyenet and D. K. Mulkey, “Retrotrapezoid nucleus and parafacial respiratory group.,” *Respir Physiol Neurobiol*, vol. 173, no. 3, pp. 244–255, Oct. 2010.

[106] J. S. Haldane and J. G. Priestley, “The regulation of the lung-ventilation.,” *J Physiol (Lond)*, vol. 32, no. 3–4, pp. 225–266, May 1905.

[107] A. W. Sheel and L. M. Romer, “Ventilation and respiratory mechanics.,” *Compr Physiol*, vol. 2, no. 2, pp. 1093–1142, Apr. 2012.

[108] N. N. Kumar, A. Velic, J. Soliz, Y. Shi, K. Li, S. Wang, J. L. Weaver, J. Sen, S. B. G. Abbott, R. M. Lazarenko, M.-G. Ludwig, E. Perez-Reyes, N. Mohebbi, C. Bettoni, M. Gassmann, T. Suply, K. Seuwen, P. G. Guyenet, C. A. Wagner, and D. A. Bayliss, “PHYSIOLOGY. Regulation of breathing by CO_2 requires the proton-activated receptor GPR4 in retrotrapezoid nucleus neurons.,” *Science*, vol. 348, no. 6240, pp. 1255–1260, Jun. 2015.

[109] C. R. Sobrinho, I. C. Wenker, E. M. Poss, A. C. Takakura, T. S. Moreira, and D. K. Mulkey, “Purinergic signalling contributes to chemoreception in the retrotrapezoid nucleus but not the nucleus of the solitary tract or medullary raphe.,” *J Physiol (Lond)*, vol. 592, no. 6, pp. 1309–1323, Mar. 2014.

[110] D. K. Mulkey, A. M. Mistry, P. G. Guyenet, and D. A. Bayliss, “Purinergic P2 receptors modulate excitability but do not mediate pH sensitivity of RTN respiratory chemoreceptors.,” *J Neurosci*, vol. 26, no. 27, pp. 7230–7233, Jul. 2006.

[111] C. R. Sobrinho, C. M. Gonçalves, A. C. Takakura, D. K. Mulkey, and T. S. Moreira, “Fluorocitrate-mediated depolarization of astrocytes in the retrotrapezoid nucleus stimulates breathing.,” *J Neurophysiol*, p. jn.00032.2017, Jul. 2017.

[112] D. K. Mulkey, I. C. Wenker, and O. Kréneisz, “Current ideas on central chemoreception by neurons and glial cells in the retrotrapezoid nucleus.,” *J*

Appl Physiol, vol. 108, no. 5, pp. 1433–1439, May 2010.

[113] E. Turovsky, S. M. Theparambil, V. Kasymov, J. W. Deitmer, A. G. Del Arroyo, G. L. Ackland, J. J. Corneveaux, A. N. Allen, M. J. Huentelman, S. Kasparov, N. Marina, and A. V. Gourine, "Mechanisms of CO2/H+ sensitivity of astrocytes.," *J Neurosci*, vol. 36, no. 42, pp. 10750–10758, Oct. 2016.

[114] E. Turovsky, A. Karagiannis, A. P. Abdala, and A. V. Gourine, "Impaired CO2 sensitivity of astrocytes in a mouse model of Rett syndrome.," *J Physiol (Lond)*, vol. 593, no. 14, pp. 3159–3168, Jul. 2015.

[115] G. Ricci, L. Volpi, L. Pasquali, L. Petrozzi, and G. Siciliano, "Astrocyte-neuron interactions in neurological disorders.," *J Biol Phys*, vol. 35, no. 4, pp. 317–336, Oct. 2009.

[116] J. J. Wade, L. J. McDaid, J. Harkin, V. Crunelli, and J. A. S. Kelso, "Bidirectional coupling between astrocytes and neurons mediates learning and dynamic coordination in the brain: a multiple modeling approach.," *PLoS ONE*, vol. 6, no. 12, p. e29445, Dec. 2011.

[117] B. Benedetti, V. Matyash, and H. Kettenmann, "Astrocytes control GABAergic inhibition of neurons in the mouse barrel cortex.," *J Physiol (Lond)*, vol. 589, no. Pt 5, pp. 1159–1172, Mar. 2011.

[118] M. Navarrete, G. Perea, D. Fernandez de Sevilla, M. Gómez-Gonzalo, A. Núñez, E. D. Martín, and A. Araque, "Astrocytes mediate in vivo cholinergic-induced synaptic plasticity.," *PLoS Biol*, vol. 10, no. 2, p. e1001259, Feb. 2012.

[119] A. M. Brown, S. B. Tekkök, and B. R. Ransom, "Glycogen regulation and functional role in mouse white matter.," *J Physiol (Lond)*, vol. 549, no. Pt 2,

pp. 501–512, Jun. 2003.

[120] F. Tang, S. Lane, A. Korsak, J. F. R. Paton, A. V. Gourine, S. Kasparov, and A. G. Teschemacher, “Lactate-mediated glia-neuronal signalling in the mammalian brain.,” *Nat Commun*, vol. 5, p. 3284, 2014.

[121] A. G. Teschemacher, A. V. Gourine, and S. Kasparov, “A Role for Astrocytes in Sensing the Brain Microenvironment and Neuro-Metabolic Integration.,” *Neurochem Res*, vol. 40, no. 12, pp. 2386–2393, Dec. 2015.

[122] D. T. Theodosis, D. A. Poulain, and S. H. R. Oliet, “Activity-dependent structural and functional plasticity of astrocyte-neuron interactions.,” *Physiol Rev*, vol. 88, no. 3, pp. 983–1008, Jul. 2008.

[123] M. Haber, L. Zhou, and K. K. Murai, “Cooperative astrocyte and dendritic spine dynamics at hippocampal excitatory synapses.,” *J Neurosci*, vol. 26, no. 35, pp. 8881–8891, Aug. 2006.

[124] E. A. Bushong, M. E. Martone, Y. Z. Jones, and M. H. Ellisman, “Protoplasmic astrocytes in CA1 stratum radiatum occupy separate anatomical domains.,” *J Neurosci*, vol. 22, no. 1, pp. 183–192, Jan. 2002.

[125] M. Tsacopoulos and P. J. Magistretti, “Metabolic coupling between glia and neurons.,” *J Neurosci*, vol. 16, no. 3, pp. 877–885, Feb. 1996.

[126] P. J. Magistretti, “Neuron-glia metabolic coupling and plasticity.,” *Exp Physiol*, vol. 96, no. 4, pp. 407–410, Apr. 2011.

[127] A. Suzuki, S. A. Stern, O. Bozdagi, G. W. Huntley, R. H. Walker, P. J. Magistretti, and C. M. Alberini, “Astrocyte-neuron lactate transport is required for long-term memory formation.,” *Cell*, vol. 144, no. 5, pp. 810–823, Mar. 2011.

[128] M. Zonta, M. C. Angulo, S. Gobbo, B. Rosengarten, K.-A. Hossmann, T. Pozzan, and G. Carmignoto, “Neuron-to-astrocyte signaling is central to the dynamic control of brain microcirculation.,” *Nat Neurosci*, vol. 6, no. 1, pp. 43–50, Jan. 2003.

[129] T. Takano, G.-F. Tian, W. Peng, N. Lou, W. Libionka, X. Han, and M. Nedergaard, “Astrocyte-mediated control of cerebral blood flow.,” *Nat Neurosci*, vol. 9, no. 2, pp. 260–267, Feb. 2006.

[130] C. Iadecola and M. Nedergaard, “Glial regulation of the cerebral microvasculature.,” *Nat Neurosci*, vol. 10, no. 11, pp. 1369–1376, Nov. 2007.

[131] G. R. J. Gordon, H. B. Choi, R. L. Rungta, G. C. R. Ellis-Davies, and B. A. MacVicar, “Brain metabolism dictates the polarity of astrocyte control over arterioles.,” *Nature*, vol. 456, no. 7223, pp. 745–749, Dec. 2008.

[132] P. G. Haydon and G. Carmignoto, “Astrocyte control of synaptic transmission and neurovascular coupling.,” *Physiol Rev*, vol. 86, no. 3, pp. 1009–1031, Jul. 2006.

[133] M. M. Halassa and P. G. Haydon, “Integrated brain circuits: astrocytic networks modulate neuronal activity and behavior.,” *Annu Rev Physiol*, vol. 72, pp. 335–355, 2010.

[134] K. Ballanyi, B. Panaitescu, and A. Ruangkittisakul, “Control of breathing by ‘nerve glue’.,” *Sci Signal*, vol. 3, no. 147, p. pe41, Nov. 2010.

[135] S. Hülsmann, Y. Oku, W. Zhang, and D. W. Richter, “Metabolic coupling between glia and neurons is necessary for maintaining respiratory activity in transverse medullary slices of neonatal mouse.,” *Eur J Neurosci*, vol. 12, no.

3, pp. 856–862, Mar. 2000.

[136] J. K. Young, I. A. Dreshaj, C. G. Wilson, R. J. Martin, S. I. A. Zaidi, and M. A. Haxhiu, “An astrocyte toxin influences the pattern of breathing and the ventilatory response to hypercapnia in neonatal rats.,” *Respir Physiol Neurobiol*, vol. 147, no. 1, pp. 19–30, May 2005.

[137] A. G. Huxtable, J. D. Zwicker, T. S. Alvares, A. Ruangkittisakul, X. Fang, L. B. Hahn, E. Posse de Chaves, G. B. Baker, K. Ballanyi, and G. D. Funk, “Glia contribute to the purinergic modulation of inspiratory rhythm-generating networks.,” *J Neurosci*, vol. 30, no. 11, pp. 3947–3958, Mar. 2010.

[138] Y. Okada, T. Sasaki, Y. Oku, N. Takahashi, M. Seki, S. Ujita, K. F. Tanaka, N. Matsuki, and Y. Ikegaya, “Preinspiratory calcium rise in putative pre-Botzinger complex astrocytes.,” *J Physiol (Lond)*, vol. 590, no. 19, pp. 4933–4944, Oct. 2012.

[139] G. D. Funk, V. Rajani, T. S. Alvares, A. L. Revill, Y. Zhang, N. Y. Chu, V. Biancardi, C. Linhares-Taxini, A. Katzell, and R. Reklow, “Neuroglia and their roles in central respiratory control; an overview.,” *Comp Biochem Physiol, Part A Mol Integr Physiol*, vol. 186, pp. 83–95, Aug. 2015.

[140] Y. Oku, J. Fresemann, F. Miwakeichi, and S. Hülsmann, “Respiratory calcium fluctuations in low-frequency oscillating astrocytes in the pre-Bötzinger complex.,” *Respir Physiol Neurobiol*, vol. 226, pp. 11–17, Jun. 2016.

[141] V. Rajani, Y. Zhang, V. Jalubula, V. Rancic, S. SheikhBahaei, J. D. Zwicker, S. Pagliardini, C. T. Dickson, K. Ballanyi, S. Kasparov, A. V. Gourine, and G. D. Funk, “Release of ATP by preBötzinger complex astrocytes contributes to the hypoxic ventilatory response via a Ca(2+) -

dependent P2Y1 receptor mechanism.," *J Physiol (Lond)*, Jul. 2017.

[142] V. Kasymov, O. Larina, C. Castaldo, N. Marina, M. Patrushev, S. Kasparov, and A. V. Gourine, "Differential sensitivity of brainstem versus cortical astrocytes to changes in pH reveals functional regional specialization of astroglia.," *J Neurosci*, vol. 33, no. 2, pp. 435–441, Jan. 2013.

[143] D. K. Mulkey and I. C. Wenker, "Astrocyte chemoreceptors: mechanisms of H+ sensing by astrocytes in the retrotrapezoid nucleus and their possible contribution to respiratory drive.," *Exp Physiol*, vol. 96, no. 4, pp. 400–406, Apr. 2011.

[144] R. T. R. Huckstepp, R. id Bihi, R. Eason, K. M. Spyer, N. Dicke, K. Willecke, N. Marina, A. V. Gourine, and N. Dale, "Connexin hemichannel-mediated CO2-dependent release of ATP in the medulla oblongata contributes to central respiratory chemosensitivity.," *J Physiol (Lond)*, vol. 588, no. Pt 20, pp. 3901–3920, Oct. 2010.

[145] A. V. Gourine, L. Atkinson, J. Deuchars, and K. M. Spyer, "Purinergic signalling in the medullary mechanisms of respiratory control in the rat: respiratory neurones express the P2X2 receptor subunit.," *J Physiol (Lond)*, vol. 552, no. Pt 1, pp. 197–211, Oct. 2003.

[146] A. V. Gourine, E. Llaudet, N. Dale, and K. M. Spyer, "ATP is a mediator of chemosensory transduction in the central nervous system.," *Nature*, vol. 436, no. 7047, pp. 108–111, Jul. 2005.

[147] J. S. Erlichman, J. C. Leiter, and A. V. Gourine, "ATP, glia and central respiratory control.," *Respir Physiol Neurobiol*, vol. 173, no. 3, pp. 305–311, Oct. 2010.

[148] A. V. Gourine, "On the peripheral and central chemoreception and control

of breathing: an emerging role of ATP.," *J Physiol (Lond)*, vol. 568, no. Pt 3, pp. 715–724, Nov. 2005.

[149] A. R. Lorier, J. Lipski, G. D. Housley, J. J. Greer, and G. D. Funk, "ATP sensitivity of preBötzinger complex neurones in neonatal rat in vitro: mechanism underlying a P2 receptor-mediated increase in inspiratory frequency.," *J Physiol (Lond)*, vol. 586, no. 5, pp. 1429–1446, Mar. 2008.

[150] A. R. Lorier, A. G. Huxtable, D. M. Robinson, J. Lipski, G. D. Housley, and G. D. Funk, "P2Y1 receptor modulation of the pre-Bötzinger complex inspiratory rhythm generating network in vitro.," *J Neurosci*, vol. 27, no. 5, pp. 993–1005, Jan. 2007.

[151] H. S. Lee, A. Ghetti, A. Pinto-Duarte, X. Wang, G. Dziewczapolski, F. Galimi, S. Huitron-Resendiz, J. C. Piña-Crespo, A. J. Roberts, I. M. Verma, T. J. Sejnowski, and S. F. Heinemann, "Astrocytes contribute to gamma oscillations and recognition memory.," *Proc Natl Acad Sci U S A*, vol. 111, no. 32, pp. E3343–52, Aug. 2014.

[152] K. E. Poskanzer and R. Yuste, "Astrocytes regulate cortical state switching in vivo.," *Proc Natl Acad Sci U S A*, vol. 113, no. 19, pp. E2675–84, May 2016.

[153] T. Fellin, M. M. Halassa, M. Terunuma, F. Succol, H. Takano, M. Frank, S. J. Moss, and P. G. Haydon, "Endogenous nonneuronal modulators of synaptic transmission control cortical slow oscillations in vivo.," *Proc Natl Acad Sci U S A*, vol. 106, no. 35, pp. 15037–15042, Sep. 2009.

[154] T. V. Dunwiddie, L. Diao, and W. R. Proctor, "Adenine nucleotides undergo rapid, quantitative conversion to adenosine in the extracellular space in rat hippocampus.," *J Neurosci*, vol. 17, no. 20, pp. 7673–7682, Oct. 1997.

[155] O. Pascual, K. B. Casper, C. Kubera, J. Zhang, R. Revilla-Sanchez, J.-Y. Sul, H. Takano, S. J. Moss, K. McCarthy, and P. G. Haydon, "Astrocytic purinergic signaling coordinates synaptic networks.," *Science*, vol. 310, no. 5745, pp. 113–116, Oct. 2005.

[156] J. Zhang, H. Wang, C. Ye, W. Ge, Y. Chen, Z. Jiang, C. Wu, M. Poo, and S. Duan, "ATP released by astrocytes mediates glutamatergic activity-dependent heterosynaptic suppression.," *Neuron*, vol. 40, no. 5, pp. 971–982, Dec. 2003.

[157] E. M. Carlsen and J.-F. Perrier, "Purines released from astrocytes inhibit excitatory synaptic transmission in the ventral horn of the spinal cord.," *Front Neural Circuits*, vol. 8, p. 60, Jun. 2014.

[158] N. Dale and D. Gilday, "Regulation of rhythmic movements by purinergic neurotransmitters in frog embryos.," *Nature*, vol. 383, no. 6597, pp. 259–263, Sep. 1996.

[159] N. Dale, "Delayed production of adenosine underlies temporal modulation of swimming in frog embryo.," *J Physiol (Lond)*, vol. 511 (Pt 1), pp. 265–272, Aug. 1998.

[160] E. C. Witts, K. M. Panetta, and G. B. Miles, "Glial-derived adenosine modulates spinal motor networks in mice.," *J Neurophysiol*, vol. 107, no. 7, pp. 1925–1934, Apr. 2012.

[161] P. Brown and N. Dale, "Adenosine A1 receptors modulate high voltage-activated Ca2+ currents and motor pattern generation in the xenopus embryo.," *J Physiol (Lond)*, vol. 525 Pt 3, pp. 655–667, Jun. 2000.

[162] G. Taccola, D. Olivieri, G. D'Angelo, P. Blackburn, L. Secchia, and K.

Ballanyi, "A_1 adenosine receptor modulation of chemically and electrically evoked lumbar locomotor network activity in isolated newborn rat spinal cords.," *Neuroscience*, vol. 222, pp. 191–204, Oct. 2012.

[163] A. G. Huxtable, J. D. Zwicker, B. Y. Poon, S. Pagliardini, S. Q. Vrouwe, J. J. Greer, and G. D. Funk, "Tripartite purinergic modulation of central respiratory networks during perinatal development: the influence of ATP, ectonucleotidases, and ATP metabolites.," *J Neurosci*, vol. 29, no. 47, pp. 14713–14725, Nov. 2009.

[164] H. Duale, S. Kasparov, J. F. R. Paton, and A. G. Teschemacher, "Differences in transductional tropism of adenoviral and lentiviral vectors in the rat brainstem.," *Exp Physiol*, vol. 90, no. 1, pp. 71–78, Jan. 2005.

[165] B. Liu, J. F. Paton, and S. Kasparov, "Viral vectors based on bidirectional cell-specific mammalian promoters and transcriptional amplification strategy for use in vitro and in vivo.," *BMC Biotechnol*, vol. 8, p. 49, May 2008.

[166] M. J. Zylka, N. A. Sowa, B. Taylor-Blake, M. A. Twomey, A. Herrala, V. Voikar, and P. Vihko, "Prostatic acid phosphatase is an ectonucleotidase and suppresses pain by generating adenosine.," *Neuron*, vol. 60, no. 1, pp. 111–122, Oct. 2008.

[167] J. A. Wells, I. N. Christie, P. S. Hosford, R. T. R. Huckstepp, P. R. Angelova, P. Vihko, S. C. Cork, A. Y. Abramov, A. G. Teschemacher, S. Kasparov, M. F. Lythgoe, and A. V. Gourine, "A critical role for purinergic signalling in the mechanisms underlying generation of BOLD fMRI responses.," *J Neurosci*, vol. 35, no. 13, pp. 5284–5292, Apr. 2015.

[168] N. Marina, F. Tang, M. Figueiredo, S. Mastitskaya, V. Kasimov, V. Mohamed-Ali, E. Roloff, A. G. Teschemacher, A. V. Gourine, and S.

Kasparov, “Purinergic signalling in the rostral ventro-lateral medulla controls sympathetic drive and contributes to the progression of heart failure following myocardial infarction in rats.,” *Basic Res Cardiol*, vol. 108, no. 1, p. 317, Jan. 2013.

[169] B. N. Armbruster, X. Li, M. H. Pausch, S. Herlitze, and B. L. Roth, “Evolving the lock to fit the key to create a family of G protein-coupled receptors potently activated by an inert ligand.,” *Proc Natl Acad Sci U S A*, vol. 104, no. 12, pp. 5163–5168, Mar. 2007.

[170] S. Coco, F. Calegari, E. Pravettoni, D. Pozzi, E. Taverna, P. Rosa, M. Matteoli, and C. Verderio, “Storage and release of ATP from astrocytes in culture.,” *J Biol Chem*, vol. 278, no. 2, pp. 1354–1362, Jan. 2003.

[171] K. Striedinger, P. Meda, and E. Scemes, “Exocytosis of ATP from astrocyte progenitors modulates spontaneous Ca2+ oscillations and cell migration.,” *Glia*, vol. 55, no. 6, pp. 652–662, Apr. 2007.

[172] E. Llaudet, S. Hatz, M. Droniou, and N. Dale, “Microelectrode biosensor for real-time measurement of ATP in biological tissue.,” *Anal Chem*, vol. 77, no. 10, pp. 3267–3273, May 2005.

[173] A. Gramsbergen, P. Schwartze, and H. F. Prechtl, “The postnatal development of behavioral states in the rat.,” *Dev Psychobiol*, vol. 3, no. 4, pp. 267–280, 1970.

[174] G. Cohen, P. Gressens, J. Gallego, and C. Gaultier, “Depression of hypoxic arousal response in adolescent mice following antenatal vasoactive intestinal polypeptide blockade.,” *J Physiol (Lond)*, vol. 540, no. Pt 2, pp. 691–699, Apr. 2002.

[175] S. Sheikhbahaei, A. V. Gourine, and J. C. Smith, “Respiratory rhythm

irregularity after carotid body denervation in rats.," *Respir Physiol Neurobiol*, Aug. 2017.

[176] G. Enhorning, S. van Schaik, C. Lundgren, and I. Vargas, "Whole-body plethysmography, does it measure tidal volume of small animals?," *Can J Physiol Pharmacol*, vol. 76, no. 10–11, pp. 945–951, Nov. 1998.

[177] J. P. Mortola and P. B. Frappell, "On the barometric method for measurements of ventilation, and its use in small animals.," *Can J Physiol Pharmacol*, vol. 76, no. 10–11, pp. 937–944, Nov. 1998.

[178] S. Trapp, S. J. Tucker, and A. V. Gourine, "Respiratory responses to hypercapnia and hypoxia in mice with genetic ablation of Kir5.1 (Kcnj16).," *Exp Physiol*, vol. 96, no. 4, pp. 451–459, Apr. 2011.

[179] H. Waki, K. Katahira, J. W. Polson, S. Kasparov, D. Murphy, and J. F. R. Paton, "Automation of analysis of cardiovascular autonomic function from chronic measurements of arterial pressure in conscious rats.," *Exp Physiol*, vol. 91, no. 1, pp. 201–213, Jan. 2006.

[180] E. B. Oliveira-Sales, D. S. A. Colombari, R. L. Davisson, S. Kasparov, A. E. Hirata, R. R. Campos, and J. F. R. Paton, "Kidney-induced hypertension depends on superoxide signaling in the rostral ventrolateral medulla.," *Hypertension*, vol. 56, no. 2, pp. 290–296, Aug. 2010.

[181] J.-M. Ramirez, "The integrative role of the sigh in psychology, physiology, pathology, and neurobiology.," *Prog Brain Res*, vol. 209, pp. 91–129, 2014.

[182] N. S. Cherniack, C. von Euler, M. Głogowska, and I. Homma, "Characteristics and rate of occurrence of spontaneous and provoked augmented breaths.," *Acta Physiol Scand*, vol. 111, no. 3, pp. 349–360, Mar. 1981.

[183] A. G. Pillai, D. de Jong, S. Kanatsou, H. Krugers, A. Knapman, J.-M. Heinzmann, F. Holsboer, R. Landgraf, M. Joëls, and C. Touma, "Dendritic morphology of hippocampal and amygdalar neurons in adolescent mice is resilient to genetic differences in stress reactivity.," *PLoS ONE*, vol. 7, no. 6, p. e38971, Jun. 2012.

[184] M. Nedergaard, B. Ransom, and S. A. Goldman, "New roles for astrocytes: redefining the functional architecture of the brain.," *Trends Neurosci*, vol. 26, no. 10, pp. 523–530, Oct. 2003.

[185] K. M. Lee and A. G. MacLean, "New advances on glial activation in health and disease.," *World J Virol*, vol. 4, no. 2, pp. 42–55, May 2015.

[186] R. D. Fields, D. H. Woo, and P. J. Basser, "Glial Regulation of the Neuronal Connectome through Local and Long-Distant Communication.," *Neuron*, vol. 86, no. 2, pp. 374–386, Apr. 2015.

[187] M. M. Halassa, T. Fellin, and P. G. Haydon, "Tripartite synapses: roles for astrocytic purines in the control of synaptic physiology and behavior.," *Neuropharmacology*, vol. 57, no. 4, pp. 343–346, Sep. 2009.

[188] M. M. Halassa, T. Fellin, H. Takano, J.-H. Dong, and P. G. Haydon, "Synaptic islands defined by the territory of a single astrocyte.," *J Neurosci*, vol. 27, no. 24, pp. 6473–6477, Jun. 2007.

[189] N. A. Oberheim, S. A. Goldman, and M. Nedergaard, "Heterogeneity of astrocytic form and function.," *Methods Mol Biol*, vol. 814, pp. 23–45, 2012.

[190] Y. Zhang and B. A. Barres, "Astrocyte heterogeneity: an underappreciated topic in neurobiology.," *Curr Opin Neurobiol*, vol. 20, no. 5, pp. 588–594,

Oct. 2010.

[191] M. C. Angulo, A. S. Kozlov, S. Charpak, and E. Audinat, “Glutamate released from glial cells synchronizes neuronal activity in the hippocampus.,” *J Neurosci*, vol. 24, no. 31, pp. 6920–6927, Aug. 2004.

[192] J. F. Burkeen, A. D. Womac, D. J. Earnest, and M. J. Zoran, “Mitochondrial calcium signaling mediates rhythmic extracellular ATP accumulation in suprachiasmatic nucleus astrocytes.,” *J Neurosci*, vol. 31, no. 23, pp. 8432–8440, Jun. 2011.

[193] P. G. Haydon, “GLIA: listening and talking to the synapse.,” *Nat Rev Neurosci*, vol. 2, no. 3, pp. 185–193, Mar. 2001.

[194] M. Amiri, F. Bahrami, and M. Janahmadi, “Functional contributions of astrocytes in synchronization of a neuronal network model.,” *J Theor Biol*, vol. 292, pp. 60–70, Jan. 2012.

[195] L. Yang, Y. Qi, and Y. Yang, “Astrocytes control food intake by inhibiting AGRP neuron activity via adenosine A1 receptors.,” *Cell Rep*, vol. 11, no. 5, pp. 798–807, May 2015.

[196] V. Rajani, Y. Zhang, A. L. Revill, and G. D. Funk, “The role of P2Y1 receptor signaling in central respiratory control.,” *Respir Physiol Neurobiol*, vol. 226, pp. 3–10, Jun. 2016.

[197] V. Rajani, S. Sheikhbahaei, Y. Zhang, N. Chu, J. Zwicker, E. Posse de Chaves, S. Pagliardini, J. Smith, S. Kasparov, A. Gourine, and G. Funk, “Exocytotic Release of ATP from preBötzinger Complex Astrocytes Contributes to the Hypoxic Ventilatory Response via a P2Y1 Receptor, PLC, PKC-Dependent Mechanism,” *The FASEB Journal* , 2015.

[198] J. Eugenín León, M. J. Olivares, and S. Beltrán-Castillo, “Role of astrocytes in central respiratory chemoreception.,” *Adv Exp Med Biol*, vol. 949, pp. 109–145, 2016.

[199] J. D. Zwicker, V. Rajani, L. B. Hahn, and G. D. Funk, “Purinergic modulation of preBötzinger complex inspiratory rhythm in rodents: the interaction between ATP and adenosine.,” *J Physiol (Lond)*, vol. 589, no. Pt 18, pp. 4583–4600, Sep. 2011.

[200] H. Koizumi, C. G. Wilson, S. Wong, T. Yamanishi, N. Koshiya, and J. C. Smith, “Functional imaging, spatial reconstruction, and biophysical analysis of a respiratory motor circuit isolated in vitro.,” *J Neurosci*, vol. 28, no. 10, pp. 2353–2365, Mar. 2008.

[201] D. A. Sholl, “Dendritic organization in the neurons of the visual and motor cortices of the cat.,” *J Anat*, vol. 87, no. 4, pp. 387–406, Oct. 1953.

[202] P. Morquette, D. Verdier, A. Kadala, J. Féthière, A. G. Philippe, R. Robitaille, and A. Kolta, “An astrocyte-dependent mechanism for neuronal rhythmogenesis.,” *Nat Neurosci*, vol. 18, no. 6, pp. 844–854, Jun. 2015.

[203] J. L. Feldman and C. A. Del Negro, “Looking for inspiration: new perspectives on respiratory rhythm.,” *Nat Rev Neurosci*, vol. 7, no. 3, pp. 232–242, Mar. 2006.

[204] H. J. Bell, C. Ferguson, V. Kehoe, and P. Haouzi, “Hypocapnia increases the prevalence of hypoxia-induced augmented breaths.,” *Am J Physiol Regul Integr Comp Physiol*, vol. 296, no. 2, pp. R334–44, Feb. 2009.

[205] S. P. Lieske, M. Thoby-Brisson, P. Telgkamp, and J. M. Ramirez, “Reconfiguration of the neural network controlling multiple breathing patterns: eupnea, sighs and gasps [see comment].,” *Nat Neurosci*, vol. 3, no.

6, pp. 600–607, Jun. 2000.

[206] T. W. Lyons, C. T. Reinhard, and N. J. Planavsky, “The rise of oxygen in Earth’s early ocean and atmosphere.,” *Nature*, vol. 506, no. 7488, pp. 307–315, Feb. 2014.

[207] M. Thoby-Brisson and J. M. Ramirez, “Role of inspiratory pacemaker neurons in mediating the hypoxic response of the respiratory network in vitro.,” *J Neurosci*, vol. 20, no. 15, pp. 5858–5866, Aug. 2000.

[208] A. Ruangkittisakul, B. Panaitescu, and K. Ballanyi, “K(+) and Ca^2(+) dependence of inspiratory-related rhythm in novel ‘calibrated’ mouse brainstem slices.,” *Respir Physiol Neurobiol*, vol. 175, no. 1, pp. 37–48, Jan. 2011.

[209] N. Marina, R. Ang, A. Machhada, V. Kasymov, A. Karagiannis, P. S. Hosford, V. Mosienko, A. G. Teschemacher, P. Vihko, J. F. R. Paton, S. Kasparov, and A. V. Gourine, “Brainstem hypoxia contributes to the development of hypertension in the spontaneously hypertensive rat.,” *Hypertension*, vol. 65, no. 4, pp. 775–783, Apr. 2015.

[210] F. Peña, M. A. Parkis, A. K. Tryba, and J.-M. Ramirez, “Differential contribution of pacemaker properties to the generation of respiratory rhythms during normoxia and hypoxia.,” *Neuron*, vol. 43, no. 1, pp. 105–117, Jul. 2004.

[211] A. K. Tryba, F. Peña, S. P. Lieske, J.-C. Viemari, M. Thoby-Brisson, and J.-M. Ramirez, “Differential modulation of neural network and pacemaker activity underlying eupnea and sigh-breathing activities.,” *J Neurophysiol*, vol. 99, no. 5, pp. 2114–2125, May 2008.

[212] G. D. Funk, A. G. Huxtable, and A. R. Lorier, “ATP in central respiratory

control: a three-part signaling system.," *Respir Physiol Neurobiol*, vol. 164, no. 1–2, pp. 131–142, Dec. 2008.

[213] C. Henneberger, T. Papouin, S. H. R. Oliet, and D. A. Rusakov, "Long-term potentiation depends on release of D-serine from astrocytes.," *Nature*, vol. 463, no. 7278, pp. 232–236, Jan. 2010.

[214] E. Nattie, "CO2, brainstem chemoreceptors and breathing.," *Prog Neurobiol*, vol. 59, no. 4, pp. 299–331, Nov. 1999.

[215] G. B. Richerson, "Serotonergic neurons as carbon dioxide sensors that maintain pH homeostasis.," *Nat Rev Neurosci*, vol. 5, no. 6, pp. 449–461, Jun. 2004.

[216] D. A. Burton, K. Stokes, and G. M. Hall, "Physiological effects of exercise," *Continuing Education in Anaesthesia, Critical Care & Pain*, vol. 4, no. 6, pp. 185–188, Dec. 2004.

[217] H. V. Forster, P. Haouzi, and J. A. Dempsey, "Control of breathing during exercise.," *Compr Physiol*, vol. 2, no. 1, pp. 743–777, Jan. 2012.

[218] J. A. Dempsey, G. S. Mitchell, and C. A. Smith, "Exercise and chemoreception.," *Am Rev Respir Dis*, vol. 129, no. 2 Pt 2, pp. S31–4, Feb. 1984.

[219] J. Duffin, "Exercise & the Control of Breathing," 2007.

[220] F. L. Eldridge, D. E. Millhorn, J. P. Kiley, and T. G. Waldrop, "Stimulation by central command of locomotion, respiration and circulation during exercise.," *Respir Physiol*, vol. 59, no. 3, pp. 313–337, Mar. 1985.

[221] J. W. Williamson, "Autonomic responses to exercise: where is central

command?," *Auton Neurosci*, vol. 188, pp. 3–4, Mar. 2015.

[222] P. Haouzi, B. Chenuel, and B. Chalon, "The control of ventilation is dissociated from locomotion during walking in sheep.," *J Physiol (Lond)*, vol. 559, no. Pt 1, pp. 315–325, Aug. 2004.

[223] K. Matsukawa, "Central command: control of cardiac sympathetic and vagal efferent nerve activity and the arterial baroreflex during spontaneous motor behaviour in animals.," *Exp Physiol*, vol. 97, no. 1, pp. 20–28, Jan. 2012.

[224] A. C. L. Nobrega, D. O'Leary, B. M. Silva, E. Marongiu, M. F. Piepoli, and A. Crisafulli, "Neural regulation of cardiovascular response to exercise: role of central command and peripheral afferents.," *Biomed Res Int*, vol. 2014, p. 478965, Apr. 2014.

[225] M. P. Kaufman and H. V. Forster, "Reflexes controlling circulatory, ventilatory and airway responses to exercise," in *Comprehensive Physiology*, R. Terjung, Ed. Hoboken, NJ, USA: John Wiley & Sons, Inc., 2010.

[226] B. D. Johnson, W. G. Reddan, D. F. Pegelow, K. C. Seow, and J. A. Dempsey, "Flow limitation and regulation of functional residual capacity during exercise in a physically active aging population.," *Am Rev Respir Dis*, vol. 143, no. 5 Pt 1, pp. 960–967, May 1991.

[227] B. F. Barna, A. C. Takakura, and T. S. Moreira, "Acute exercise-induced activation of Phox2b-expressing neurons of the retrotrapezoid nucleus in rats may involve the hypothalamus.," *Neuroscience*, vol. 258, pp. 355–363, Jan. 2014.

[228] I. C. Wenker, C. R. Sobrinho, A. C. Takakura, T. S. Moreira, and D. K. Mulkey, "Regulation of ventral surface CO2/H+-sensitive neurons by

purinergic signalling.," *J Physiol (Lond)*, vol. 590, no. 9, pp. 2137–2150, May 2012.

[229] J. S. Erlichman and J. C. Leiter, "Glia modulation of the extracellular milieu as a factor in central CO2 chemosensitivity and respiratory control.," *J Appl Physiol*, vol. 108, no. 6, pp. 1803–1811, Jun. 2010.

[230] D. Accorsi-Mendonça, D. B. Zoccal, L. G. H. Bonagamba, and B. H. Machado, "Glial cells modulate the synaptic transmission of NTS neurons sending projections to ventral medulla of Wistar rats.," *Physiol Rep*, vol. 1, no. 4, p. e00080, Sep. 2013.

[231] K. R. Jessen, R. Thorpe, and R. Mirsky, "Molecular identity, distribution and heterogeneity of glial fibrillary acidic protein: an immunoblotting and immunohistochemical study of Schwann cells, satellite cells, enteric glia and astrocytes.," *J Neurocytol*, vol. 13, no. 2, pp. 187–200, Apr. 1984.

[232] L. F. Eng, "Glial fibrillary acidic protein (GFAP): the major protein of glial intermediate filaments in differentiated astrocytes.," *J Neuroimmunol*, vol. 8, no. 4–6, pp. 203–214, Jun. 1985.

[233] D. E. Weinstein, M. L. Shelanski, and R. K. Liem, "Suppression by antisense mRNA demonstrates a requirement for the glial fibrillary acidic protein in the formation of stable astrocytic processes in response to neurons.," *J Cell Biol*, vol. 112, no. 6, pp. 1205–1213, Mar. 1991.

[234] E. Fuchs and K. Weber, "Intermediate filaments: structure, dynamics, function, and disease.," *Annu Rev Biochem*, vol. 63, pp. 345–382, 1994.

[235] H. Gomi, T. Yokoyama, and S. Itohara, "Role of GFAP in morphological retention and distribution of reactive astrocytes induced by scrapie encephalopathy in mice.," *Brain Res*, vol. 1312, pp. 156–167, Feb. 2010.

[236] J. Middeldorp and E. M. Hol, “GFAP in health and disease.,” *Prog Neurobiol*, vol. 93, no. 3, pp. 421–443, Mar. 2011.

[237] A. Catalani, M. Sabbatini, C. Consoli, C. Cinque, D. Tomassoni, E. Azmitia, L. Angelucci, and F. Amenta, “Glial fibrillary acidic protein immunoreactive astrocytes in developing rat hippocampus.,” *Mech Ageing Dev*, vol. 123, no. 5, pp. 481–490, Mar. 2002.

[238] Y. Wu, A.-Q. Zhang, and D. T. Yew, “Age related changes of various markers of astrocytes in senescence-accelerated mice hippocampus.,” *Neurochem Int*, vol. 46, no. 7, pp. 565–574, Jun. 2005.

[239] H.-G. Bernstein, J. Bannier, G. Meyer-Lotz, J. Steiner, G. Keilhoff, H. Dobrowolny, M. Walter, and B. Bogerts, “Distribution of immunoreactive glutamine synthetase in the adult human and mouse brain. Qualitative and quantitative observations with special emphasis on extra-astroglial protein localization.,” *J Chem Neuroanat*, vol. 61–62, pp. 33–50, Nov. 2014.

[240] F. A. Tansey, M. Farooq, and W. Cammer, “Glutamine synthetase in oligodendrocytes and astrocytes: new biochemical and immunocytochemical evidence.,” *J Neurochem*, vol. 56, no. 1, pp. 266–272, Jan. 1991.

[241] D. Dahl, D. C. Rueger, A. Bignami, K. Weber, and M. Osborn, “Vimentin, the 57 000 molecular weight protein of fibroblast filaments, is the major cytoskeletal component in immature glia.,” *Eur J Cell Biol*, vol. 24, no. 2, pp. 191–196, Jun. 1981.

[242] S. K. Pixley and J. de Vellis, “Transition between immature radial glia and mature astrocytes studied with a monoclonal antibody to vimentin.,” *Brain Res*, vol. 317, no. 2, pp. 201–209, Aug. 1984.

[243] L. Saur, P. P. A. Baptista, P. N. de Senna, M. F. Paim, P. do Nascimento, J. Ilha, P. B. Bagatini, M. Achaval, and L. L. Xavier, "Physical exercise increases GFAP expression and induces morphological changes in hippocampal astrocytes.," *Brain Struct Funct*, vol. 219, no. 1, pp. 293–302, Jan. 2014.

[244] M. Zhang, W.-B. Li, Y.-X. Liu, C.-J. Liang, L.-Z. Liu, X. Cui, J.-X. Gong, S.-J. Gong, Y.-Y. Hu, and X.-H. Xian, "High expression of GLT-1 in hippocampal CA3 and dentate gyrus subfields contributes to their inherent resistance to ischemia in rats.," *Neurochem Int*, vol. 59, no. 7, pp. 1019–1028, Dec. 2011.

[245] W. Sun, A. Cornwell, J. Li, S. Peng, M. J. Osorio, N. A. Su Wanga, A. Benraiss, N. Lou, S. A. Goldman, and M. Nedergaard, "SOX9 is an astrocyte-specific nuclear marker in the adult brain outside the neurogenic regions.," *J Neurosci*, Mar. 2017.

[246] N. A. Oberheim, G.-F. Tian, X. Han, W. Peng, T. Takano, B. Ransom, and M. Nedergaard, "Loss of astrocytic domain organization in the epileptic brain.," *J Neurosci*, vol. 28, no. 13, pp. 3264–3276, Mar. 2008.

[247] K. Ogata and T. Kosaka, "Structural and quantitative analysis of astrocytes in the mouse hippocampus.," *Neuroscience*, vol. 113, no. 1, pp. 221–233, 2002.

[248] Y. Imura, Y. Morizawa, R. Komatsu, K. Shibata, Y. Shinozaki, H. Kasai, K. Moriishi, Y. Moriyama, and S. Koizumi, "Microglia release ATP by exocytosis.," *Glia*, vol. 61, no. 8, pp. 1320–1330, Aug. 2013.

[249] M. Mori, C. Heuss, B. H. Gähwiler, and U. Gerber, "Fast synaptic transmission mediated by P2X receptors in CA3 pyramidal cells of rat

hippocampal slice cultures.," *J Physiol (Lond)*, vol. 535, no. Pt 1, pp. 115–123, Aug. 2001.

[250] P. B. Guthrie, J. Knappenberger, M. Segal, M. V. Bennett, A. C. Charles, and S. B. Kater, "ATP released from astrocytes mediates glial calcium waves.," *J Neurosci*, vol. 19, no. 2, pp. 520–528, Jan. 1999.

[251] P. Li, W. A. Janczewski, K. Yackle, K. Kam, S. Pagliardini, M. A. Krasnow, and J. L. Feldman, "The peptidergic control circuit for sighing.," *Nature*, vol. 530, no. 7590, pp. 293–297, Feb. 2016.

[252] T. Dashevskiy, J. Bloom, and J.-M. Ramirez, "To Sigh Or Not To Sigh: Role Of Glia In Sigh Generation," *FASEB J*, Jan. 2016.

[253] E. E. Nattie and A. Li, "Substance P-saporin lesion of neurons with NK1 receptors in one chemoreceptor site in rats decreases ventilation and chemosensitivity.," *J Physiol (Lond)*, vol. 544, no. Pt 2, pp. 603–616, Oct. 2002.

[254] T. Lonergan, A. G. Teschemacher, D. Y. Hwang, K. S. Kim, A. E. Pickering, and S. Kasparov, "Targeting brain stem centers of cardiovascular control using adenoviral vectors: impact of promoters on transgene expression.," *Physiol Genomics*, vol. 20, no. 2, pp. 165–172, Jan. 2005.

[255] J. Korecka, M. Schouten, R. Eggers, A. Ulusoy, K. Bossers, and J. Verhaagen, "Comparison of AAV Serotypes for Gene Delivery to Dopaminergic Neurons in the Substantia Nigra," in *Viral GeneTherapy*, K. Xe, Ed. China: InTech, 2011, pp. 205–224.

[256] S. B. G. Abbott, R. L. Stornetta, M. G. Fortuna, S. D. Depuy, G. H. West, T. E. Harris, and P. G. Guyenet, "Photostimulation of retrotrapezoid nucleus phox2b-expressing neurons in vivo produces long-lasting activation of

breathing in rats.," *J Neurosci*, vol. 29, no. 18, pp. 5806–5819, May 2009.

[257] S. B. G. Abbott, S. D. DePuy, T. Nguyen, M. B. Coates, R. L. Stornetta, and P. G. Guyenet, "Selective optogenetic activation of rostral ventrolateral medullary catecholaminergic neurons produces cardiorespiratory stimulation in conscious mice.," *J Neurosci*, vol. 33, no. 7, pp. 3164–3177, Feb. 2013.

[258] M. P. Matott, D. D. Kline, and E. M. Hasser, "Glial EAAT2 regulation of extracellular nTS glutamate critically controls neuronal activity and cardiorespiratory reflexes.," *J Physiol (Lond)*, Jul. 2017.

[259] R. Huda, D. R. McCrimmon, and M. Martina, "pH modulation of glial glutamate transporters regulates synaptic transmission in the nucleus of the solitary tract.," *J Neurophysiol*, vol. 110, no. 2, pp. 368–377, Jul. 2013.

[260] J. S. Erlichman, A. C. Boyer, P. Reagan, R. W. Putnam, N. A. Ritucci, and J. C. Leiter, "Chemosensory responses to CO2 in multiple brain stem nuclei determined using a voltage-sensitive dye in brain slices from rats.," *J Neurophysiol*, vol. 102, no. 3, pp. 1577–1590, Sep. 2009.

[261] J. S. Erlichman, A. Hewitt, T. L. Damon, M. Hart, J. Kurascz, A. Li, and J. C. Leiter, "Inhibition of monocarboxylate transporter 2 in the retrotrapezoid nucleus in rats: a test of the astrocyte-neuron lactate-shuttle hypothesis.," *J Neurosci*, vol. 28, no. 19, pp. 4888–4896, May 2008.

[262] R. L. Stornetta, T. S. Moreira, A. C. Takakura, B. J. Kang, D. A. Chang, G. H. West, J. F. Brunet, D. K. Mulkey, D. A. Bayliss, and P. G. Guyenet, "Expression of Phox2b by brainstem neurons involved in chemosensory integration in the adult rat.," *J Neurosci*, vol. 26, no. 40, pp. 10305–10314, Oct. 2006.

[263] J. A. Dempsey, C. A. Smith, T. Przybylowski, B. Chenuel, A. Xie, H. Nakayama, and J. B. Skatrud, “The ventilatory responsiveness to CO(2) below eupnoea as a determinant of ventilatory stability in sleep.,” *J Physiol (Lond)*, vol. 560, no. Pt 1, pp. 1–11, Oct. 2004.

[264] R. Meeusen and K. De Meirleir, “Exercise and brain neurotransmission.,” *Sports Med*, vol. 20, no. 3, pp. 160–188, Sep. 1995.

[265] M. Dworak, P. Diel, S. Voss, W. Hollmann, and H. K. Strüder, “Intense exercise increases adenosine concentrations in rat brain: implications for a homeostatic sleep drive.,” *Neuroscience*, vol. 150, no. 4, pp. 789–795, Dec. 2007.

[266] F. Ding, J. O’Donnell, A. S. Thrane, D. Zeppenfeld, H. Kang, L. Xie, F. Wang, and M. Nedergaard, “α1-Adrenergic receptors mediate coordinated Ca2+ signaling of cortical astrocytes in awake, behaving mice.,” *Cell Calcium*, vol. 54, no. 6, pp. 387–394, Dec. 2013.

[267] Y. Pankratov and U. Lalo, “Role for astroglial α1-adrenoreceptors in gliotransmission and control of synaptic plasticity in the neocortex.,” *Front Cell Neurosci*, vol. 9, p. 230, Jun. 2015.

[268] C. Schnell, M. Negm, J. Driehaus, A. Scheller, and S. Hülsmann, “Norepinephrine-induced calcium signaling in astrocytes in the respiratory network of the ventrolateral medulla.,” *Respir Physiol Neurobiol*, vol. 226, pp. 18–23, Jun. 2016.

[269] M. Paukert, A. Agarwal, J. Cha, V. A. Doze, J. U. Kang, and D. E. Bergles, “Norepinephrine controls astroglial responsiveness to local circuit activity.,” *Neuron*, vol. 82, no. 6, pp. 1263–1270, Jun. 2014.

[270] T. Matsui, H. Omuro, Y.-F. Liu, M. Soya, T. Shima, B. S. McEwen, and H.

Soya, “Astrocytic glycogen-derived lactate fuels the brain during exhaustive exercise to maintain endurance capacity.,” *Proc Natl Acad Sci U S A*, vol. 114, no. 24, pp. 6358–6363, Jun. 2017.

[271] G. E. Bisgard, H. V. Forster, B. Byrnes, K. Stanek, J. Klein, and M. Manohar, “Cerebrospinal fluid acid-base balance during muscular exercise.,” *J Appl Physiol*, vol. 45, no. 1, pp. 94–101, Jul. 1978.

[272] E. Vlemincx, J. L. Abelson, P. M. Lehrer, P. W. Davenport, I. Van Diest, and O. Van den Bergh, “Respiratory variability and sighing: a psychophysiological reset model.,” *Biol Psychol*, vol. 93, no. 1, pp. 24–32, Apr. 2013.

[273] E. Vlemincx, I. Van Diest, and O. Van den Bergh, “Emotion, sighing, and respiratory variability.,” *Psychophysiology*, vol. 52, no. 5, pp. 657–666, May 2015.

[274] K. Yackle, L. A. Schwarz, K. Kam, J. M. Sorokin, J. R. Huguenard, J. L. Feldman, L. Luo, and M. A. Krasnow, “Breathing control center neurons that promote arousal in mice.,” *Science*, vol. 355, no. 6332, pp. 1411–1415, Mar. 2017.